Optimally Braked Landing Response of a Nonlinear Aircraft Model

A Thesis Submitted
in Partial Fulfillment of the Requirements
for the Degree of
Master of Technology

by
Sharad Agarwal

to the

DEPARTMENT OF AEROSPACE ENGINEERING
INDIAN INSTITUTE OF TECHNOLOGY, KANPUR

June 1995

CERTIFICATE

This is to certify that the work contained in the thesis titled **Optimally Braked Landing Response of a Nonlinear Aircraft Model** by **Sharad Agarwal**, has been carried out under my supervision and that this work has not been submitted elsewhere for a degree.

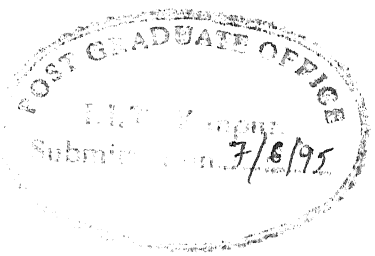

June 1995

(Dr. D. Yadav)
Professor
Dept. of Aerospace Engineering
Indian Institute of Technology
Kanpur.

Abstract

A short landing run requirement for an aircraft is important from economic, operational and strategic considerations. An anti-skid optimal braking scheme is presented to achieve the shortest possible (optimal) landing run. The heave model of the aircraft with nonlinear oleopneumatic shock strut is considered. The track profile is simulated as superimposition of a random process over a deterministic mean. A linear-predictor algorithm is used to predict the braking force one step ahead in time. Effects of variations in sink and glide velocities and mean profile, on the system response is presented. Considerable reduction in the ground distance travelled shows the efficacy of the proposed anti-skid optimal braking scheme.

Acknowledgements

I wish to express my deep sense of indebtedness and gratitude to my thesis supervisor Dr. D. Yadav, who helped and guided me throughout the progress and stagnance of the work. I am thankful to him for his persistent efforts and uncountable suggestions without which this thesis would not have been in the present state.

Among many close friends, Sarvesh and Maneesh will always be special for having boosted my morale from unimaginable depths to unbelievable heights. I wish to thank my friends Manoj, Magar, Gagan and Amit for their consistent support. I thank Dixitji, K. D. Kumar and Vineet for having provided a nice company.

Sharad Agarwal

Contents

Nomenclature

B	Braking force on the tyre
C_D	Drag coefficient
C_{Do}	Zero drag coefficient
C_{Do_r}	Zero drag coefficient during ground roll
C_{Do_r}	Zero drag coefficient at touch down
C_L	Lift coefficient
C_{Lo}	Zero lift coefficient
$C_{L\alpha}$	Lift curve slope
D	Aerodynamic drag on the aircraft
D_m	Free outer diameter of the wheel
F_a	Pneumatic force in the shock strut
F_{fj}	Journal friction force in the shock strut
F_{fm}	Seal friction force in the shock strut
F_h	Hydraulic force in the shock strut
F_s	Total axial force in the shock strut
F_{hg}	Horizontal force (friction force) between the tyre and the ground
F_{vg}	Vertical ground reaction
g	Gravitational acceleration
h_{det}	Mean ground variation (as a function of time)
h_{sd}	Randomness in the track profile (as a function of space)
K	Aspect ratio of the wings
L	Aerodynamic lift on the aircraft
S	Wing area of the aircraft

s	Tyre slip
s_d	Ground distance travelled by the aircraft
s_m	Shock strut stroke
$\dot{s}_m$	Strut telescoping velocity
T_b	Applied braking torque
V	Aircraft forward velocity
V_{sink}	Aircraft sink velocity
W	Total weight of the aircraft
W_1	Weight of the sprung mass
W_2	Weight of the unsprung mass
Z	Radial deflection in the tyre
Z_1	Vertical displacement of the sprung mass
Z_2	Vertical displacement of the unsprung mass
$\dot{Z}_1$	Sprung mass velocity
$\dot{Z}_2$	Unsprung mass velocity
$\ddot{Z}_1$	Sprung mass acceleration
$\ddot{Z}_2$	Unsprung mass acceleration
α	Angle of attack
α_1	Correlation constant for roughness of the track
α_s	Stalling angle
μ	Coefficient of slip friction between the tyre and the ground
Ω	Spatial frequency
Ω_o	Cut off Nyquist frequency
ω	Angular velocity of the wheel
$\dot{\omega}$	Angular acceleration of the wheel
ω_o	Free roll angular velocity of the wheel
ρ	Density of the air
σ	Standard deviation of the track profile

List of Tables

List of Figures

Chapter 1

Introduction

1.1 The Problem

In general, the aircrafts, all over the world, take-off and land from well prepared and large airstrips. But sometimes, in emergency, it may have to land on short and rough fields. This is particularly true in the case of military and rescue aircrafts, where they may have to land on badly prepared and different kinds of runways. The requirement of short landing run also arises for navy aircrafts, where the aircrafts have to take-off and land on aircraft carrier ships. This necessitates the development of a specialised mechanism to halt the aircraft in a short landing distance.

The length of the landing run depends on the way in which the brake is applied. If the applied brake is low, the stopping distance is large, while if the brake force is large, wheels lock and skidding takes place. The skidding is always a undesirable phenomenon, as it leads to instability of the vehicle.

When a wheel rolls on the ground, it has got inherent stability due to the stabilising gyroscopic forces, which arise due to rolling motion of the wheel. These tend to oppose the effects of any destabilising moments that may exist due to unbalanced or misaligned forces on the wheel.

A wheel can roll on the ground only if there is sufficient friction force between the tyres and the ground. If the braking force, applied on the wheel, is greater than the maximum sustainable friction force between the tyre and the ground, the wheel locks and the rolling motion is transformed into skidding motion. As soon as the skidding starts, the stabilizing gyroscopic forces disappear. Consequently, the control on the wheel is lost and this may lead to an accident. At this stage, to regain the control on

the vehicle, the only corrective step will be to release the brakes. Thus, to achieve the optimal landing run (the shortest stopping run without skidding), the braking force has to be varied to match the frictional force at all times.

The above criteria points to the design of a braking mechanism for an aircraft, which can reduce the landing distance substantially, on any kind of surface with no skidding during the braking operation.

The friction force between the tyre and the ground depends on the coefficient of friction between the tyre and the ground and the vertical ground reaction. The coefficient of friction depends on the roughness of the surface in contact, ground conditions and the slip of the tyre. The variation of μ with slip is shown in Fig.1.1 [1]. It has a maxima with the slip somewhere between 0.05 and 0.3. The slip s is defined as [1]

$$s = 1 - \frac{\omega}{\omega_a} \tag{1.1}$$

where ω is the angular velocity of the wheel at any instant of time and ω_a is the free roll angular velocity at that speed, defined as:

$$\omega_a = \frac{V}{\text{rolling radius}} = \frac{V}{\frac{D_m}{2} - \frac{Z}{3}} \tag{1.2}$$

where D_m is the free outer diameter of the tyre, Z is the tyre deflection and V is the forward velocity of the aircraft.

Furthermore, as the aircraft runs on a track, its weight is transferred to the ground, filtered through the suspension mechanism, such as shock absorbers and the tyres. If the track is uneven, the aircraft will oscillate under the influence of inputs through the wheels. Consequently, the reaction of the ground on the tyres also varies with time. These induced oscillations depend on the vehicle suspension mechanism, its forward velocity and the characteristics of the track profile. The time variable reaction of the ground on the wheels causes the maximum sustainable friction force also to vary with time. Both these forces are random in nature due to the randomness in the track profile.

This implies that in order to have optimal braking characteristic without skid, the brake torque should constantly match the wheel-ground friction torque. For this, either the braking force or the aircraft parameters, corresponding to the friction torque, should be varied continuously, while simultaneously maintaining the slip in the optimal range.

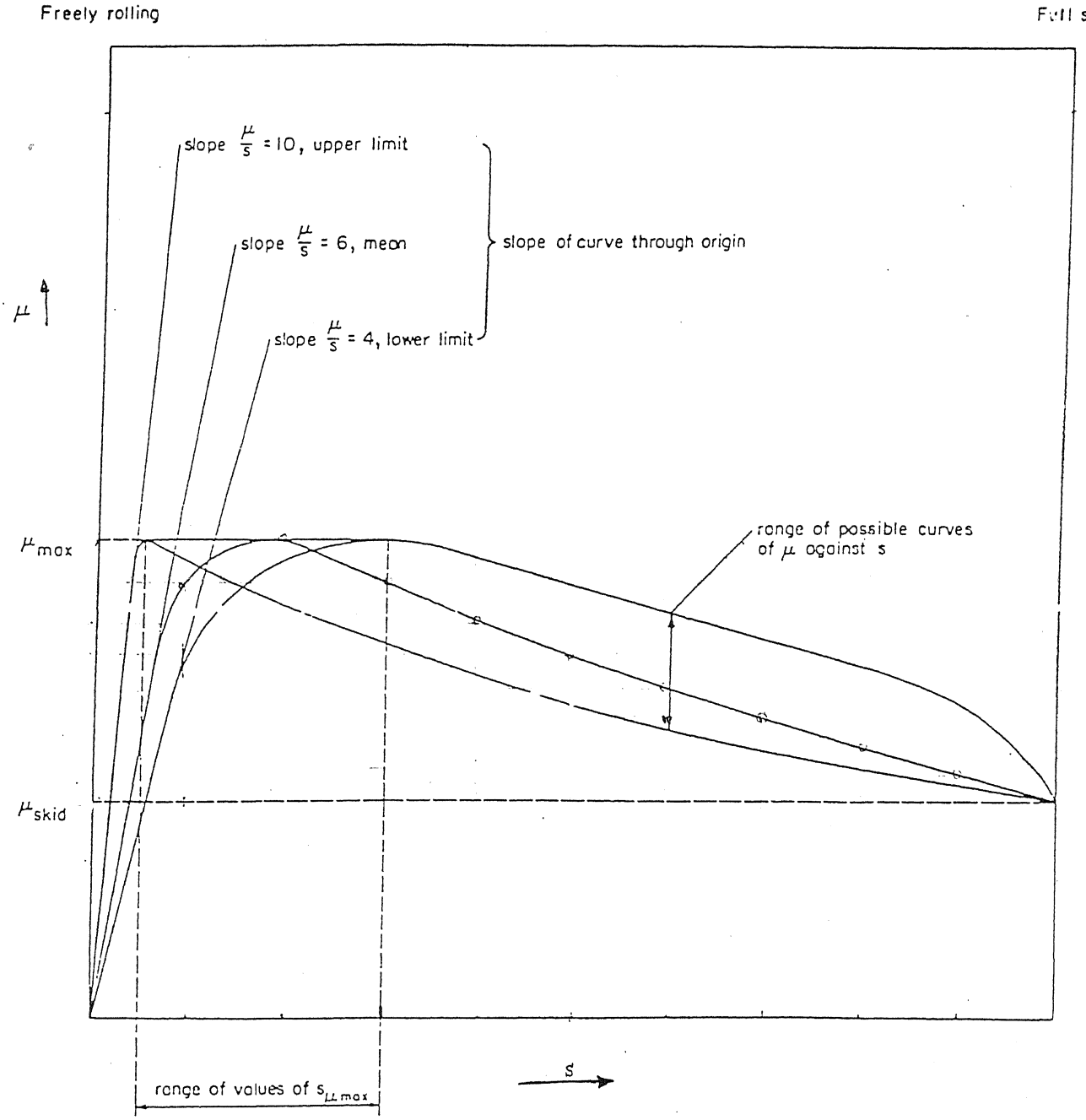

Figure 1.1: Variation of friction coefficient μ with tyre slip

It is physically impossible for any device to react instantaneously to a stimulus. This is manily due to the time taken :

- to detect the stimulus and its nature.
- to calculate the response.
- by the device to activate its sensors and achieve fully the response, due to the inherent physical inertia of the servo-mechanism.

Thus a continually varying braking force will lag behind the impulse by a small time interval. Therefore, to achieve optimality, the friction force between the wheel and the track should be known ahead of time by at least one worst lag interval. This necessitates to apply a prediction method applicable in the environment.

Short run anti-skid braking is also an important need for all road vehicles for safe operation on modern roads. These vehicles require strong deceleration to avoid collision, while negotiating curves and bad road patches, as well as for stopping. The stopping/slowing distance requirements are becoming ever more stringent with increase in operating speed. The control problem is very similar to the anti-skid optimal braking of the aircraft, and this study can be used for road vehicles as well.

1.2 Literature Survey

The optimal antiskid braking study involves a vehicle and track system modelling and response evaluation, optimal brake force prediction and its implementation on the vehicle system. A brief discussion is presented for the literature available on these aspects.

Analytical study of vehicle dynamics due to track induced excitation started with a linear model moving on a rigid pavement at a constant velocity [2]. The track was modelled to have discrete bumps and dips occurring at intersections and uneven settlements. Silsby [3] has studied analytically the effects of various linear landing gear parameters on the airplane response to runway roughness. Tung et al.[4] have carried out an investigation of runway-excited vibrations by a deterministic as well as statistical approach. They linearised the model using perturbation and equivalent linearisation techniques. The analysis yielded the statistics of displacements of mass center and the wheel masses during constant velocity runs. Kirk and Perry [5]

have carried out the analysis of uniform velocity taxing-induced vibrations of a linearised subsonic aircraft by the power spectral density method. Comparing the r.m.s. accelerations obtained statistically with those computed from the deterministic analysis of [2] they have concluded that the assumption of stationarity leads to an overestimate of the dynamic response. Kirk [6] has obtained the closed form solution of the response of the aircraft due to track induced excitations taking a heave-pitch model and adopting a equivalent linearisation technique. Virchis and Robson [7], and Sobczyk and Macvean [8] applied the time domain approach to determine the response statistics for a single-degree-of-freedom model in constant-velocity runs. Yadav and Nigam [9] have used a frequency domain formulation and a evolutionary spectra approach for response evaluation for lumped mass models in variable-velocity runs. Closed form solutions for response statistics were obtained for the linear model while a numerical technique was resorted to for the non-linear model. Hammond and Harrison [10,11] adopted a state space approach to obtain the non-stationary response of a vehicle modelled by linear dynamics. They have shown that the non-stationary response for some form of velocity variation may depart significantly from an approximating stationary solution. In another paper, Hammond and Harrison [12] modelled a non-linear system, but used statistical linearisation to overcome the non-linearity. They have demonstrated that the state space approach is tractable provided that the ground profile can be modelled by a linear spatially varying filter.

In all above studies, it has been assumed that the track profile is homogeneous and the shock absorber is linear, with the exceptions of [11] and [9,12], in which non-homogeneous track and non-linear shock absorbers, respectively, have been considered.

Yadav and Kapadia [13] have evaluated the second order response statistics of a vehicle in a variable velocity run over a non-homogeneous track using Monte Carlo simulation technique. They have assumed the vehicle suspension system to consist a articulated shock absorber carrying a oleopneumatic shock strut. The shock absorber has been modelled to have a non-linear spring and damper. The effects of suspension linkages on the vehicle dynamics has also been incorporated. Narayanan and Raju [14] tried to control the non-stationary vehicle response by use of active suspension taking a single degree of freedom model with variable velocity. Optimal solution has been obtained by using stochastic optimal control theory based on perfect and complete measurements. The road has been simulated as the output of a second

order linear spatial shaping filter to white noise input. Yadav and Ramamoorthy [15] have presented an analysis for the aircraft dynamics with a heave-pitch model having telescoping main gears and articulated nose gear. The formulation includes linkage dynamics and the non-linearities in the oleopneumatic shock struts for the two gears. The response and its second order statistics have been evaluated by the Monte-Carlo approach with simulation of the random track profile as a known mean superimposed over by a zero mean random process. Solutions have been presented for uniform taxi, accelerating take-off and decelerating landing runs. Yadav and Upadhyay [16,17] have studied the dynamics of the vehicles in variable velocity runs over non-homogeneous flexible track and foundation. The vehicle has been taken as a heave-pitch model with shock absorbers replaced by linear springs and dampers.

Not much work has been done on anti-skid braking. Yadav and Singh [18] have designed an anti-skid algorithm for an optimal braking problem. The braking force has been predicted one step ahead in time using adaptive linear algorithm. The vehicle has been modelled as a rigid body with heave degrees of freedom supported on a linear shock absorber consisting of a spring and a damper over a single wheel. The track profile has been taken to be random with a given power spectral density and known variable mean.

1.3 Present Work

In aircraft braking system, presently there exist two types of commercially available anti-skid mechanisms. These are briefly introduced here.

1. Pulsed braking system :

   In this system the braking force is applied in discrete pulses. The wheel is braked for a short period of time with no concessions to skidding and then released. During the period of free roll the wheel recovers from any skid it might have entered. This process is repeated until the aircraft is brought to a halt. This is a rugged design even though very sub-optimal.

2. Skid monitoring system : In this type of landing gear the motion of the aircraft is monitored during braking to detect any skidding, with the help of sensors. When a skid is sensed, the wheel is released to roll freely and come out of skid. This process is repeated until the aircraft is brought to a halt.

In both the above methods the braking force is kept constant. As the maximum allowable braking force varies continuously with the ground reaction and the wheel skid, these approaches are suboptimal.

In the present work, an attempt is made to produce an optimal anti-skid braking system by varying the brake force continuously to match the frictional force, so that the aircraft comes to a stop with the shortest possible run without skidding. A one-step prediction scheme is also used to overcome the inertia effect and achieve optimality.

1.4 Mathematical Model Used

1.4.1 The Vehicle Model

In this study, the heave model of the aircraft is considered. The aircraft is assumed to possess telescopic landing gear with oleo-pneumatic shock strut.

The hydraulic, pneumatic and friction forces of the shock strut have been taken into account for the study. Other forces included on the model are the wing lift forces and the drag loads.

1.4.2 The Track Surface Model

The track is modelled as a random process in the space domain. It can be expressed as a superimposition of

- a variable mean process, and
- a random zero mean process described by its statistical characteristics.

The PSD of the zero mean process has been found to conform to a "flat bell shape". Various approximations to this shape have been used to describe the PSD distribution, depending upon the primary variable chosen, namely velocity or distance.

The optimal braking scheme is tested with numerically simulated computer runs. For this, the random track unevenness has been generated using the cosine filter [19] with a uniform deviate. The track heights generated from this, as a function of distance, are added to the corresponding deterministic means which are taken as simple algebraic or transcendental functions of distance.

1.4.3 Prediction Algorithm

Prediction is required to cover the lag period of the response evaluation and the brake actuating servo system. The ground reaction is selected for prediction in the present work and is used to obtain the required brake force at the next interval. An auto-regressive algorithm [20] has been adopted for this purpose. In this algorithm the predicted value has been taken to be a weighted average of the time series' history.

Chapter 2

System Equations

The modelling and development of the system equations are presented in this chapter to study the dynamic behaviour of a vehicle. A small fighter plane is selected for the anti-skid landing run with optimal braking. The system equations are specific to the vehicle selected and the model adopted. The same sequence of steps can be followed for other vehicles and models used.

The accuracy with which the behaviour of any dynamic system is predicted depends to a large extent on the model chosen to idealize the physical system. Here, the heave model of the aircraft is selected for study and the landing gear is taken to be of telescopic type. The aircraft fuselage and wings are modelled as a lumped rigid sprung mass. The wheels and part of the landing gears are clubbed as lumped unsprung mass. The two masses are assumed to vibrate in the vertical plane with only heave degrees of freedom. This effectively means that the two main landing gears and main wheels are are considered to act as a single shock strut and single wheel. The landing gear is assumed to be infinitely rigid in bending. The aerodynamic lift and drag forces are assumed to act only during initial phase in the landing run.

The dynamic system considered for the analysis is shown in Fig.2.1. Oleo-pneumatic shock strut is inflated to some finite air pressure in the fully extended condition. The strut does not begin to deflect under compression until sufficient force is developed to overcome the preload F_{S0} due to the extended air pressure and internal friction.

In the landing run the aircraft approaches the landing strip with a vertical sink velocity and a horizontal glide velocity. The landing gear is out and locked-in position. The shock strut is fully stretched as it is unloaded in air before touch-down. The landing touch-down can be one point, two point or three point depending on whether

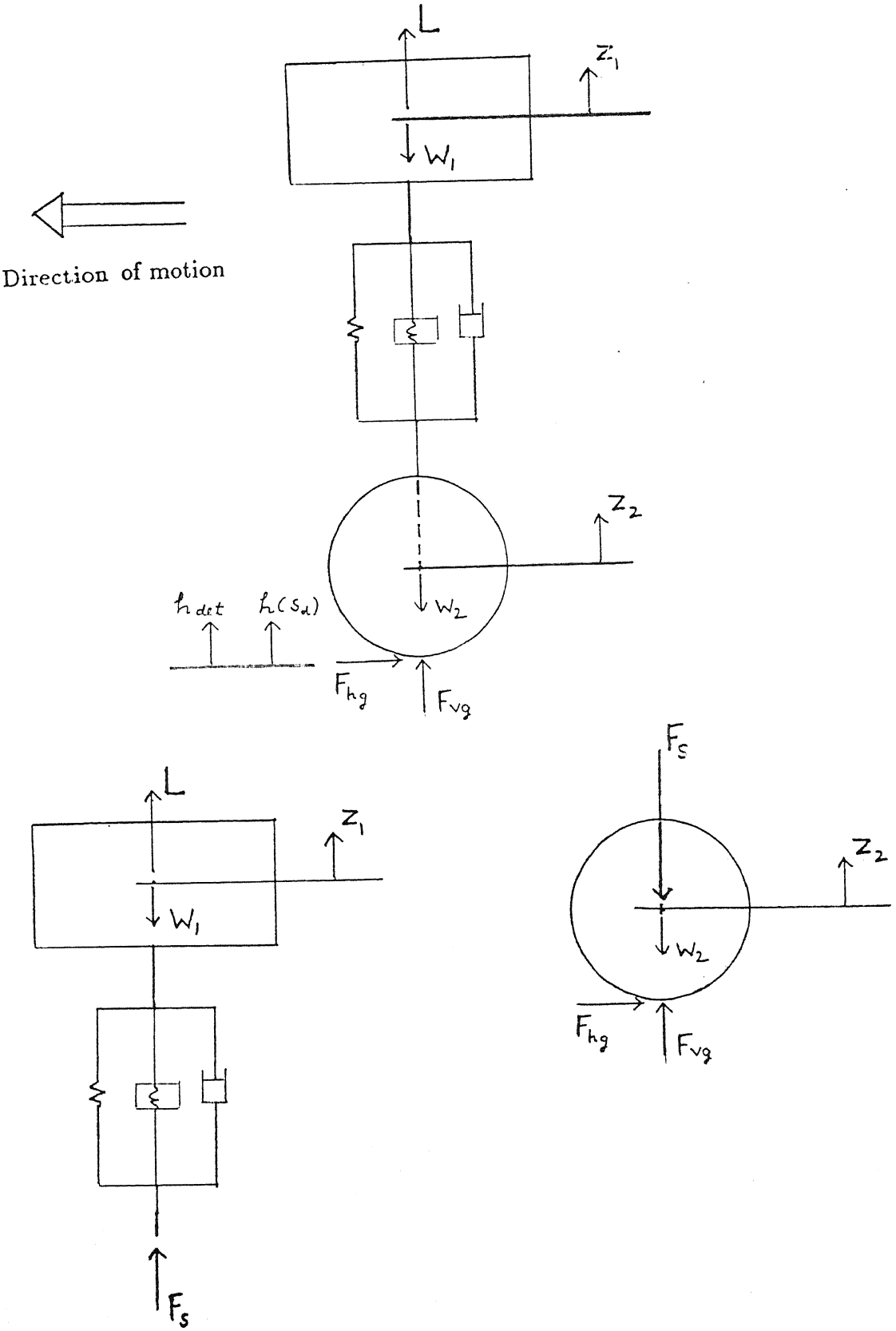

Figure 2.1: Aircraft Telescopic Heave Model

only one wheel (main wheel), or two wheels (main wheels) or all the three wheels make contact with the ground simultaneously. The study considers a normal landing with two point touch-down of the main wheels. For the heave model used, this is the only condition possible. At touch-down, since the strut is comparatively rigid in bending and compression, initially the shock strut is locked and the tyre alone compress with the system behaving as a single degree of freedom system. With passage of time, once the preload is exceeded, the shock strut becomes operational and the degree of freedoms of the system increases.

2.1 Forces on The Model

The external forces acting on the aircraft are Lift, Drag, Gravity, Reaction, and Braking force. The effect of gravity is incorporated via the mass of the vehicle. The expression for the other forces are as follows.

2.1.1 Lift Force on The Aircraft

Lift on the aircraft acts only during the initial phase of the landing, and after that it is assumed to be lost. Lift on the aircraft is defined as

$$L = \frac{1}{2}\rho V^2 S C_L \tag{2.1}$$

where ρ is the density of the air, V is the forward velocity of the aircraft, S is the wing area and C_L is the coefficient of lift given by

$$C_L = \begin{cases} C_{L0} + \alpha C_{L\alpha} & \text{if } \alpha \leq \alpha_{stall} \\ 0 & \alpha > \alpha_{stall} \end{cases} \tag{2.2}$$

where α is the angle of attack, α_{stall} is the stalling angle, C_{L0} is the zero lift coefficient and $C_{L\alpha}$ is the lift curve slope. For most cases in the range of operation, the lift varies linearly with the angle of attack, and so the lift curve slope is a constant for the operational range.

2.1.2 Drag Force on The Aircraft

The Drag on the aircraft is given by

$$D = \frac{1}{2}\rho V^2 S C_D \tag{2.3}$$

where C_D is the drag coefficient, usually described by the "drag polar"

$$C_D = C_{Do} + KC_L^2 \tag{2.4}$$

C_{Do} is the zero drag coefficient and K is the aspect ratio of the wings of the aircraft.

2.1.3 Forces On The Tyre

The tyre experiences forces from the ground in the vertical and the horizontal directions. The vertical force F_{vg} in the inflated tyre is developed due to polytropic compression of the enclosed air and is taken to be of exponential type.

$$F_{vg} = mZ^r \tag{2.5}$$

where

m, r = constants corresponding to various regimes of tyre-deflection process

Z = radial deflection of the tyre

The horizontal force F_{hg}, between the tyre and the ground, is given by

$$F_{hg} = \mu F_{vg} \tag{2.6}$$

where μ is the coefficient of slip-friction between the tyre and the ground.

2.1.4 Braking Forces Applied on The Aircraft

The braking force on the aircraft is limited by the dynamics of the vehicle as shown in § 1.1. The maximum applicable braking force is given as

$$B = \mu_{max} F_{vg} \tag{2.7}$$

where μ is given as a function of slip s in equation 1.1.

Coefficient of friction also depends on the vehicle speed, tyre inflation pressure, tread depth and ground surface conditions [1].

2.2 Forces In The Shock Strut

The telescopic shock strut, considered here, is of oleo-pneumatic type. The total force in the shock strut is due to hydraulic resistance, air compression and internal friction

[21]. As the shock strut telescopes, the hydraulic fluid is forced through the orifice to the lower chamber providing the non-linear damping. When the fluid enters the lower chamber, it pushes the separator down and compresses the air in the process. The polytropic compression of air provides the non-linear spring behaviour.

Loss of energy in the shock absorber due to heating, secondary vibrations such as vibrations of the shock absorber wall, emission of sound etc., are assumed not to effect the behaviour of the shock absorber.

2.2.1 Pneumatic Force

The pneumatic force in the shock strut is determined by the initial air pressure, initial air and oil volumes, pneumatic area, oil bulk modulus and the air compression process. The pneumatic force in the shock strut is given by [21]

$$F_a = P_{a_0} A_a \left(\frac{V_{a_0}}{V_{a_0} - A_a s_m + V_{o_0} \left(\frac{P_a - P_{a_0}}{\beta} \right)} \right)^n \tag{2.8}$$

where

A_a	=	pneumatic area
n	=	polytropic exponent of the air compression process
P_a	=	instantaneous air pressure
P_{a_0}	=	initial air pressure
s_m	=	shock strut stroke
V_{a_0}	=	initial air volume
V_{o_0}	=	initial oil volume
β	=	bulk modulus of oil

2.2.2 Hydraulic Force

The hydraulic resistance F_h due to the telescoping of the strut is given by [22]

$$F_h = \frac{\dot{s}_m}{\|\dot{s}_m\|} \frac{\rho_f A_h^2}{2(C_d A_n)^2} \dot{s}_m^2 \tag{2.9}$$

where

A_h = hydraulic area

A_n = net orifice area

C_d = coefficient of discharge

$\dot{s}_m$ = strut telescoping velocity

ρ_f = mass density of fluid

2.2.3 Friction Force

The journal friction force F_{fj} can be written as [23]

$$F_{fj} = \frac{\dot{s}_m}{\|\dot{s}_m\|}(\mu_{j1}\|F_1\| + \mu_{j2}\|F_2\|) \tag{2.10}$$

where

F_1 = normal force on the upper bearing

F_2 = normal force on the lower bearing

μ_{j1} = coefficient of friction of upper bearing (attached to the inner cylinder) on the shock strut

μ_{j2} = coefficient of friction of lower bearing (attached to the outer cylinder) on the shock strut

From the balance of moments, F_1 and F_2 can be obtained.

$$F_1 = \left(\frac{l_2 - s_m}{l_1 + s_m}\right) F_n \; and \; F_2 = \left(\frac{l_1 + l_2}{l_1 + s_m}\right) F_n$$

where

l_1 = axial distance between lower and upper bearings on fully extended shock strut

l_2 = axial distance between lower bearings and point of attachement of shock strut

F_n = normal force on the shock strut

The seal friction force F_{fm} is given by [21]

$$F_{fm} = \frac{\dot{s}_m}{\|\dot{s}_m\|}\mu_s F_a \tag{2.11}$$

where

F_a = pneumatic force in the shock strut

μ_s = coefficient of seal friction

The total axial force in the shock strut is the sum of all the forces [21].

$$F_s = F_a + F_h + F_{fj} + F_{fm} \tag{2.12}$$

2.3 Dynamics of The Aircraft

The aircraft is modelled as a two degree of freedom lumped mass system with vertical displacements due to the rigid body translation of the sprung and unsprung masses. All motions are assumed to be restricted to the vertical plane through the center of gravity of the aircraft.

Depending upon the force acting on it, the shock strut can be either locked or unlocked. Equations of motion for both the cases are developed in the following subsections.

2.3.1 Equations Of Motion With Locked Shock Strut

When the force in the shock strut is less than the preload, the shock strut is locked and only the tyre is compressed. The displacement of the two lumped masses is same in this case and the system has only one degree of freedom.

If Z_1 and Z_2 are the vertical displacements of the sprung and unsprung masses respectively, then according to the locked condition :

$$Z_1 = Z_2 \tag{2.13}$$

The equation of motion of the system for vertical motion is

$$\frac{W}{g}(\ddot{Z}_1 + \ddot{h}_{det}) - L + W - F_{vg}(Z) = 0 \tag{2.14}$$

where

h_{det}	=	mean ground variation (as a function of time)
F_{vg}	=	vertical ground reaction (function of Z)
W	=	$W_1 + W_2$ (total weight of the aircraft)
W_1	=	weight of the sprung mass
W_2	=	weight of the unsprung mass
Z	=	$-Z_2 + h(s_d)$
$h(s_d)$	=	randomness in track profile, function of ground distance travelled by the aircraft in time t

On solving the equation 2.14 the response of the two lumped masses is obtained.

To obtain the force F_s in the shock strut, writing the the vertical equilibrium equation of motion of the wheel (unsprung mass) :

$$F_s = -\frac{W_2}{g}\ddot{Z}_2 - W_2 + F_{vg} \tag{2.15}$$

The system is converted to two degrees of freedom system, when the force F_s in the shock strut exceeds the preload.

2.3.2 Equations Of Motion For Unlocked Case

The system has two degrees of freedom when shock strut starts operating. The shock strut stroke s_m and the strut telescoping velocity $\dot{s}_m$ are given by

$$s_m = Z_2 - Z_1 \tag{2.16}$$

and

$$\dot{s}_m = \dot{Z}_2 - \dot{Z}_1 \tag{2.17}$$

Since $F_s = F_s(s_m, \dot{s}_m)$, the force F_s in the shock strut can be determined with equations 2.8 to 2.12.

The vertical equilibrium consideration gives the equation of motion of the sprung mass as

$$\frac{W_1}{g}\ddot{Z}_1 - L + W_1 - F_s = 0 \tag{2.18}$$

and for the unsprung mass as

$$\frac{W_2}{g}\ddot{Z}_2 + W_2 - F_{vg} + F_s = 0 \tag{2.19}$$

Equations 2.18 and 2.19 are solved simultaneously to obtain the response.

Chapter 3

Track Profile Generation

As the aircraft runs on the track, the wheels get a vertical input from the undulations in the track. The system equations, thus get an excitation dependent on the track unevenness and the vehicle forward velocity. A knowledge of the track profile is required for integration of the system differential equations.

As mentioned earlier, the ground surface is modelled as a zero mean random process superimposed over a deterministic mean profile.

3.1 The Mean Track Profile

In general the prepared tracks are planned to have a flat mean level. Achieving the perfectly flat mean track, however, may be difficult and uneconomical. Hence, some tracks have variable mean level from the beginning. During working life of the track its use, wear and tear and loading of the track results in further deformations, inducing inclined, wavy, stepped and other types of deformations in the mean level. Bombing by enemy, during war, can also cause changes in the mean profile.

The profile can be described by infinitely many combinations of simple algebraic or transcendental functions to satisfy some physical properties of a given runway, such as

- differential settlement of concrete slabs
- inclined runways
- parabolic or curved runway surfaces

- bomb craters covered with repair mats
- unevenness in the landing decks of aircraft carriers.

Following three types of mean runway profiles have been considered here,

- a stepped runway, such as a crater covered with a repair mat
- an inclined runway, and
- a sinusoidal runway.

The deterministic variable mean process can be generated by using the appropriate shapes and their combinations for the different cases.

3.2 The Random Zero Mean Process

The zero mean track unevenness has been characterised as homogeneous random process in space coordinates [14]. It is common to describe the road unevenness by the auto-correlation function or the PSD function. Out of various forms available in literature, the following correlation function is selected for the present study [24] :

$$R(s_d) = \sigma^2 e^{-\alpha_1 {\delta_1}^2} \tag{3.1}$$

where

s_d = ground distance travelled by the aircraft in time t

α_1 = correlation constant

δ_1 = space lag

σ = standard deviation

with the following PSD function

$$\Phi(\Omega) = \frac{\sigma^2}{2\alpha_1\sqrt{\pi}} e^{-\frac{\Omega^2}{4{\alpha_1}^2}} \tag{3.2}$$

where Ω = spatial frequency.

The random process for the road, with zero mean and above PSD is simulated in terms of the sum of cosine functions with random frequencies and random phase angles [19], as below

$$h(s_d) = \sigma \left(\frac{2}{N}\right)^{\frac{1}{2}} \sum_{k=1}^{N} \cos(\Omega_k t + \psi_k) \tag{3.3}$$

where

$$\sigma = \left(\int_{-\infty}^{\infty} \Phi_0(\Omega) d\Omega\right)^{\frac{1}{2}} \tag{3.4}$$

is the standard deviation of the process $h(s_d)$, $\Omega_k (k = 1, 2, ..., N)$ are independent random variables identically distributed with the density function $g(\Omega) = g(\Omega_k)$ obtained by normalising $\Phi_0(\Omega)$,

$$g(\omega) = \frac{\Phi_0(\omega)}{\sigma^2} \tag{3.5}$$

and ψ_k are independent random variables identically distributed with the uniform density $1/(2\pi)$ between 0 and 2π. Ω_k and $\psi_l (k, l = 1, 2, .., N)$ are independent.

The generated random process can be easily seen to be of zero mean and the required PSD [19].

The track induced input to the system equations comes as a time parametered process. However, the actual track profile is in the space domain, which gets modified by the vehicle forward velocity to act as the system input. Therefore, in this study, the runway has been generated in the space domain and then converted to the time domain via the space-time relationship. Hence, for generating the random process the spatial PSD and the spatial frequency have been used. Also, since a discrete process is generated, the sampling theorem dictates a cut-off frequency, within which region only the PSD need be integrated. Thus equation 3.2 becomes

$$\phi(\Omega) = \begin{cases} \frac{\sigma^2}{2\alpha\sqrt{\pi}} e^{-\frac{\Omega^2}{4\alpha^2}} & \text{if } \|\Omega\| \leq \Omega_0 \\ 0 & \text{otherwise} \end{cases} \tag{3.6}$$

Ω_0 is the cut-off frequency, given by :

$$\Omega_0 = \frac{1}{2\Delta} \tag{3.7}$$

where Δ is the sampling interval.

3.3 Space-Time Relationship

In this study, the track profile is generated in space domain whereas the equations of motion are solved in time domain. To get the track height at any instant of time, a space-time relation is required. From the Newton's second law of equation of motion

$$\ddot{s}_d = -\frac{D+B}{W} \tag{3.8}$$

Integrating the above equation twice

$$\dot{s}_d = -\int_{t_0}^{t} \frac{D+B}{W} dt + \dot{s}_d(t_0) \tag{3.9}$$

and

$$s_d = -\int_{t_0}^{t} \dot{s}_d(t) dt + s_d(t_0) \tag{3.10}$$

Since, braking force B is continuously changing with time in a random fashion, the integration will have to be carried out numerically in real time.

3.4 Slip-Time Relationship

Variation of slip with wheel's angular velocity was defined in equation 1.1. The angular velocity depends on the variation of braking torque and the moment generated due to the shift in the centre of pressure of the radial load. The angular acceleration of the wheel is given as [1]

$$\dot{\omega} = \frac{1}{I_w}\left\{\left(\mu(\frac{D_m}{2} - Z) - X_c\right) F_{vg} - T_b\right\} \tag{3.11}$$

where X_c is the forward shift in the centre of pressure, T_b is the applied braking torque and I_w is the moment of inertia of the whole aircraft about the wheel axle.

The angular velocity of the wheel can be obtained by integrating the above equation.

$$\omega = \int_{t_0}^{t} \dot{\omega}(t) dt + \omega(t_0) \tag{3.12}$$

Chapter 4

Prediction of Braking Force

To predict the braking force, the ground reaction is predicted first, one step ahead in time. Braking force then can be obtained from the ground reaction using the coefficient of friction between the tyre and the ground.

4.1 Prediction Algorithm

The linear-predictor algorithm [20] is used here, for prediction. The predictor is a auto-regressive filter defined as [20]

$$x_n^* = \sum_{k=1}^{p} a_k x_{n-k} \tag{4.1}$$

The error in prediction is given as

$$e_n = x_n - x_n^* \tag{4.2}$$

Here, x_n^* is the predicted value at instant n, x_{n-k} is the value at instant $n-k$ and a_k are weighing coefficients which have to adjusted in order to give a good prediction.The square of the error is minimised to obtain the coefficients.

4.2 Optimisation of The Prediction Coefficients

The total squared prediction error is

$$M = \sum_n e_n^2 = \sum_n \left(x_n - \sum_{k=1}^{p} a_k x_{n-k} \right)^2 \tag{4.3}$$

To minimise M by choice of coefficients a_j, differentiating the above equation with respect to the coefficients a_j,

$$\frac{dM}{da_j} = -2\sum_n x_{n-j}\left(x_n - \sum_{k=1}^{p} a_k x_{n-k}\right) = 0 \tag{4.4}$$

so,

$$\sum_{k=1}^{p} a_k \sum_n x_{n-j}x_{n-k} = \sum_n x_n x_{n-j},\ j = 1, 2, ..., p \tag{4.5}$$

It can be seen that for a doubly infinite sum,

$$\sum_{n=-\infty}^{\infty} x_{n-j}x_{n-k} = \sum_{n=-\infty}^{\infty} x_{n-j+1}x_{n-k+1} = ... = \sum_{n=-\infty}^{\infty} x_n x_{n-k+j}$$

so now equation 4.4 transforms to

$$R_0 a_1 + R_1 a_2 + R_2 a_3 + ... = R_1$$

$$R_1 a_1 + R_0 a_2 + R_1 a_3 + ... = R_2$$

$$R_2 a_1 + R_1 a_2 + R_0 a_3 + ... = R_3$$

and so on.
where

$$R_m = \sum_n x_n x_{n+m},\ m = 0, 1, 2, ..., p$$

The above system of equations are solved for a_k. In the present work, it has been solved using the Durbin and Levinson method [20] which requires much less computational effort than other methods.

Since it's impractical and undesirable to compute the infinite sums in the above equation, a windowing procedure is used. The window is described as a set of weights spread over time as follows

$$x_n^{'} = w_n x_n$$

Here, w_n is zero outside a finite range of interest. R_m can be redefined as

$$R_m^h = \sum_{n=h}^{h+N-1} x_n^{'} x_{n+m}^{'},\ m = 0, 1, 2, ..., p$$

Chapter 5

Results and Discussion

The results of the simulated landing run of the aircraft model are presented and discussed in this chapter.

The system differential equations developed in chapter 2 have been integrated by a variable order variable step size method implementing the Backward Differentiation Formulae (NAG Library Subroutine D02NBF). The scheme keeps the accuracy within the prescribed limits while selecting the optimal step size and order of the numerical integration.

Results have been compiled at an interval of 0.5ms for study and plotting of the system behaviour. The sprung and the unsprung mass vertical displacement, velocity and acceleration have been obtained by integration which proceeds after evaluating the external forces acting on the vehicle masses. The associated values of the ground reaction and the retarding ground frictional force on the tyre have been calculated. The frictional force between the wheel and the ground is obtained by using the optimal value of the friction coefficient assuming the best slip range to be operative. The available information is used to predict the ground reaction at an interval of 0.01 seconds in future, which is expected to cover the worst time lag for the brake actuator mechanism. The matching brake force is assumed to become active after this lag period. The resulting vehicle forward velocity is calculated. All of this is repeated at the next step to progress the solution in time. The scheme is continued until the aircraft comes to a halt.

The braking comes into operation only after the free roll. It is assumed that due to optimal braking, slip always remains in the optimal range. If out of range, it can be brought back in range by using appropriate feed back control scheme. However,

in the present study, this has not been attempted.

5.1 Model Parameters

The numerical values of different parameters, used in the modelling of the aircraft, landing gear and generating the results are presented in table 5.1 and 5.2 [1,15,18].

5.2 Track Parameters

As discussed earlier, the track is simulated as superimposition of zero mean random process over a variable mean. The following values of the parameters have been adopted for the track profile.

- Zero mean random profile :

  The zero mean random process is generated using the Shinozuka filter. The parameter values used are :

  Correlation constant for roughness, $\alpha_1 = 0.0001$

  Standard deviation of the track, $\sigma = 0.01$

  Cut off Nyquist frequency, $\Omega_o = 20 rad/m$

  Number of simulated terms for the Shinozuka filter, $N = 200$

- Mean profile :

Following four different mean track profiles have been considered :

1. Zero mean runway :

   This is equivalent to a flat mean surface and is taken to have a value of zero everywhere.

2. Inclined mean runway :

   This runway is assumed to have an inclination of 5 in 1000, corresponding to an angle of inclination of $0.29°$.

3. Stepped runway :

   The mean runway is assumed to have an inclined step of height 0.02m in a length of 0.02m situated at a distance of 100m from the point of touch down.

Table 5.1: Model parameters

Symbol	Description	Value	Units
C_{Do_r}	Zero lift drag coefficient during ground roll	0.1144	
C_{Do_t}	Zero lift drag Coefficient at touch down	0.0614	
C_L	Lift coefficient	0.696-0.484	
AR	Aspect ratio	5.0	
M_1	Mass of the sprung mass	9188.0	Kg
M_2	Mass of the unsprung mass	342.0	Kg
S	Wing area	38.4	m^2
V	Aircraft landing glide velocity	75.56-90.67	m/s
V_{sink}	Aircraft sink velocity	1.0-3.0	m/s
α_s	Stalling angle	20.0	degree
	Period of free roll	0.038	

Table 5.2: Shock strut parameters

Symbol	Description	Value	Units
A_a	pneumatic area	99.0	cm^2
A_h	hydraulic area	127.2	cm^2
A_n	net orifice area	4.81	cm^2
C_d	coefficient of discharge	0.6	
l_1	axial distance between lower and upper bearings on fully extended shock strut	0.2	m
l_2	axial distance between lower bearings and point of attachement of shock strut	0.594	m
n	polytropic exponent of the air compression process	1.3	
P_{a_0}	initial air pressure	3.622	MPa
V_{a_0}	initial air volume	1462.0	cm^3
V_{o_0}	initial oil volume	1950.0	cm^3
β	bulk modulus of oil	1.172	GPa
μ_{j1}	coefficient of friction of upper bearing (attached to the inner cylinder) on the shock strut	0.075	
μ_{j2}	coefficient of friction of lower bearing (attached to the outer cylinder) on the shock strut	0.075	
μ_s	coefficient of seal friction	0.0	
ρ_f	mass density of fluid	850.0	Kg/m^3

4. Sinusoidal mean runway :

   The sinusoidal mean profile is generated as a sine wave with an amplitude of 0.01m and a wavelength of 10m.

5.3 Aircraft Response in the Landing Run

The effect of variations in three different parameters, namely aircraft sink and glide velocities and runway mean profile on the system response has been studied. The graphs of the system response, namely sprung and unsprung masses vertical displacement, velocity, acceleration, ground reaction (actual and predicted), aircraft glide velocity and ground distance covered are plotted as a function of time.

The case for glide velocity=75.56 m/s, sink velocity=1.0 m/s and flat runway profile is considered first. During the initial phase of landing, the sprung and unsprung mass displacements show strong oscillatory motions (Fig. 5.1 and 5.2). This is due to the landing impact. The peaks attained in this period can be more clearly seen in the inset of the corresponding figures. Although the amplitude of the vibration decreases after the effect of impact, the masses continue to oscillate about the mean value and the response subsides to steady state pattern of random motion. The randomness in the response is due to the ground undulations which is random in nature.

When the forward motion of the aircraft comes to a halt, it continues to oscillate in the vertical plane for some time before it attains the equilibrium state.

The slightly larger amplitude during the last phase of landing can be due to the matching of frequencies of oscillation of the system with the distributed frequencies of ground PSD, resulting in a resonance like effect.

The unsprung mass displacement is found to be larger than the sprung mass displacement.

Like displacement response, the velocity response of the two masses also have a large variation in amplitude during the impact (Fig. 5.3 and 5.4). The variation in velocity response of the unsprung mass is more than that of the sprung mass. The general behaviour of the velocity response is similar to the displacement response.

The effect of landing impact on sprung mass acceleration, as strong oscillations, can be seen in Fig. 5.5. However, it is not clear in the unsprung mass acceleration response as the strong oscillations persist well beyond the impact stage (Fig. 5.6).

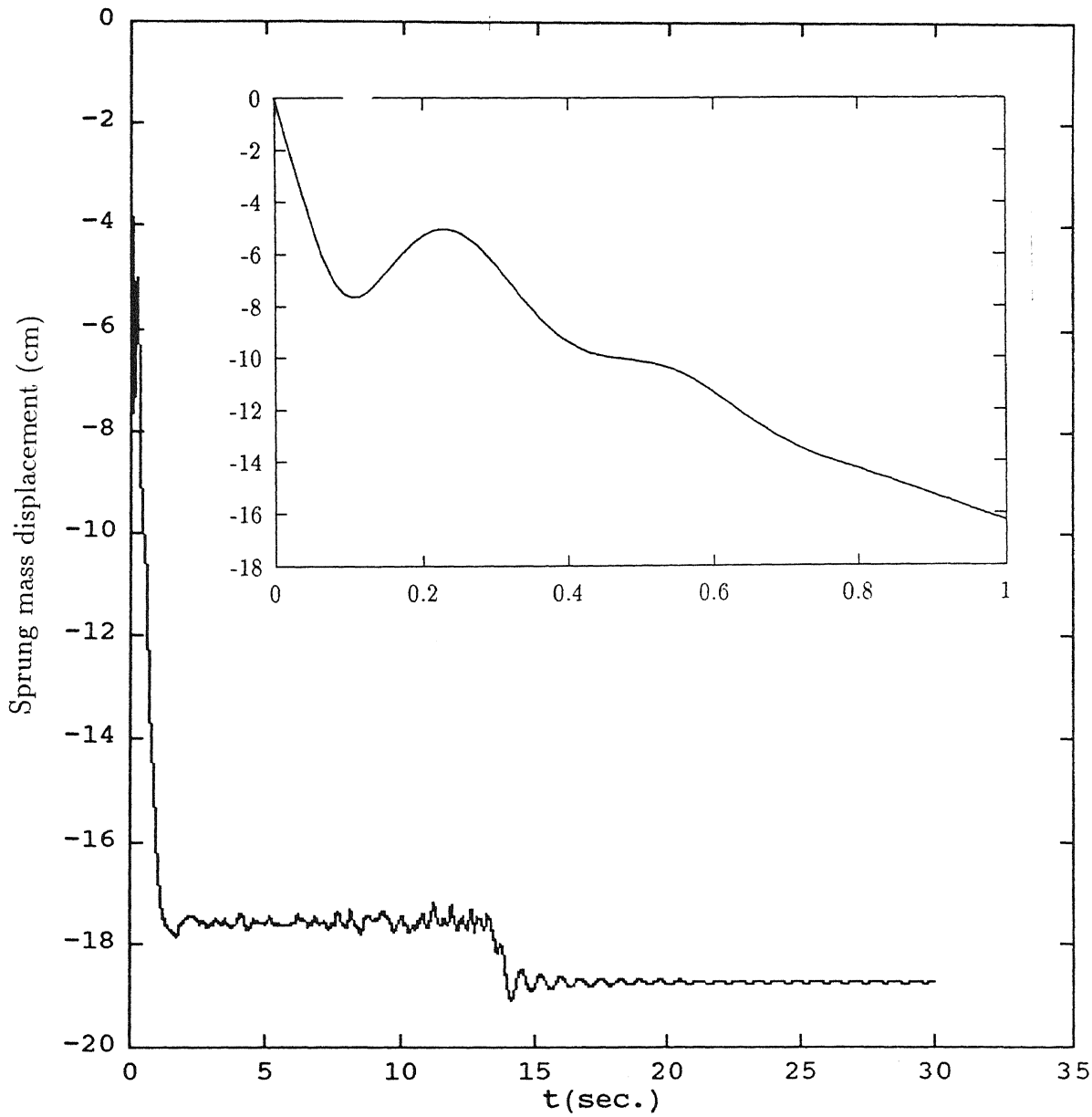

Figure 5.1: Sprung mass displacement for zero mean runway, Glide velocity=75.56 m/s, Sink velocity=1.0 m/s

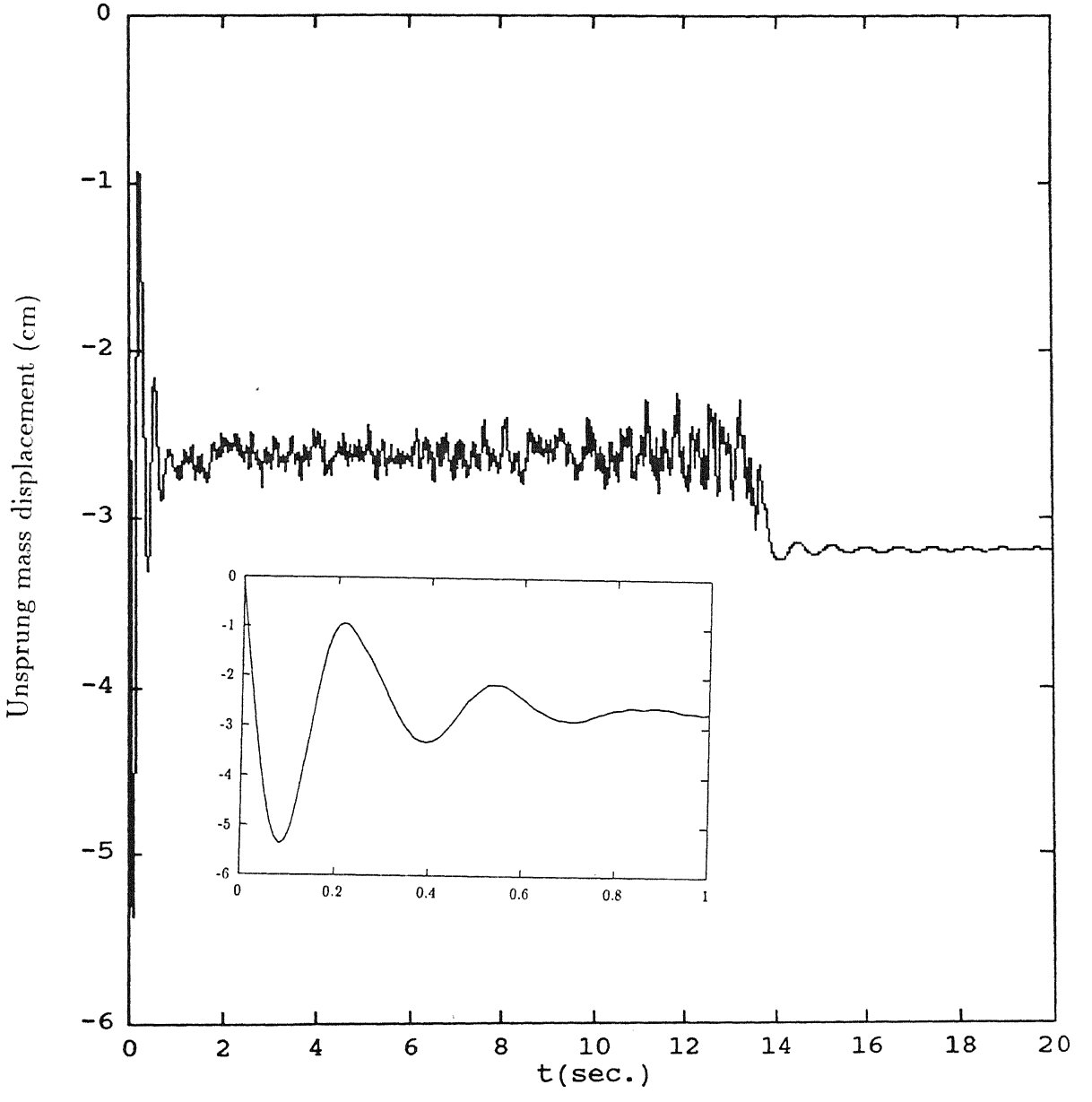

Figure 5.2: Unsprung mass displacement for zero mean runway, Glide velocity=75.56 m/s, Sink velocity=1.0 m/s

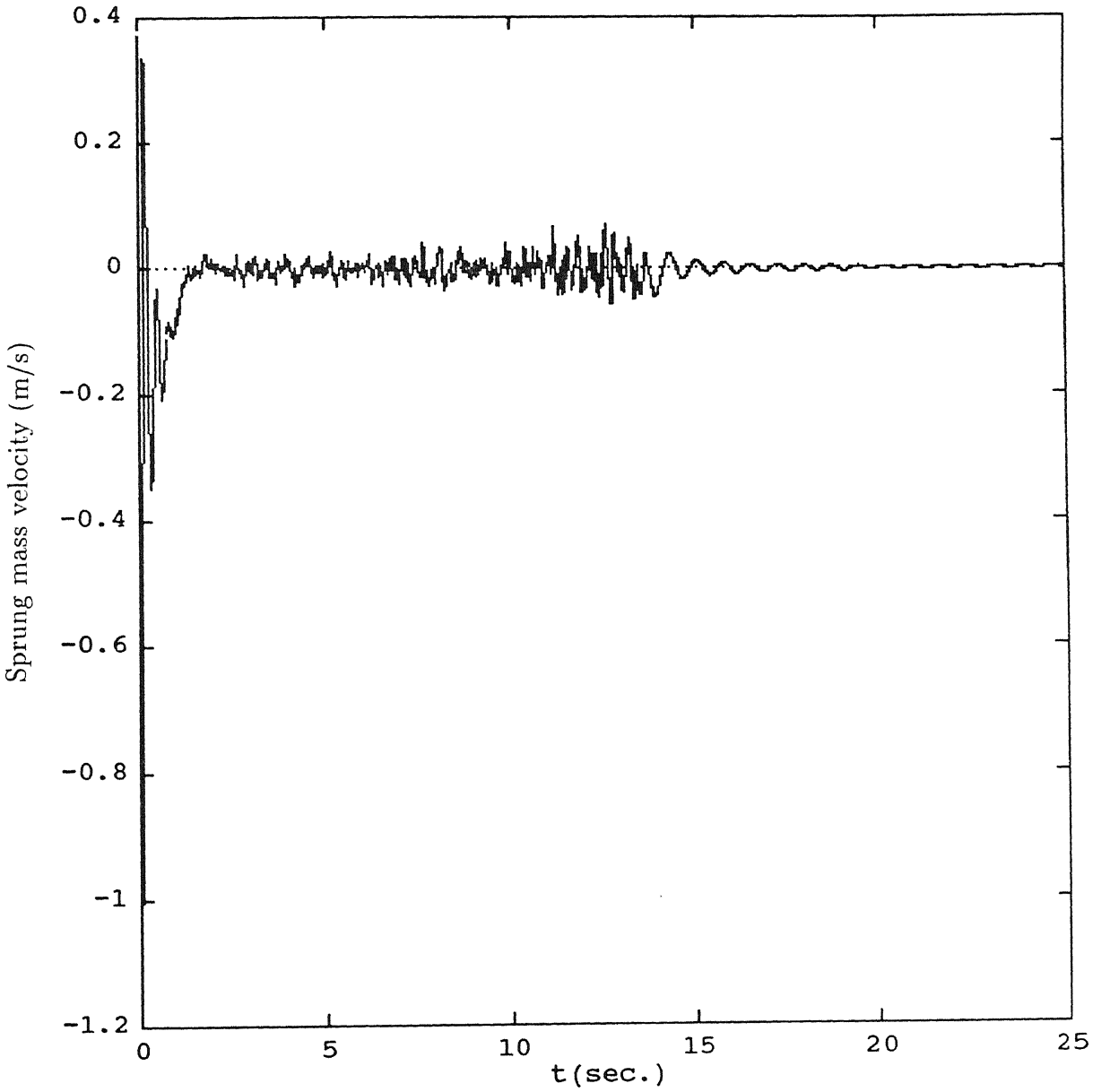

Figure 5.3: Sprung mass velocity for zero mean runway, Glide velocity=75.56 m/s, Sink velocity=1.0 m/s

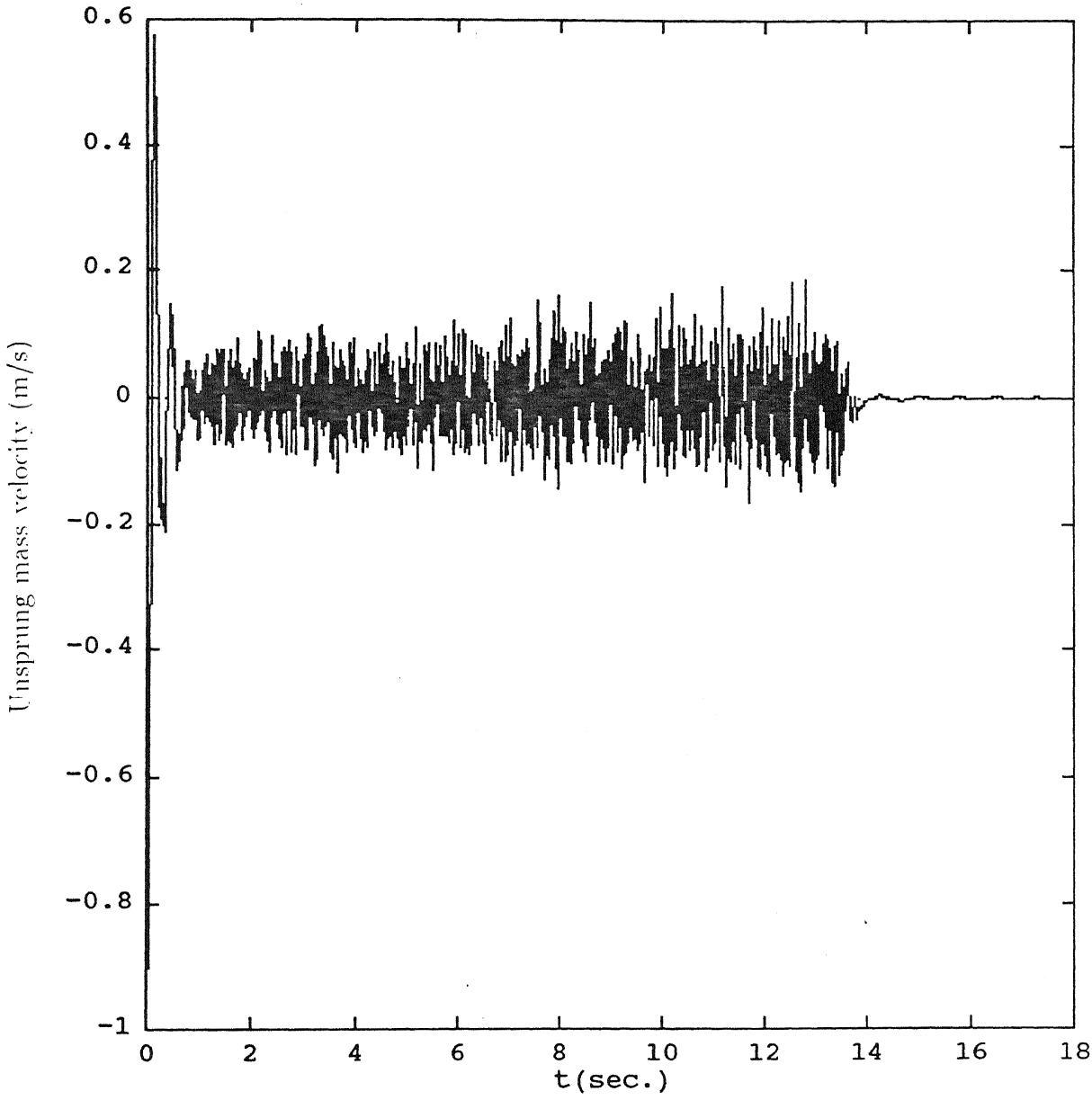

Figure 5.4: Unsprung mass velocity for zero mean runway, Glide velocity=75.56 m/s, Sink velocity=1.0 m/s

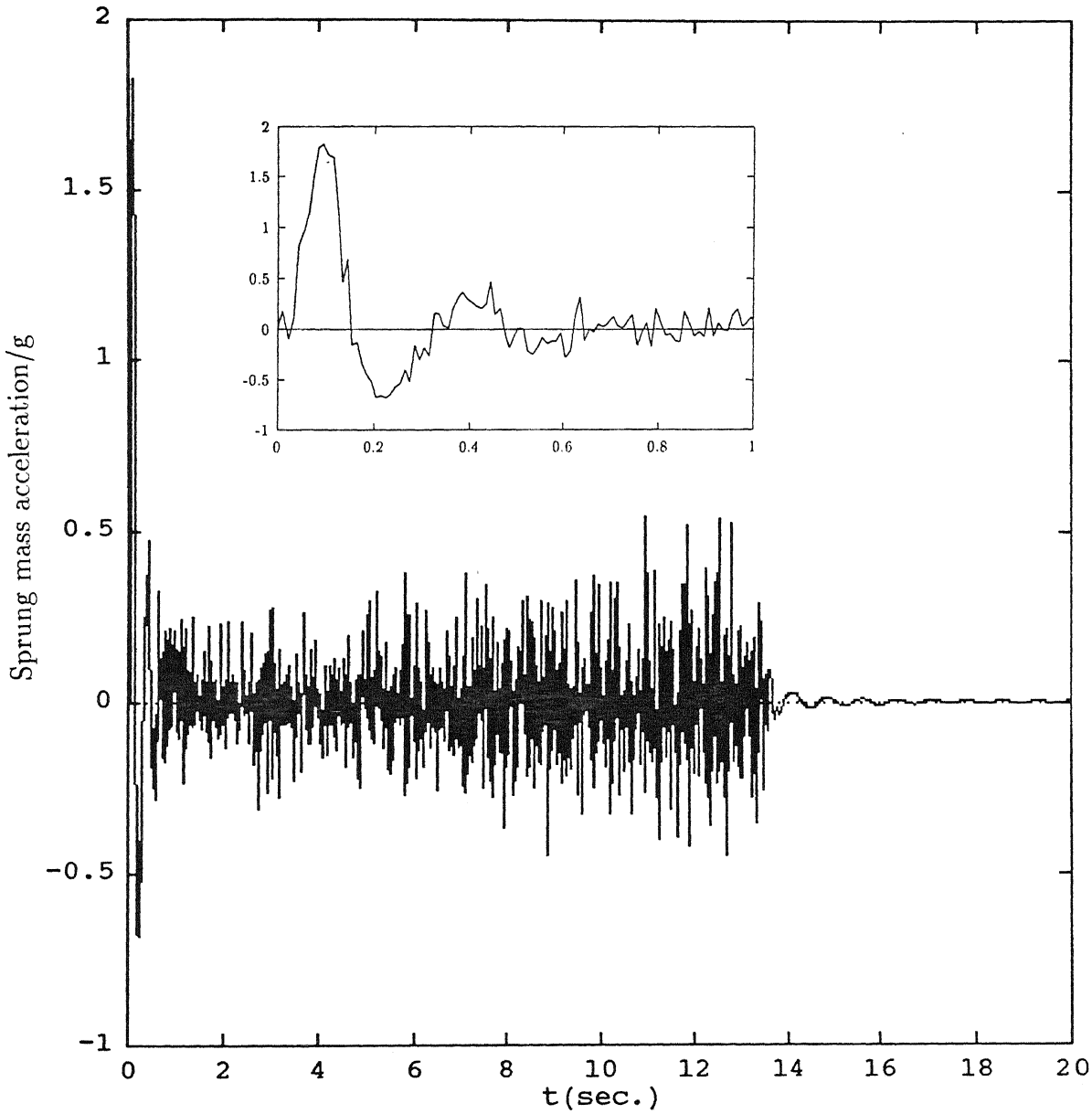

Figure 5.5: Sprung mass acceleration for zero mean runway, Glide velocity=75.56 m/s, Sink velocity=1.0 m/s

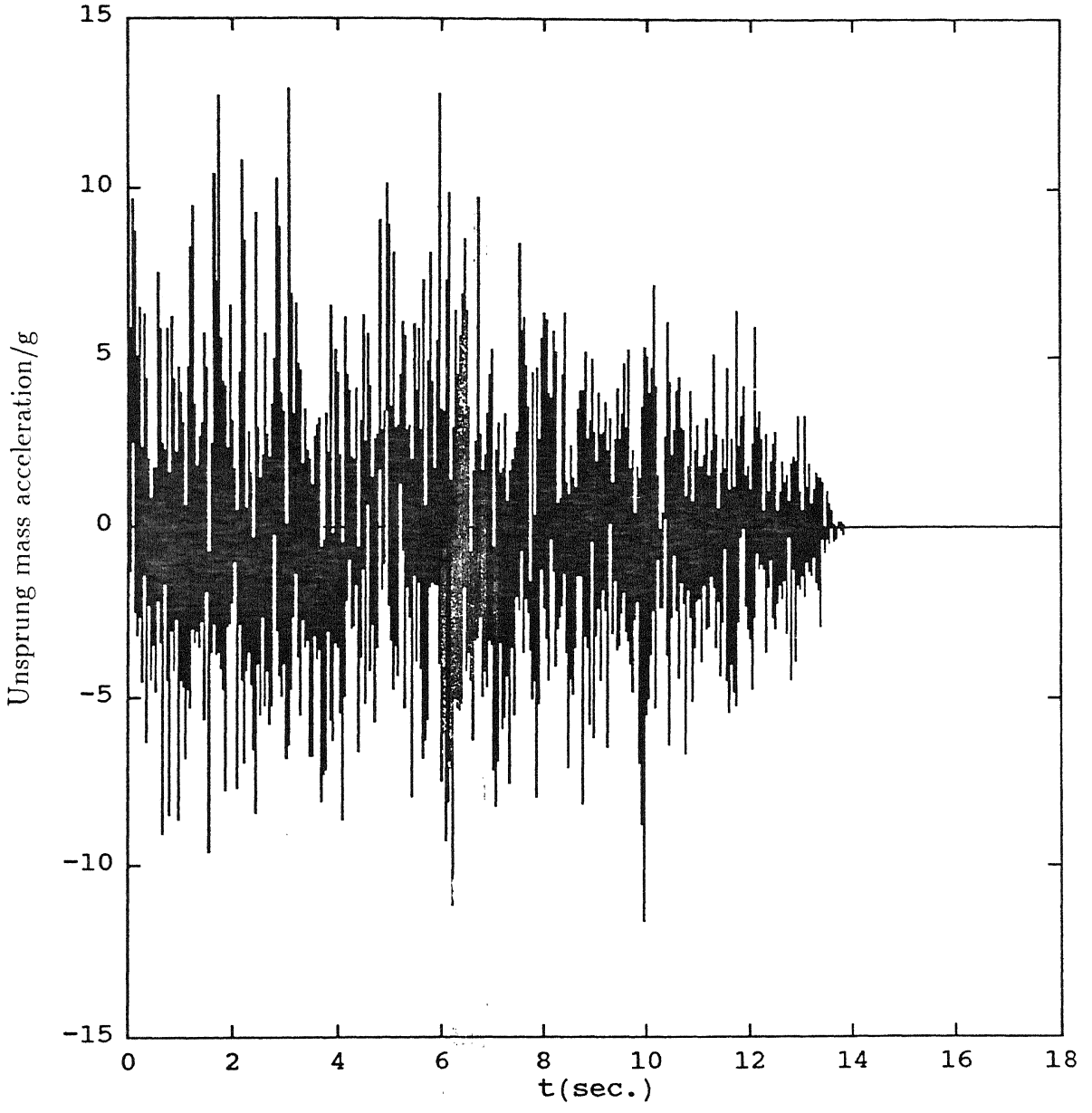

Figure 5.6: Unsprung mass acceleration for zero mean runway, Glide velocity=75.56 m/s, Sink velocity=1.0 m/s (Inset on next page)

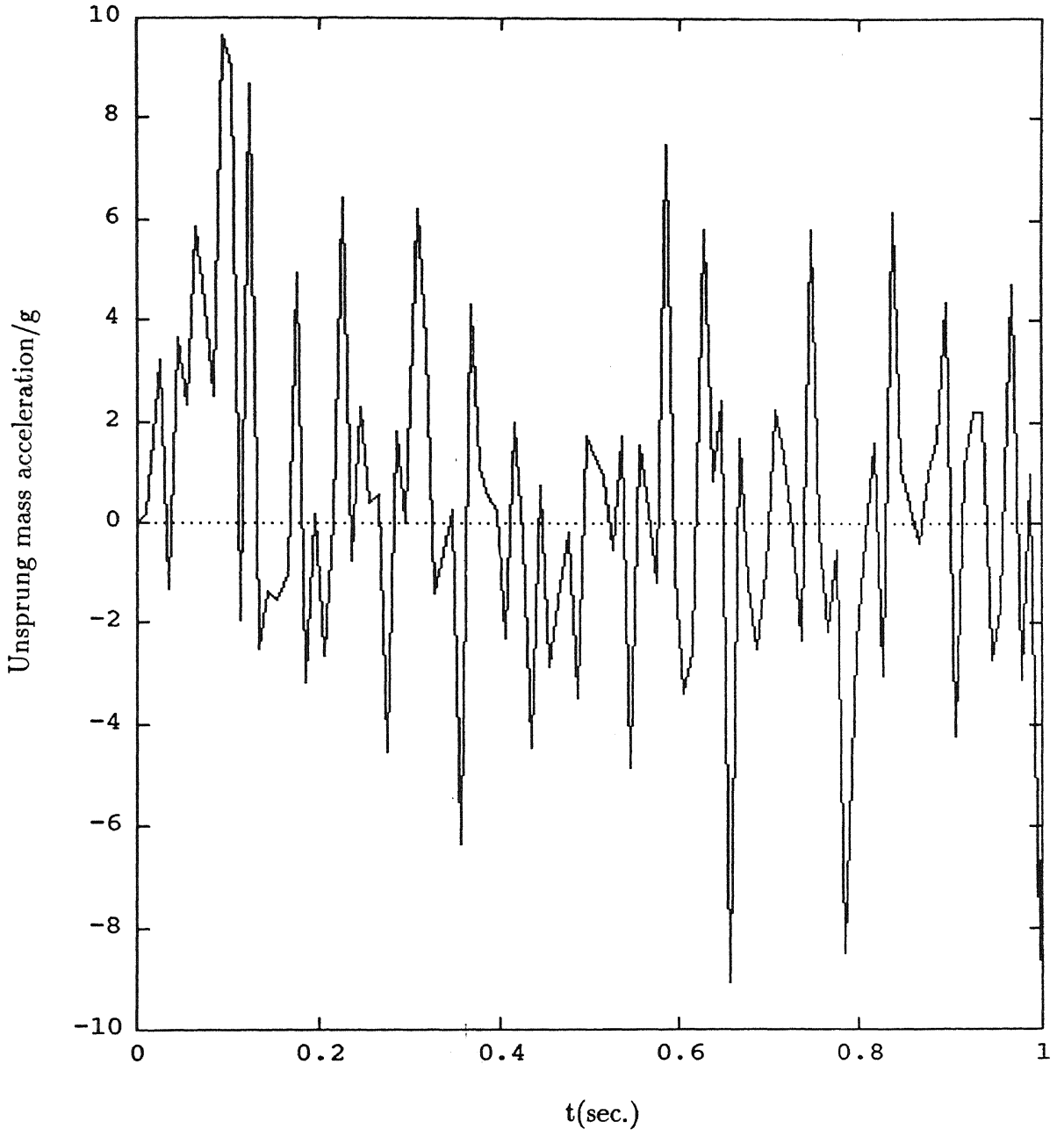

Inset figure of Fig. 5.6

The large variations in acceleration response of unsprung mass represent the larger loads acting on it which pass to the main mass after being filtered through the landing gear. The effect of ground undulations can be clearly seen in acceleration response which has got much more variation than displacement and velocity responses. Like the displacement and velocity response, the amplitude of sprung mass acceleration response increases as the forward velocity of the aircraft decreases. The unsprung mass amplitude, however, shows a marginal decrease with decrease in the aircraft forward velocity.

The ground reaction variation is shown in Fig. 5.7. The initial value of ground reaction is very high, due to the large impact load. Following the displacement of the unsprung mass, the ground reaction shows larger oscillations at impact with subsequent steady state random pattern.

The reaction in future can be predicted only after some time because some data is always required to initiate the prediction scheme. The actual and the predicted values do not match initially, but as the integration proceeds, the prediction turns out to be a very close one except sometimes at the peaks.

The drop in the forward velocity of the aircraft with time is nonlinear (Fig. 5.8). The rate of change of velocity decreases with time, since the braking force reduces the ground reaction.

The ground distance travelled is obtained by integrating the forward velocity and is plotted as a function of time (Fig. 5.9).

5.3.1 Variation in Sink Velocity

The sink velocity is varied from 1.0 m/s to 2.0 and 3.0 m/s keeping glide velocity and runway mean profile same as in the previous case.

The general behaviour of the system response is similar for the three sink velocities studied.

With increase in sink velocity, the peaks in the displacement curves of the sprung and the unsprung masses attain higher values, showing a stronger motion (Fig. 5.10 to 5.13). Aircraft ballooning has taken place after the impact for the two higher sink velocities, the effect being stronger with increase in the sink velocity. This has happened due to higher impact load. Except during the impact, the pattern of the displacement curves of the two masses are almost the same as in the previous case.

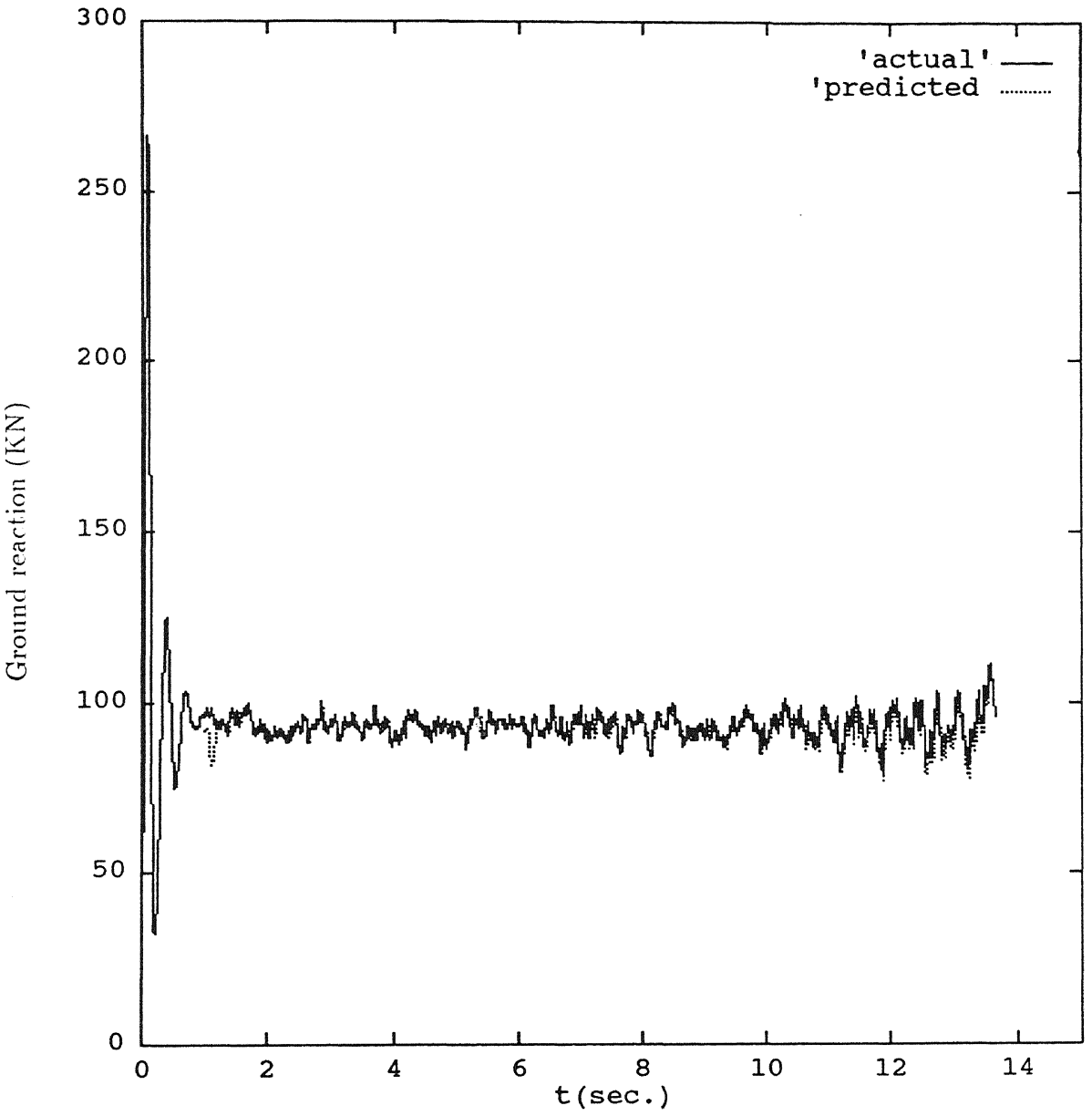

Figure 5.7: Ground Reaction for zero mean runway, Glide velocity=75.56 m/s, Sink velocity=1.0 m/s

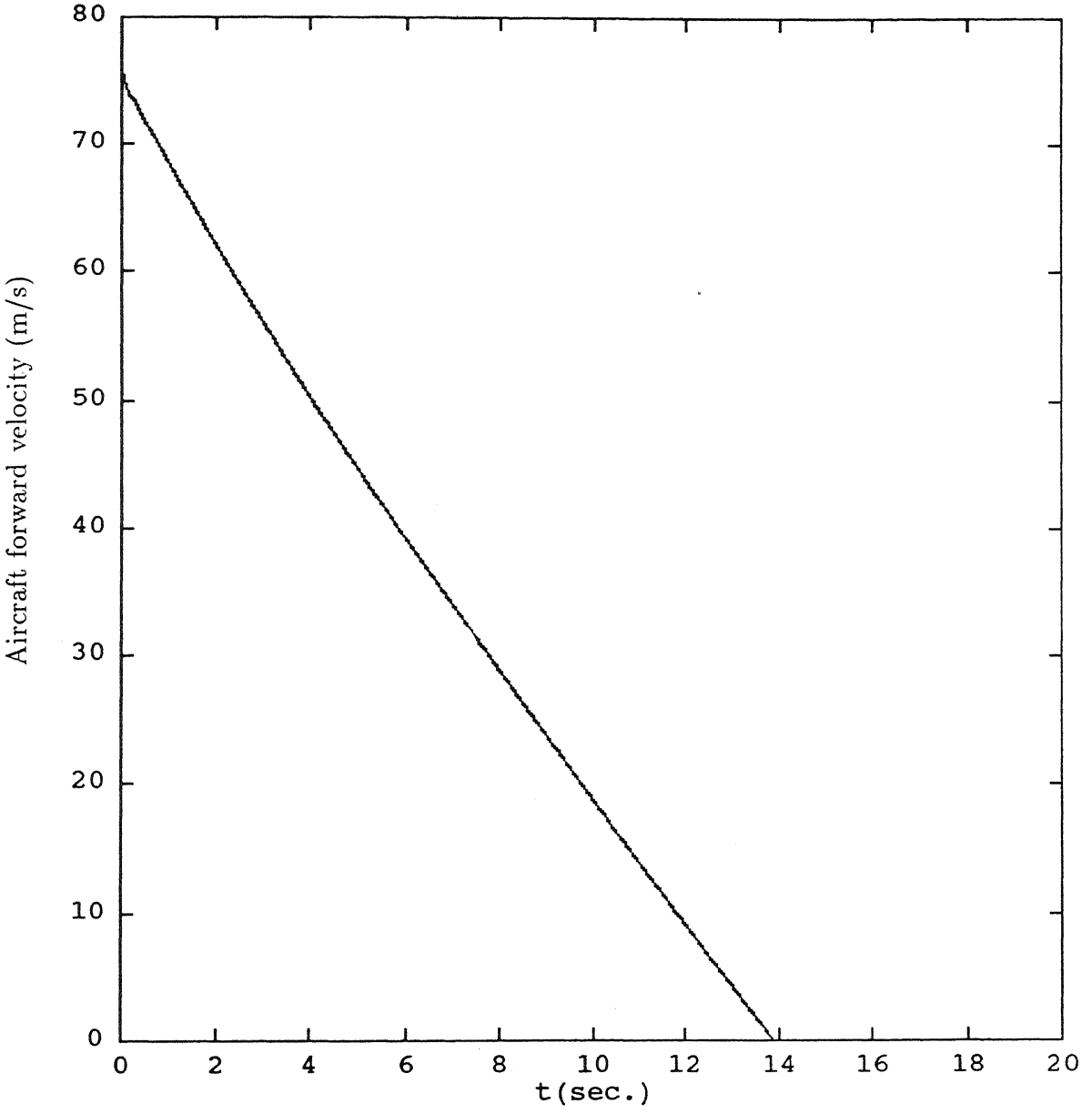

Figure 5.8: Aircraft forward velocity for zero mean runway, Glide velocity=75.56 m/s, Sink velocity=1.0 m/s

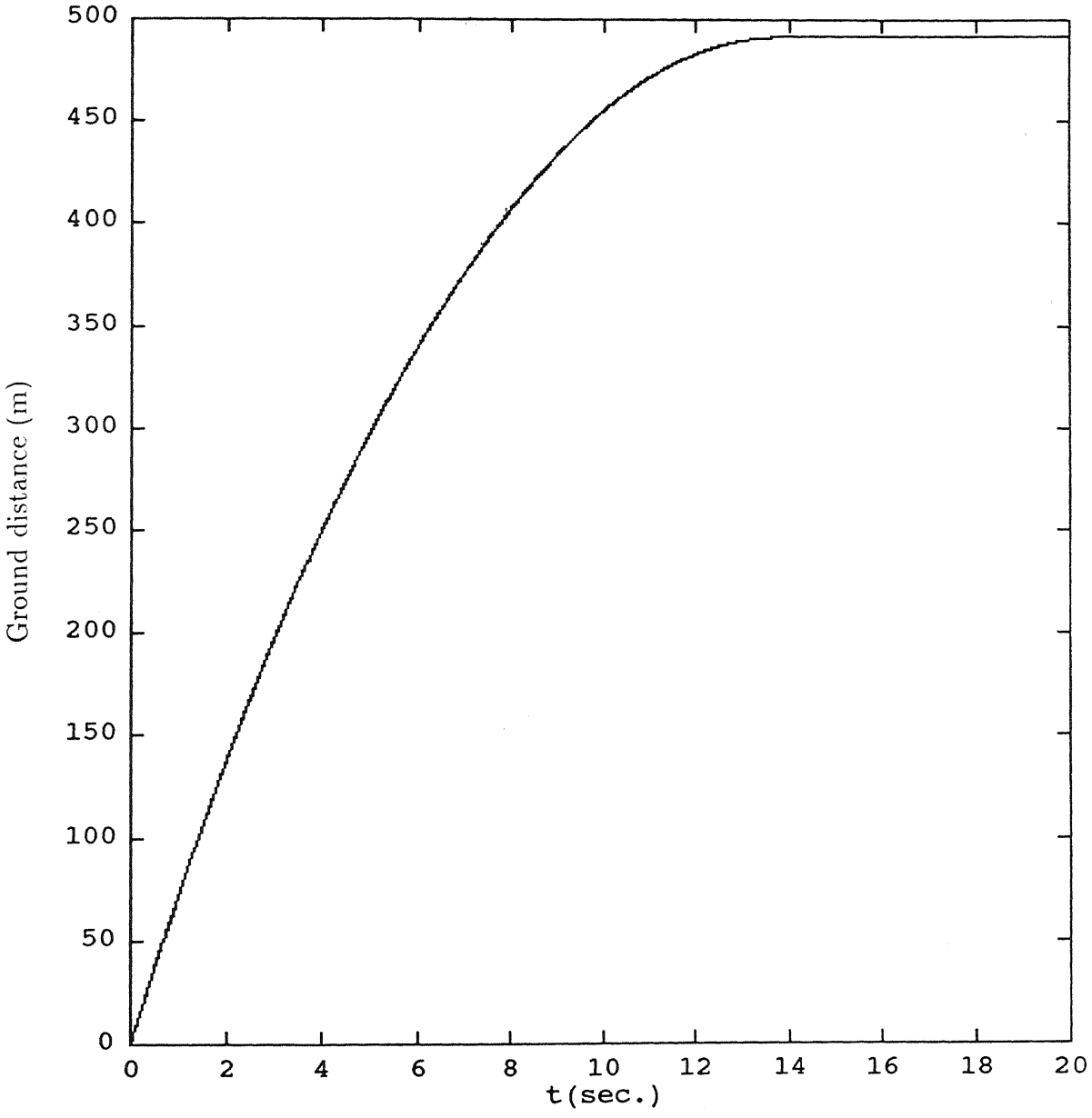

Figure 5.9: Ground distance travelled for zero mean runway, Glide velocity=75.56 m/s, Sink velocity=1.0 m/s

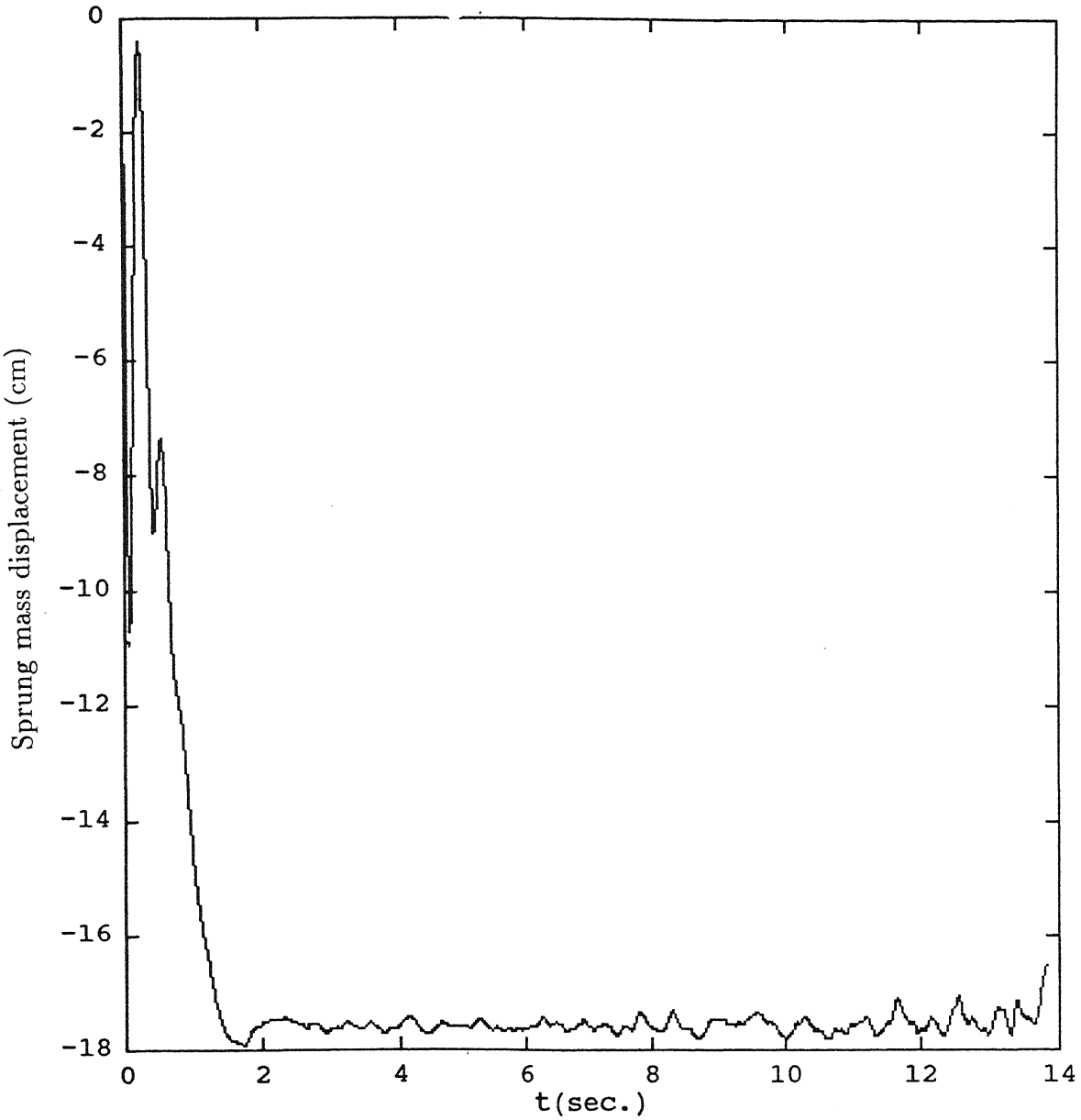

Figure 5.10: Sprung mass displacement for zero mean runway, Glide velocity=75.56 m/s, Sink velocity=2.0 m/s

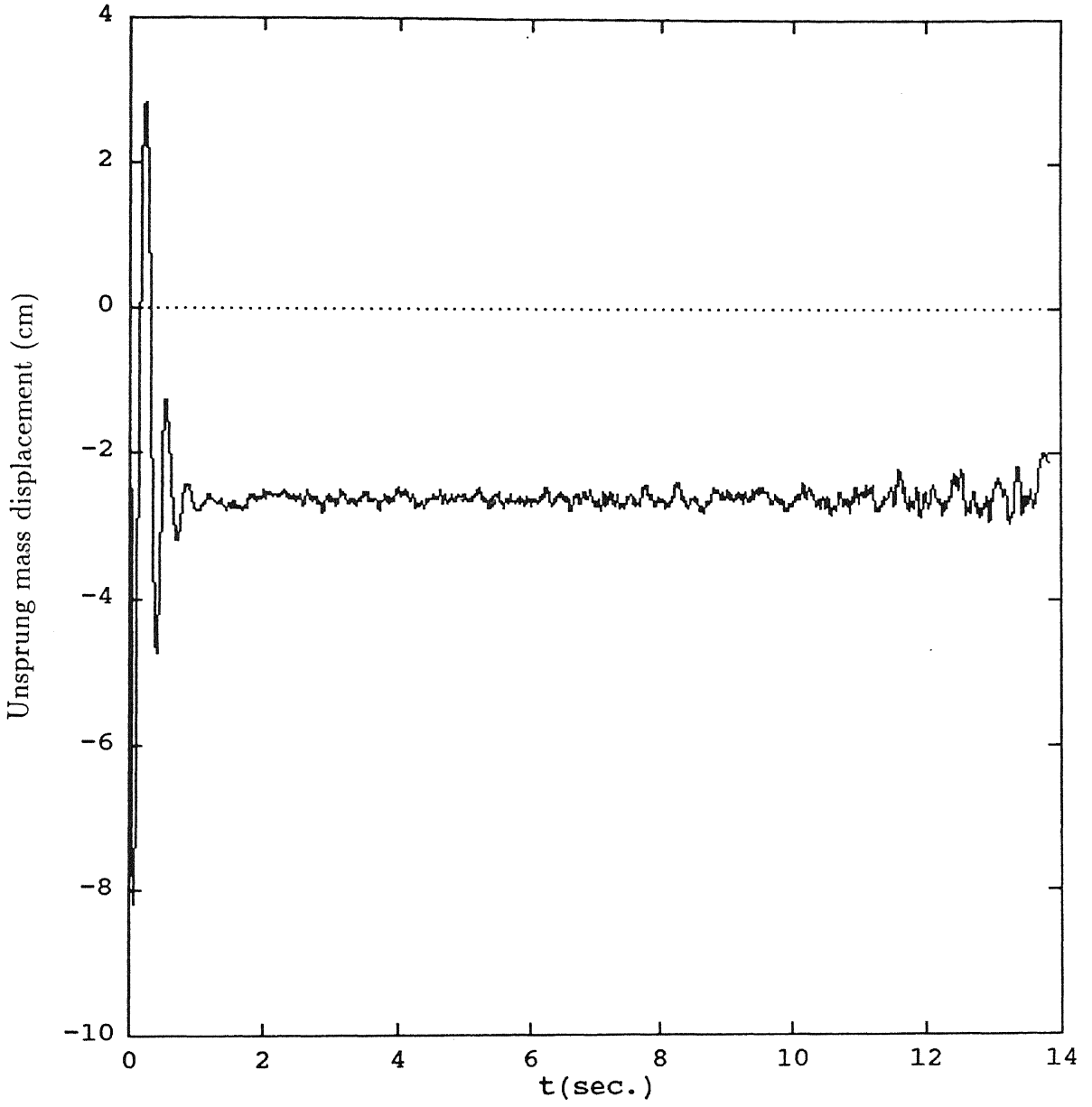

Figure 5.11: Unsprung mass displacement for zero mean runway, Glide velocity=75.56 m/s, Sink velocity=2.0 m/s

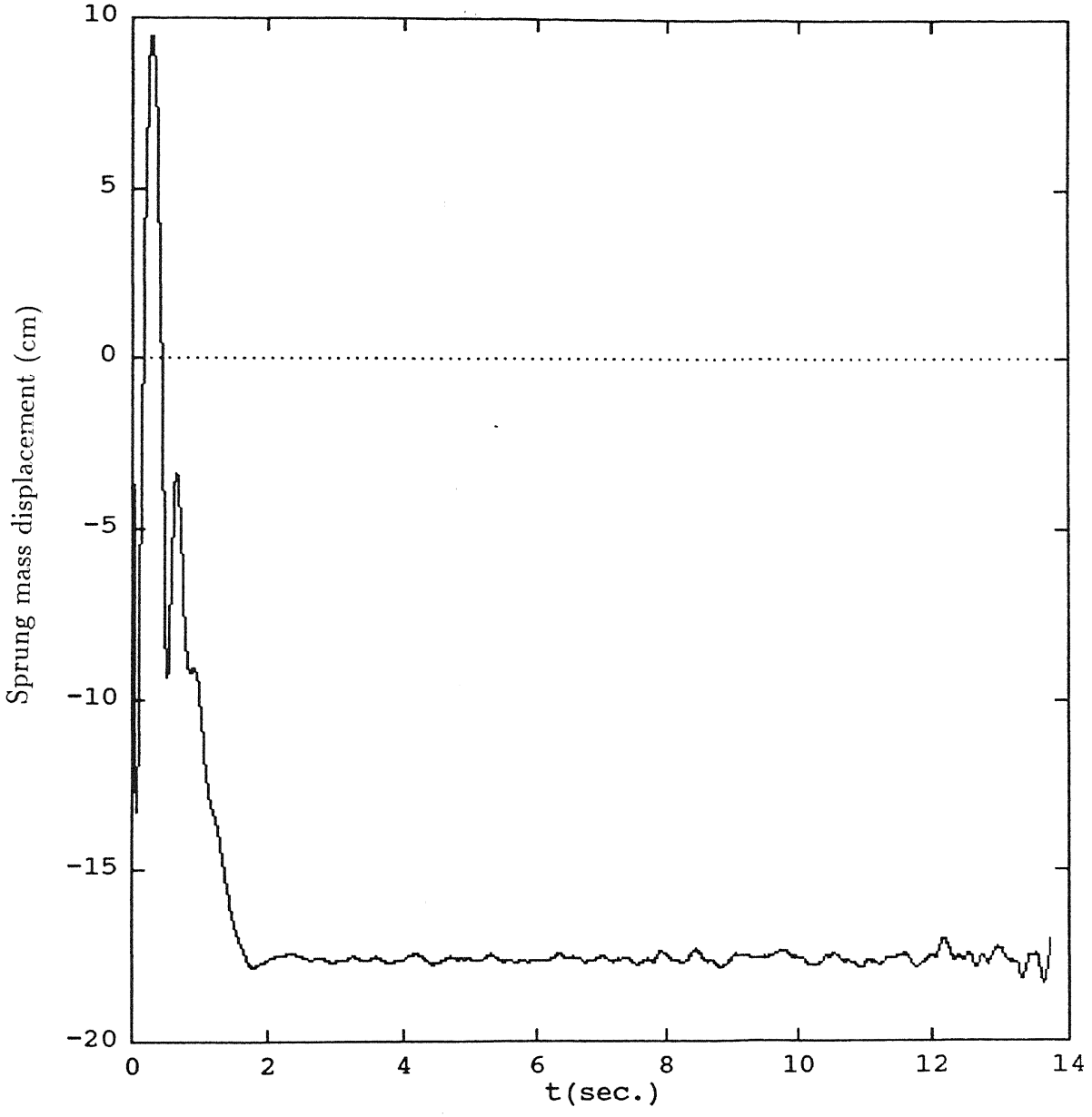

Figure 5.12: Sprung mass displacement for zero mean runway, Glide velocity=75.56 m/s, Sink velocity=3.0 m/s

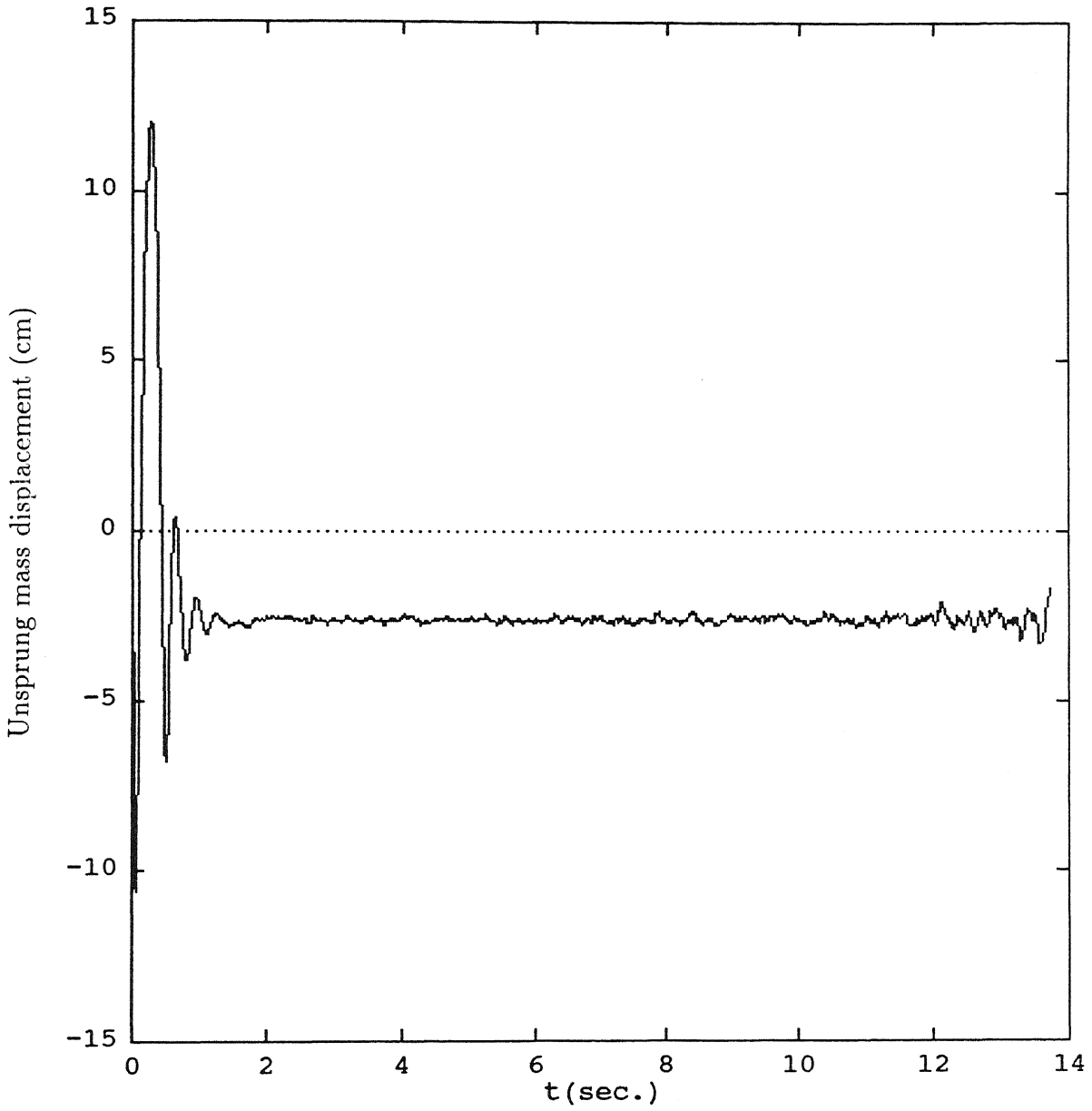

Figure 5.13: Unsprung mass displacement for zero mean runway, Glide velocity=75.56 m/s, Sink velocity=3.0 m/s

In the velocity response of the two masses, the number of peaks during the initial phase of landing, are increased with increase in sink velocity showing a stronger effect of larger sink velocities. The remaining changes in the velocity response of the two masses, compared with the previous case, are of the similar type as in displacement response (Fig. 5.14 to 5.17).

During the period of ballooning the acceleration response of the two masses show a constant value for some time (Fig. 5.18 to 5.21). With increase in sink velocity, the amplitude of acceleration response is increased. This is due to higher impact energy.

The ground reaction variation for the sink velocities of 2.0 and 3.0 m/s are shown in Fig. 5.22 and 5.23. The ground reaction is zero during ballooning. With increase in sink velocity the initial mismatching in the actual and predicted values is reduced.

The nonlinearity in the forward velocity of the aircraft, during the initial phase of landing, is increased with increase in sink velocity (Fig. 5.24 and 5.25). The stopping time is reduced with increase in sink velocity.

5.3.2 Variation in Glide Velocity

Two more values of glide velocity 83.12 and 90.67 m/s, have been considered to study its effect on system response. The sink velocity is 1.0 m/s and track profile is zero mean surface.

In general the response pattern is similar for the three glide velocities used. No significant difference is seen in the displacement and velocity response of the two masses with increase in the glide velocity (Fig. 5.26 to 5.33). The slight increase in the amplitude of the system response towards the stoppage of the aircraft can be due to the resonance phenomenon as was explained in the first case.

The acceleration responses of the two masses do not seem to follow any definite pattern, during the initial phase of landing, with increase in glide velocity (Fig. 5.34 to 5.37). This may be due to having taken only one sample of ground variations. However, the amplitude, after the landing impact, is increased as the glide velocity is increased.

The only difference found in the ground reaction plot compared to the first case is that with increase in glide velocity the initial prediction becomes worse (Fig. 5.38 and 5.39).

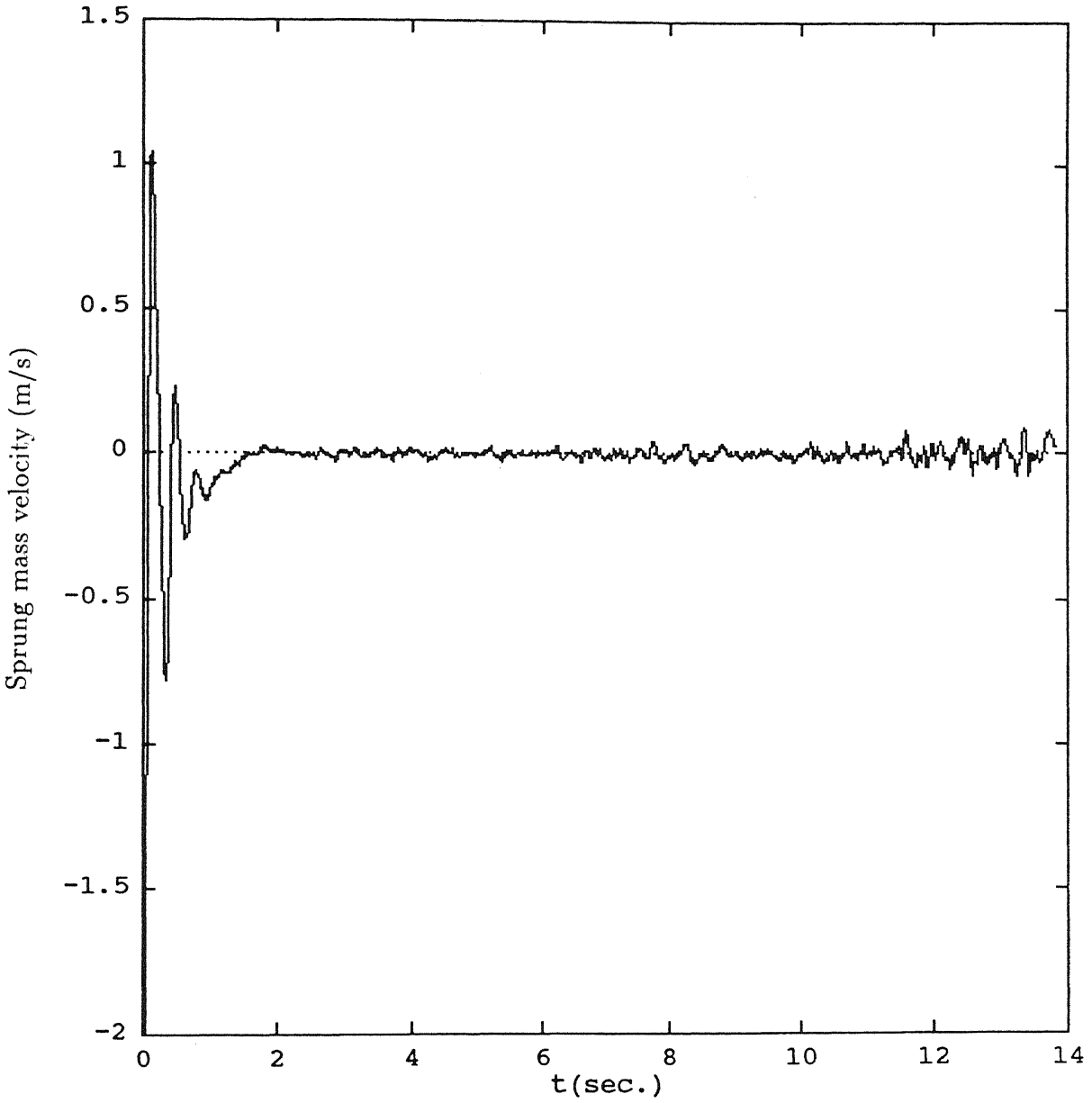

Figure 5.14: Sprung mass velocity for zero mean runway, Glide velocity=75.56 m/s, Sink velocity=2.0 m/s

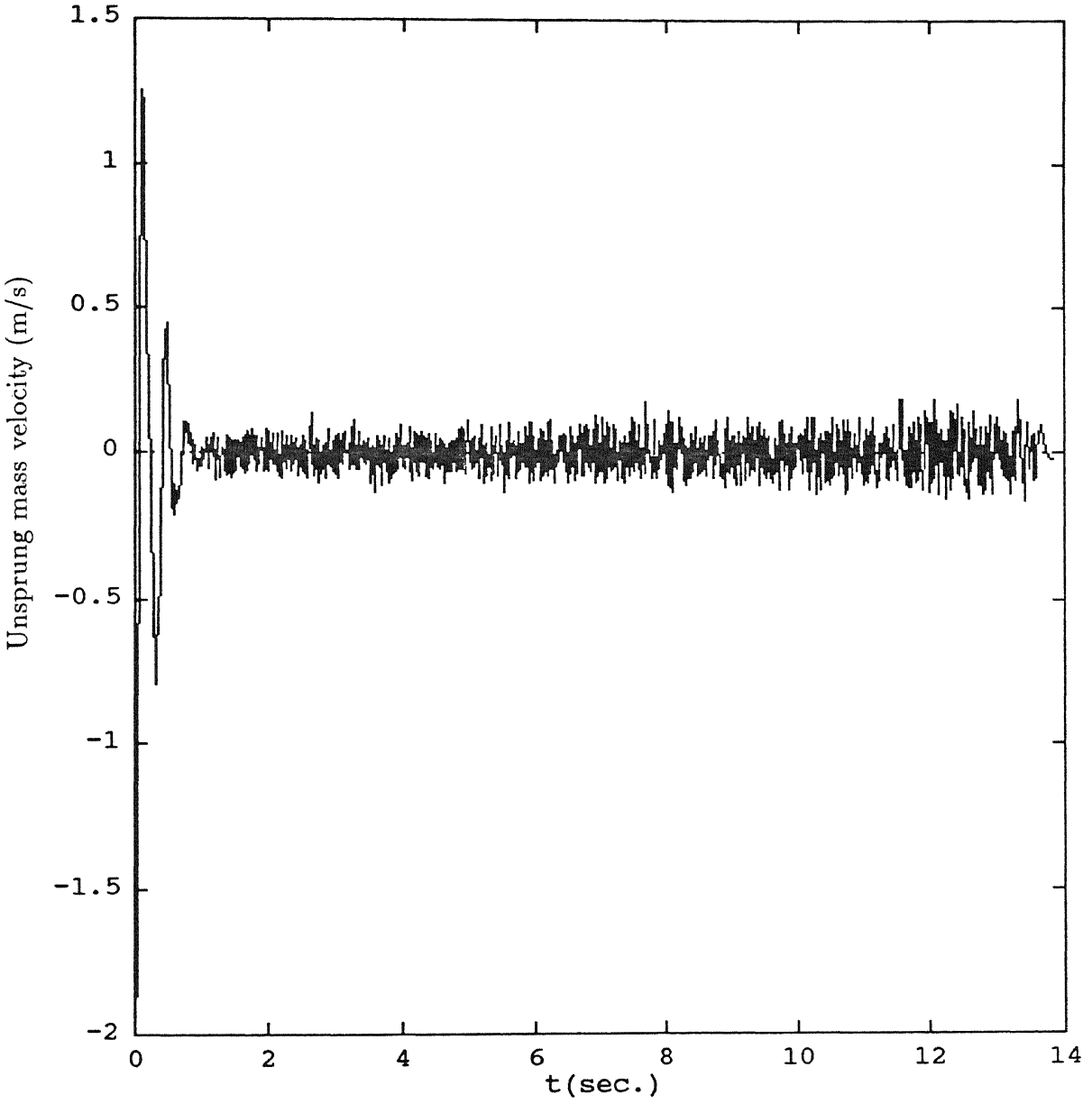

Figure 5.15: Unsprung mass velocity for zero mean runway, Glide velocity=75.56 m/s, Sink velocity=2.0 m/s

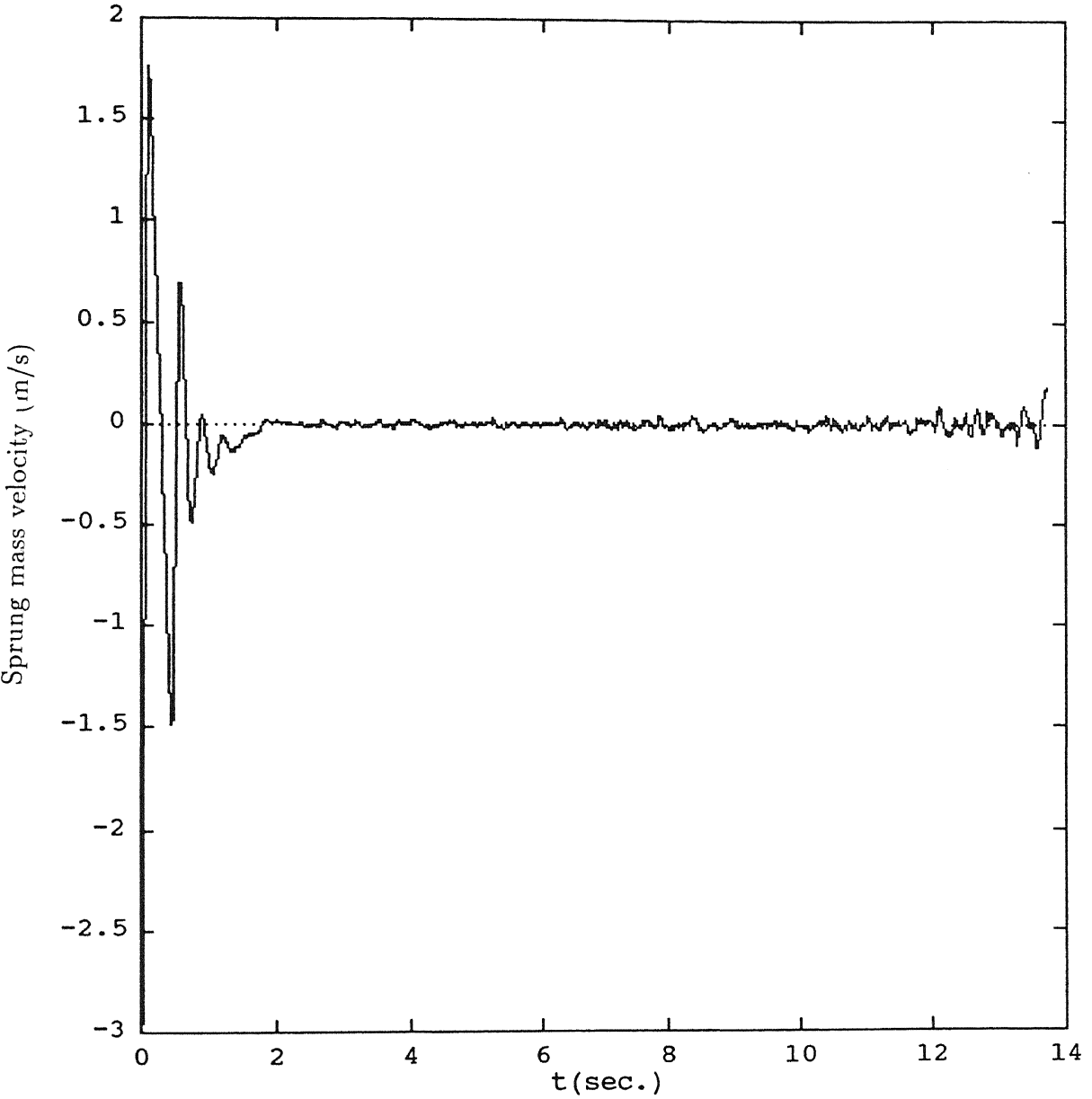

Figure 5.16: Sprung mass velocity for zero mean runway, Glide velocity=75.56 m/s, Sink velocity=3.0 m/s

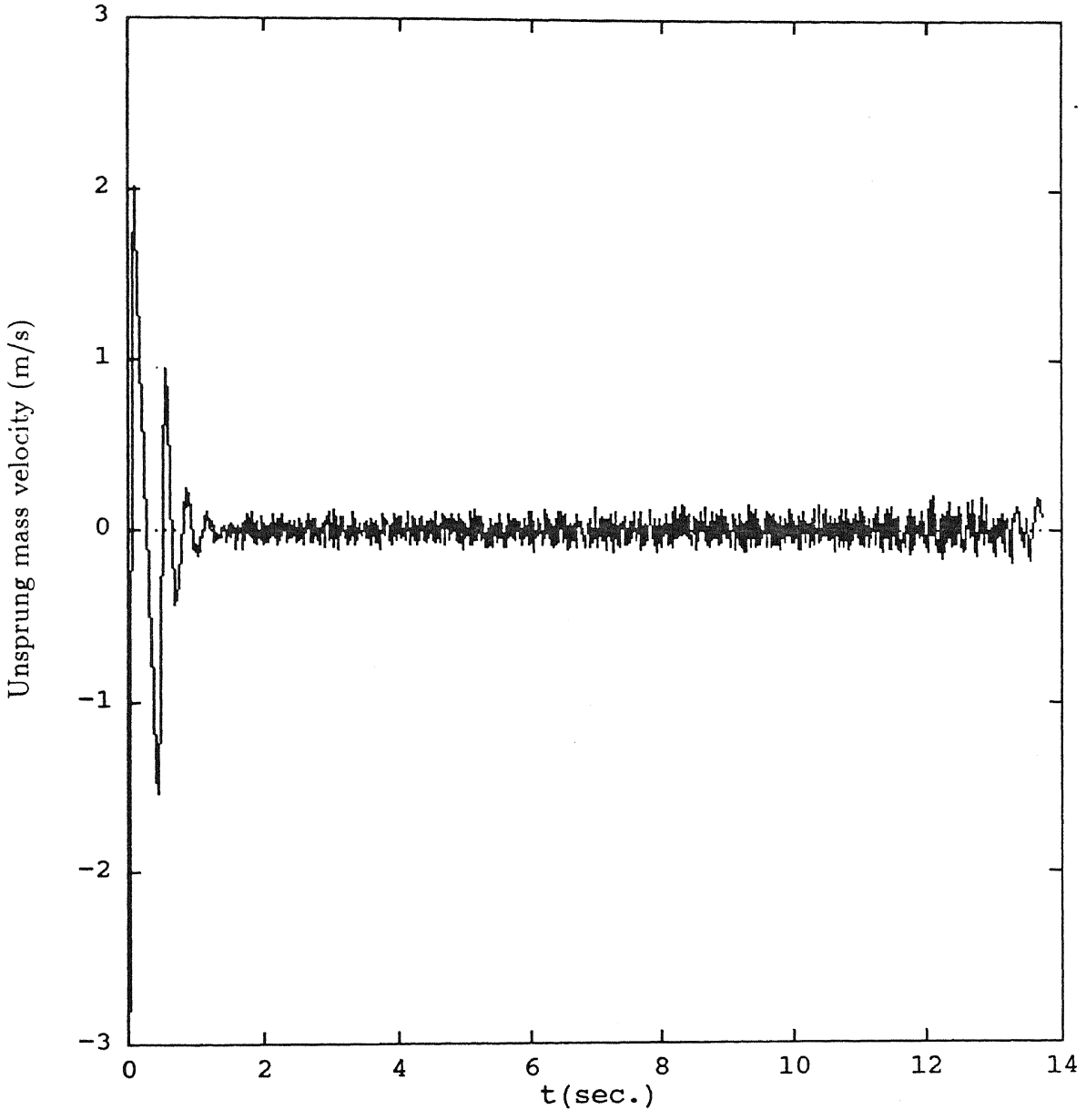

Figure 5.17: Unsprung mass velocity for zero mean runway, Glide velocity=75.56 m/s, Sink velocity=3.0 m/s

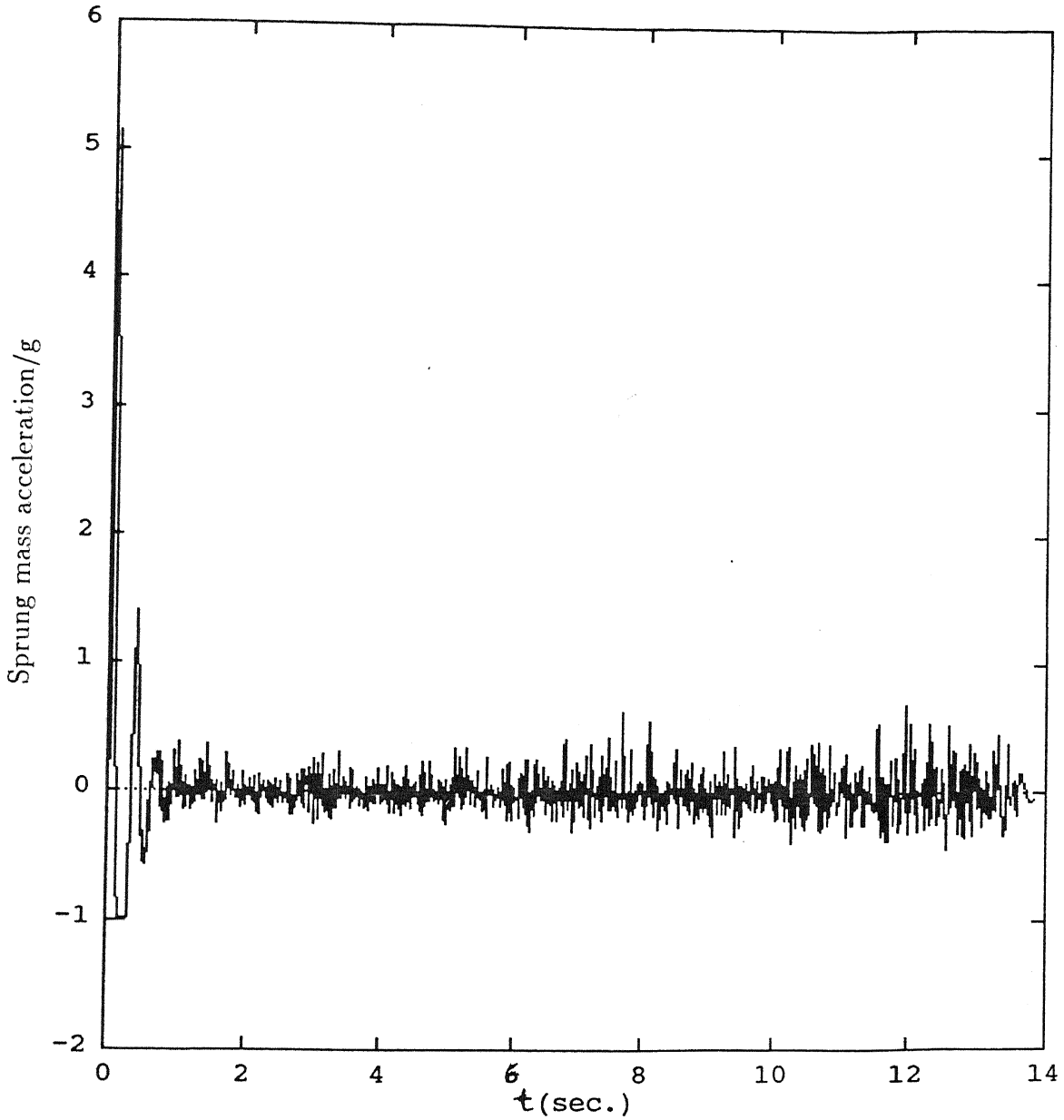

Figure 5.18: Sprung mass acceleration for zero mean runway, Glide velocity=75.56 m/s, Sink velocity=2.0 m/s

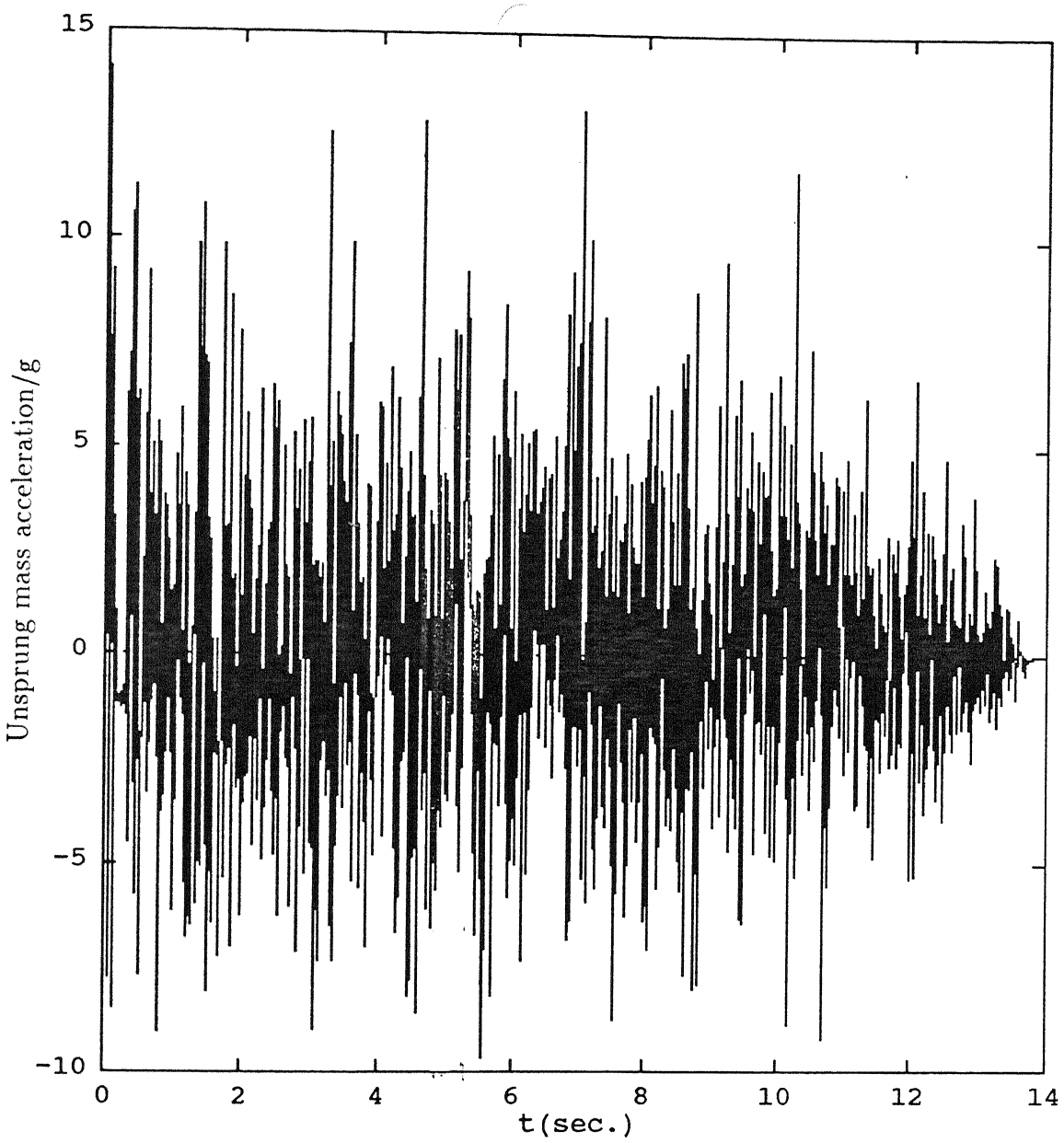

Figure 5.19: Unsprung mass acceleration for zero mean runway, Glide velocity=75.56 m/s, Sink velocity=2.0 m/s

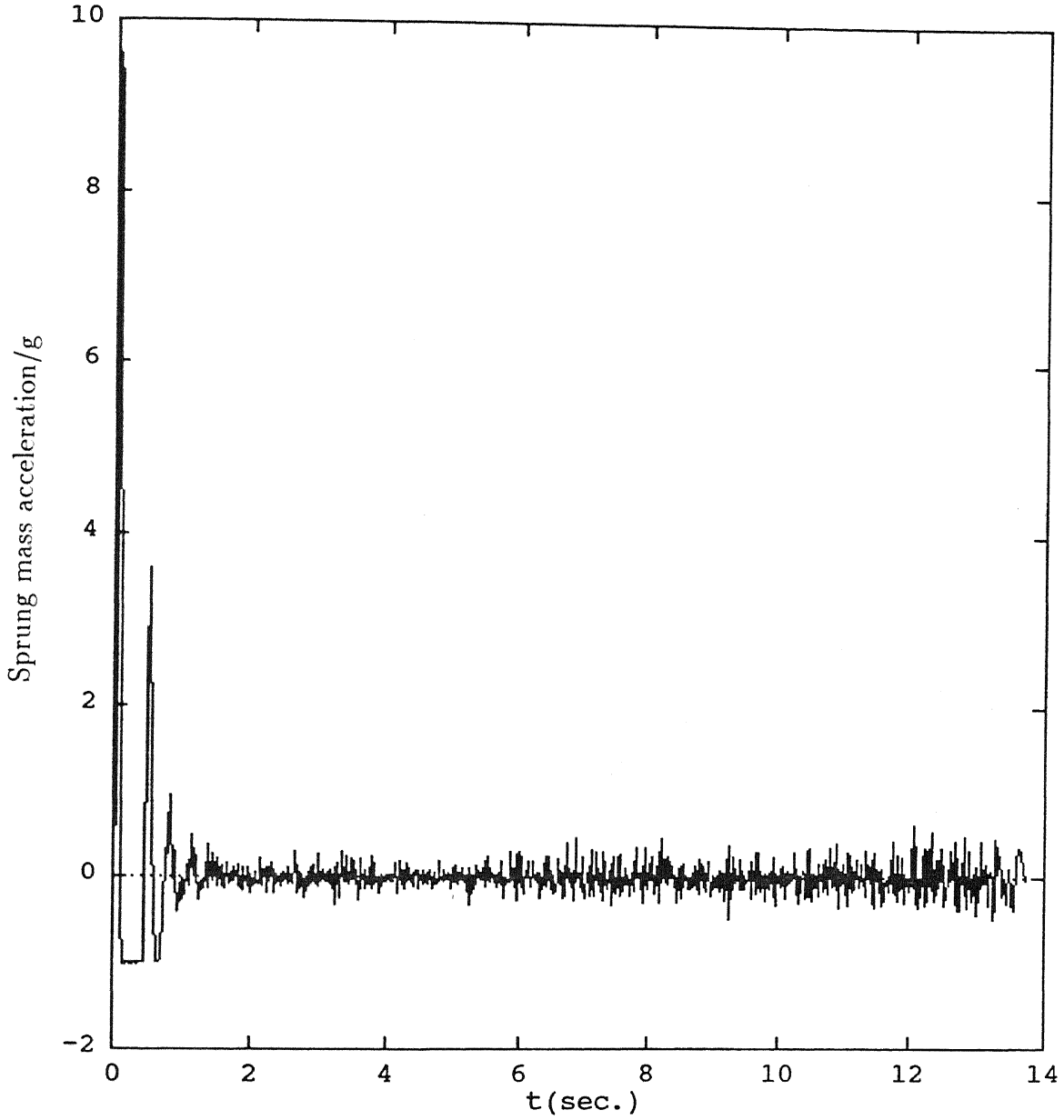

Figure 5.20: Sprung mass acceleration for zero mean runway, Glide velocity=75.56 m/s, Sink velocity=3.0 m/s

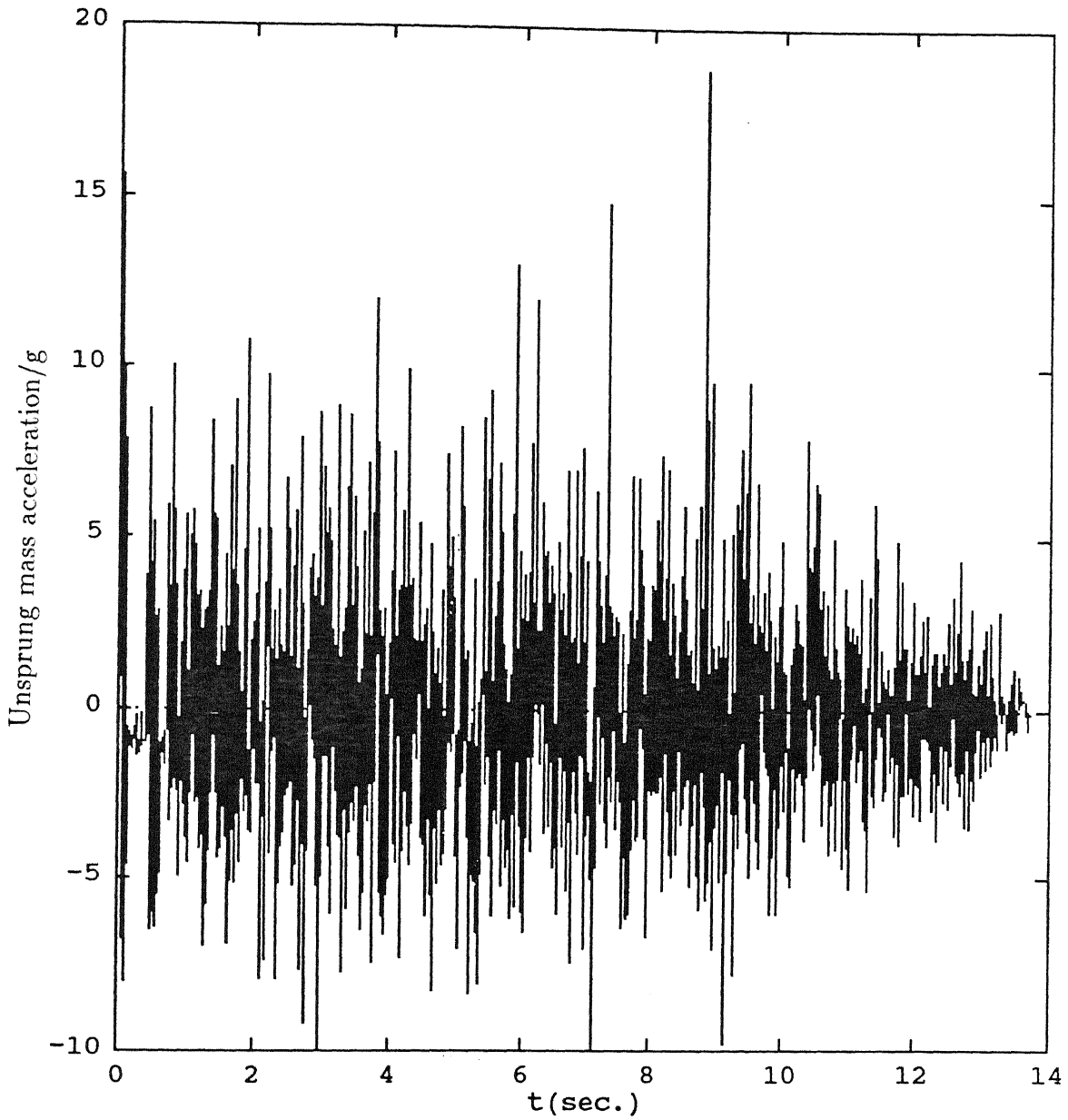

Figure 5.21: Unsprung mass acceleration for zero mean runway, Glide velocity=75.56 m/s, Sink velocity=3.0 m/s

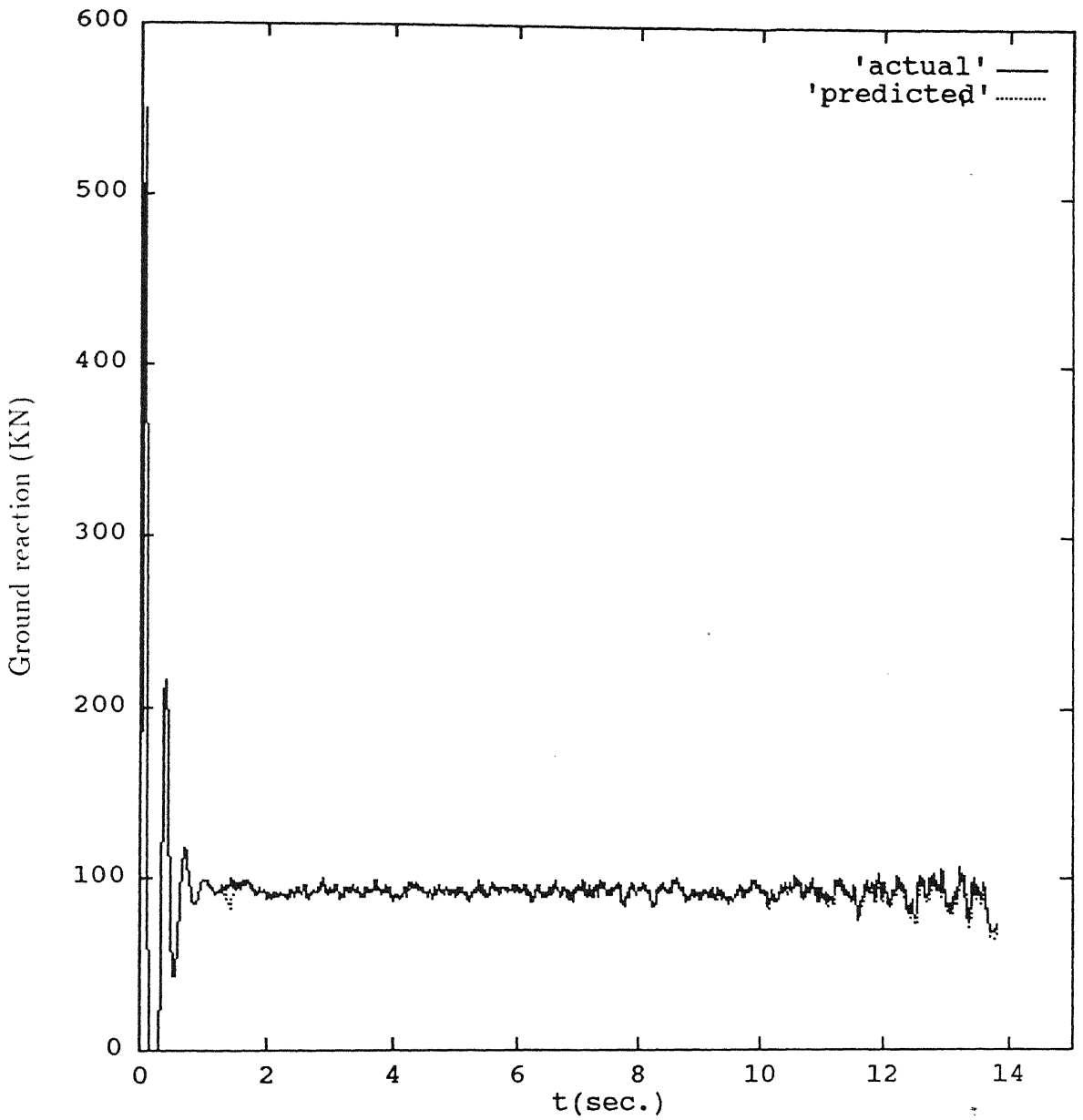

Figure 5.22: Ground Reaction for zero mean runway, Glide velocity=75.56 m/s, Sink velocity=2.0 m/s

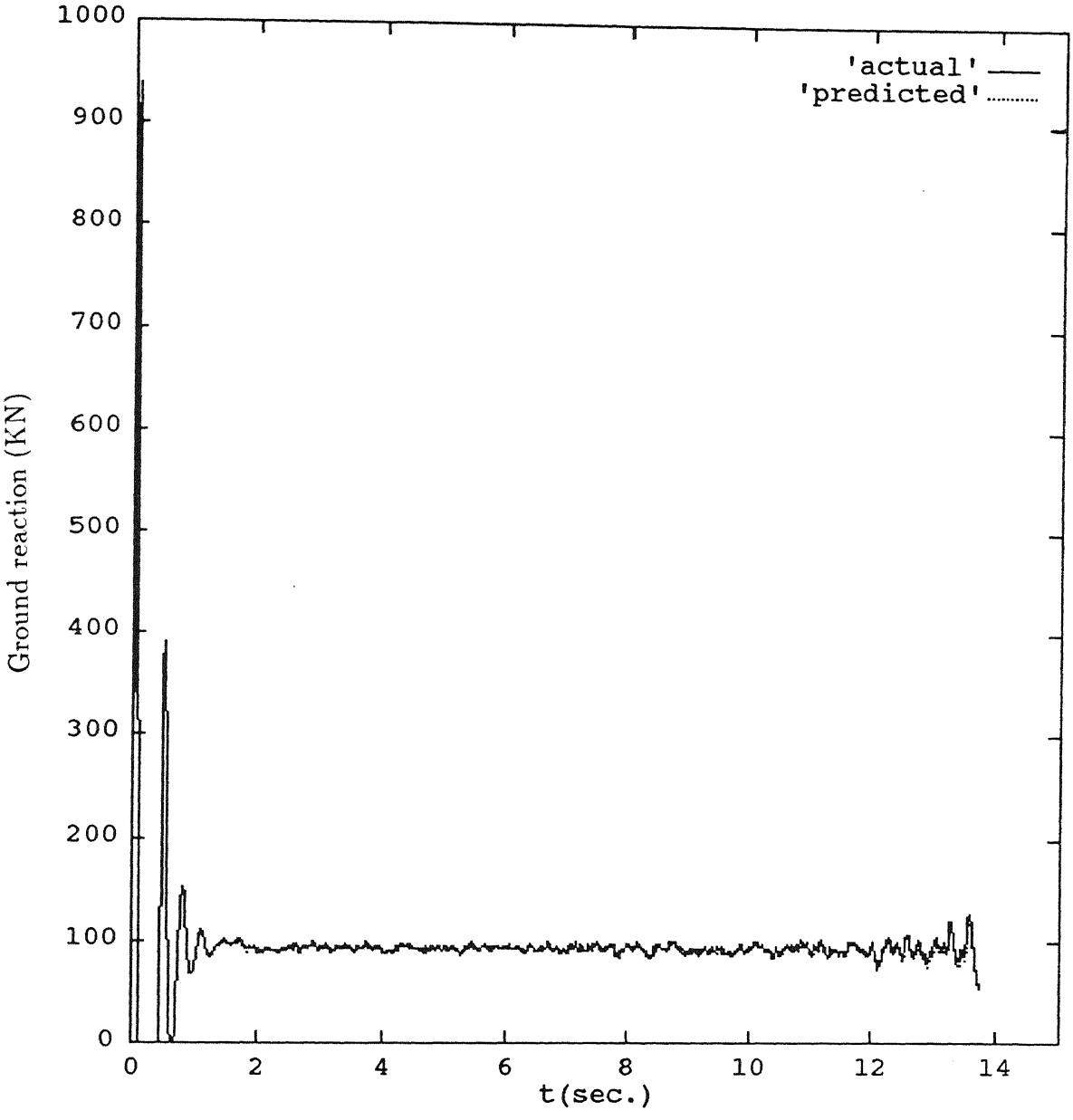

Figure 5.23: Ground Reaction for zero mean runway, Glide velocity=75.56 m/s, Sink velocity=3.0 m/s

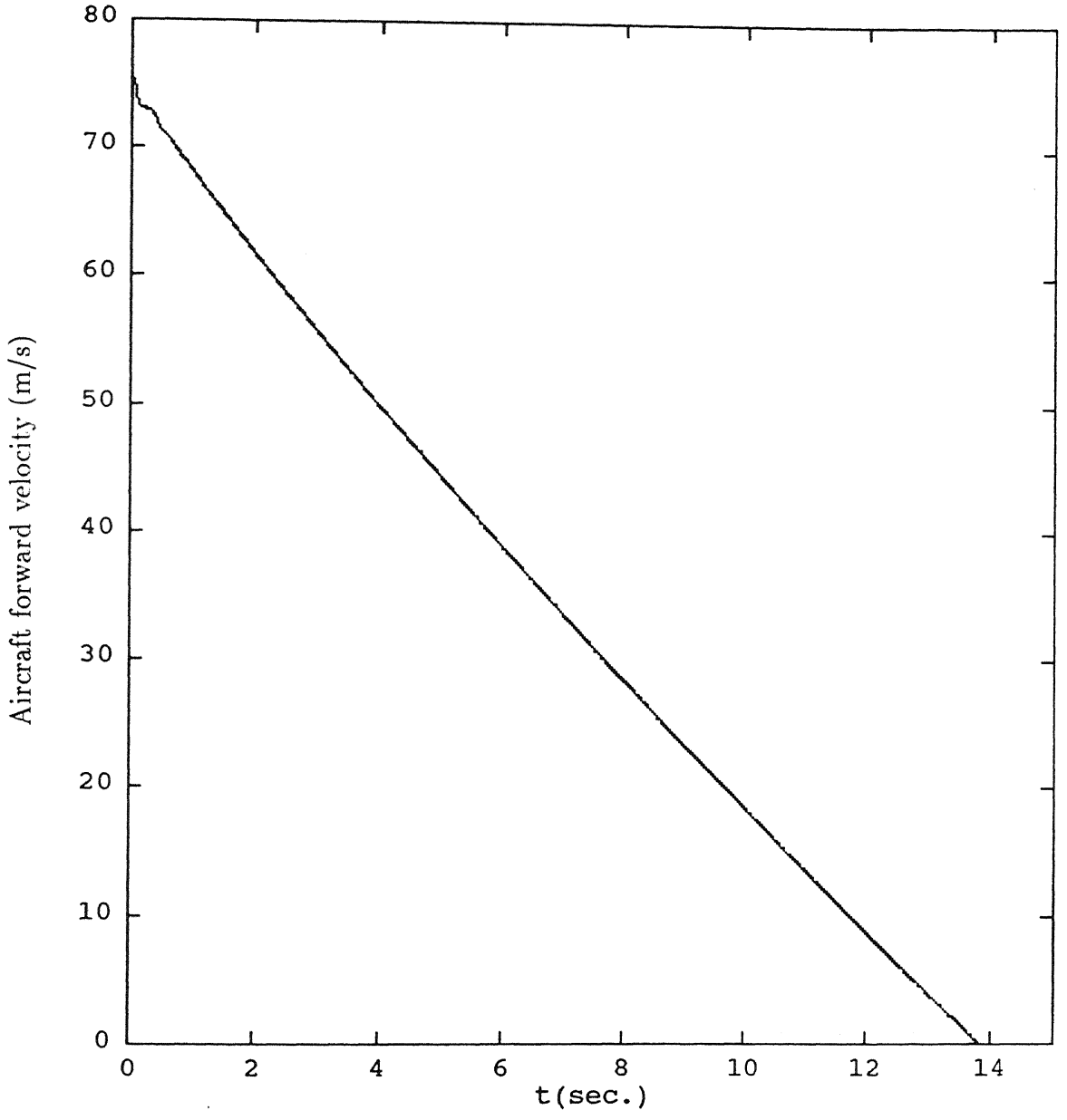

Figure 5.24: Aircraft forward velocity for zero mean runway, Glide velocity=75.56 m/s, Sink velocity=2.0 m/s

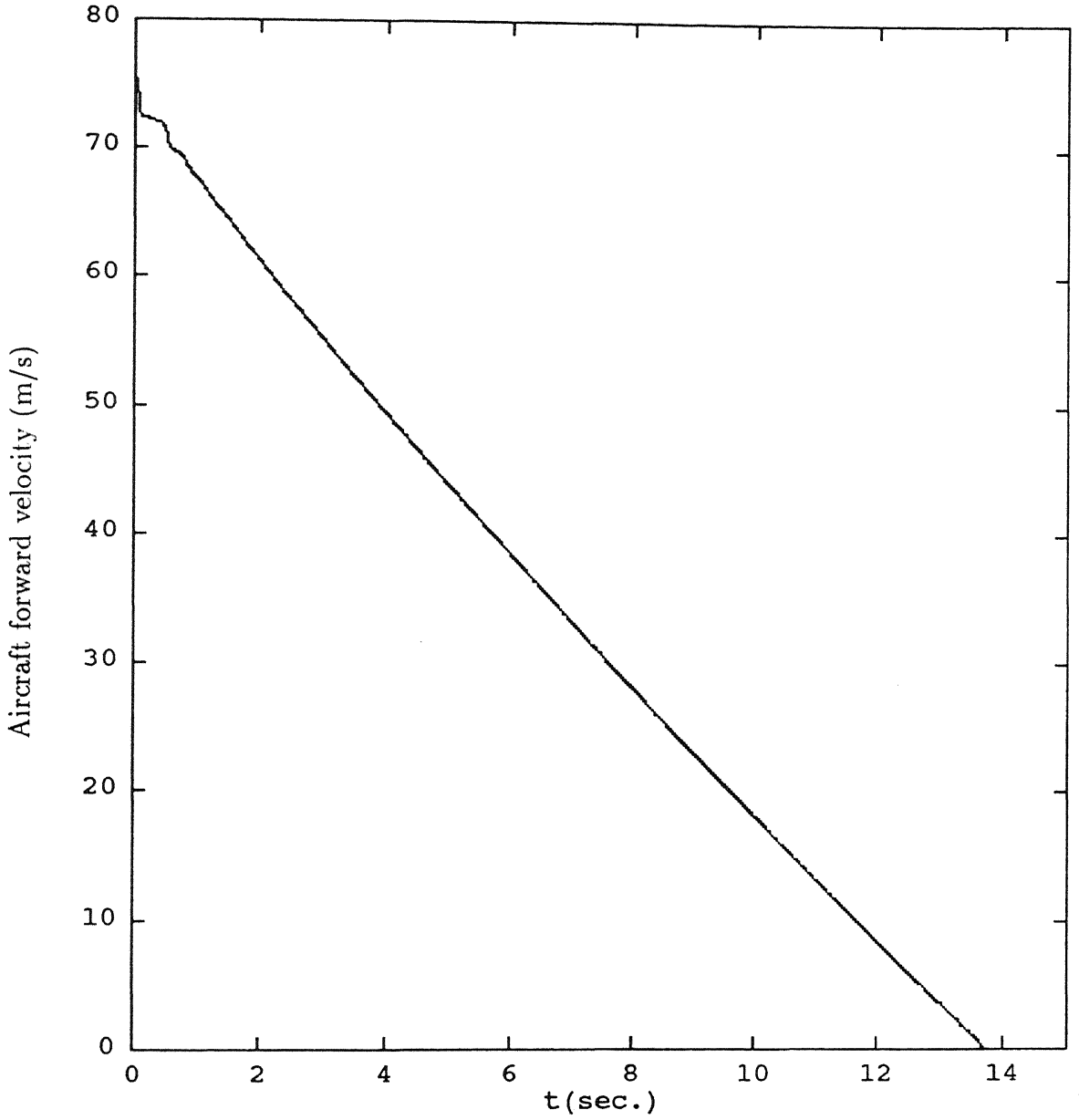

Figure 5.25: Aircraft forward velocity for zero mean runway, Glide velocity=75.56 m/s, Sink velocity=3.0 m/s

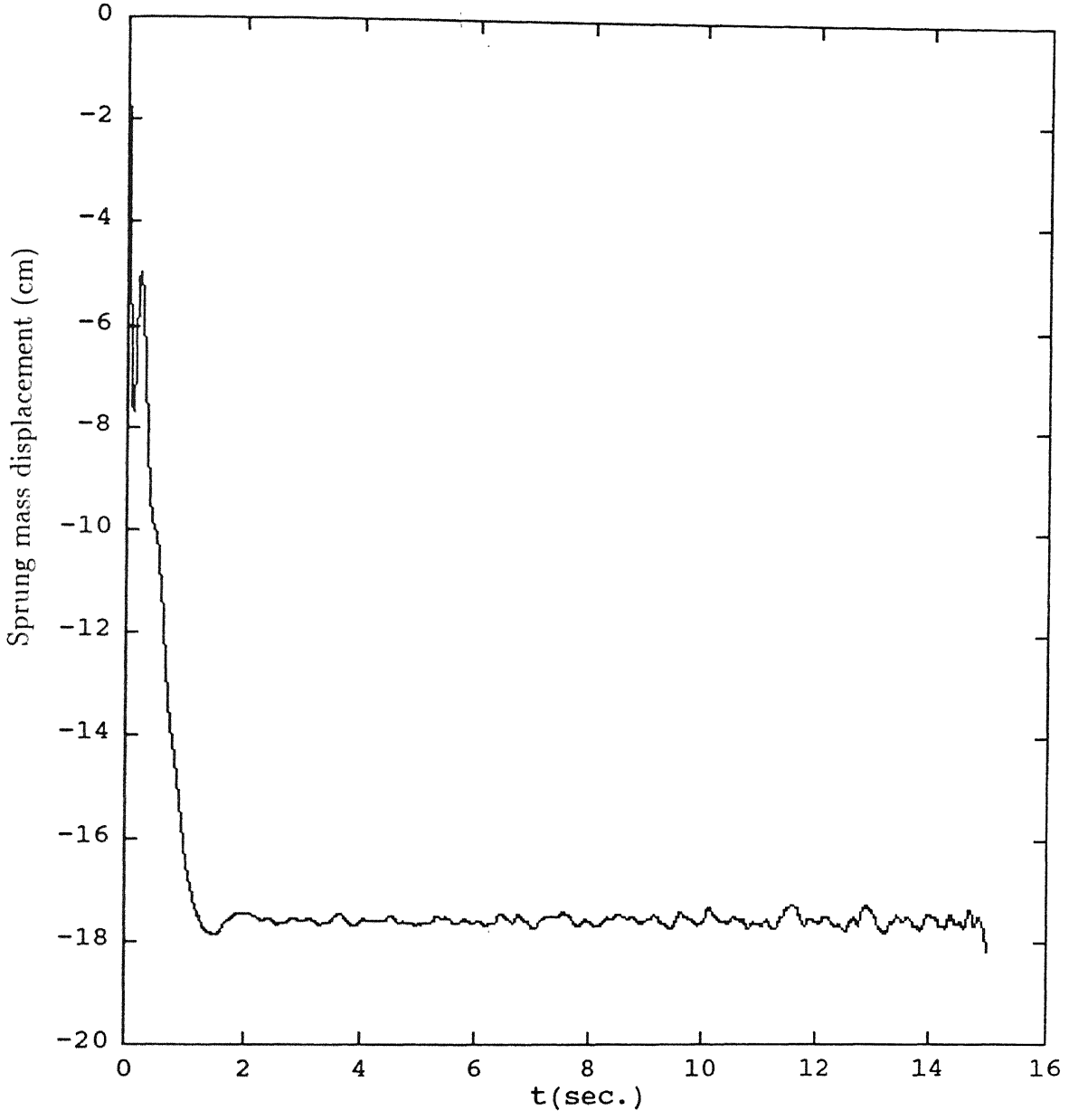

Figure 5.26: Sprung mass displacement for zero mean runway, Glide velocity=83.12 m/s, Sink velocity=1.0 m/s

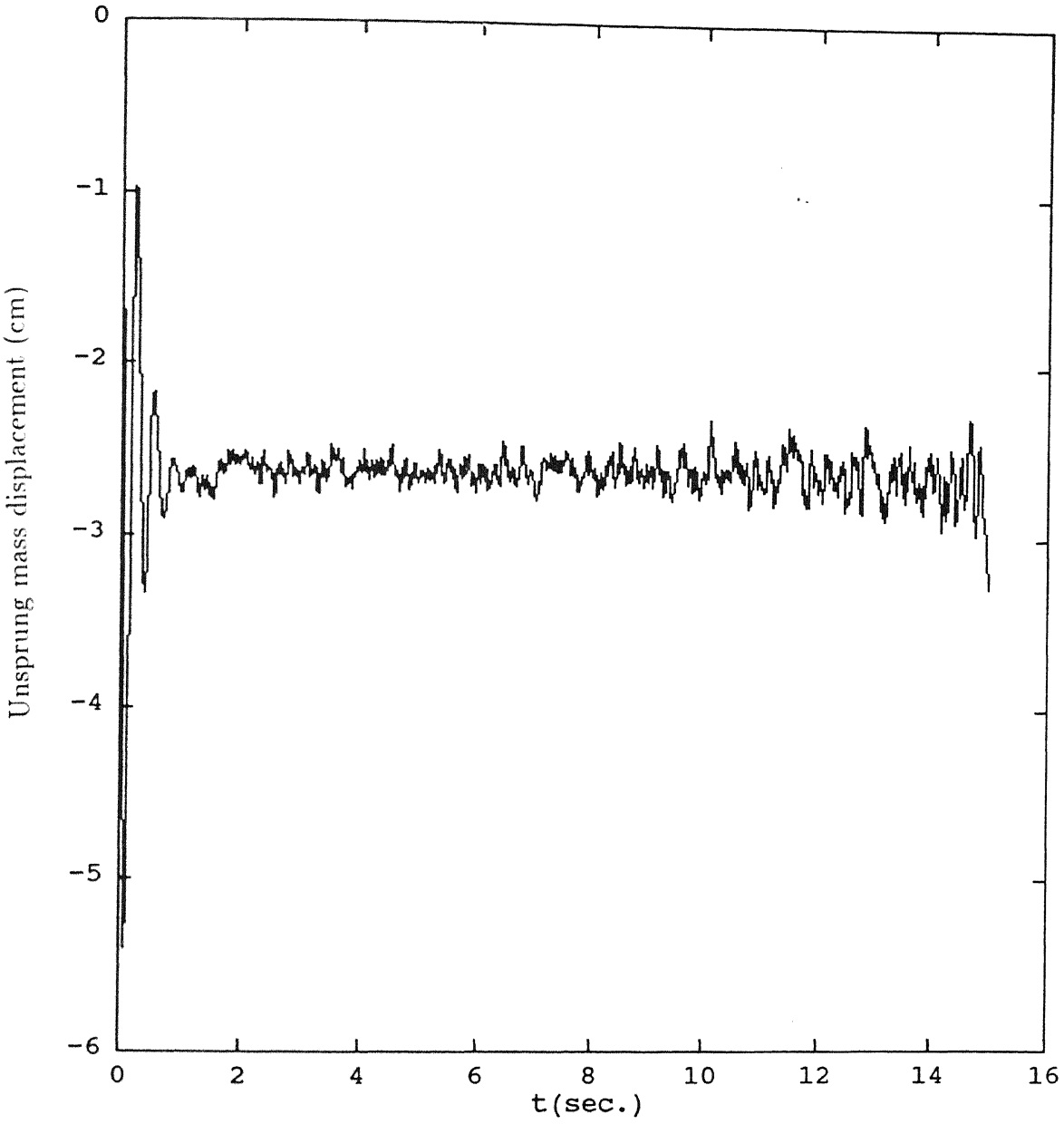

Figure 5.27: Unsprung mass displacement for zero mean runway, Glide velocity=83.12 m/s, Sink velocity=1.0 m/s

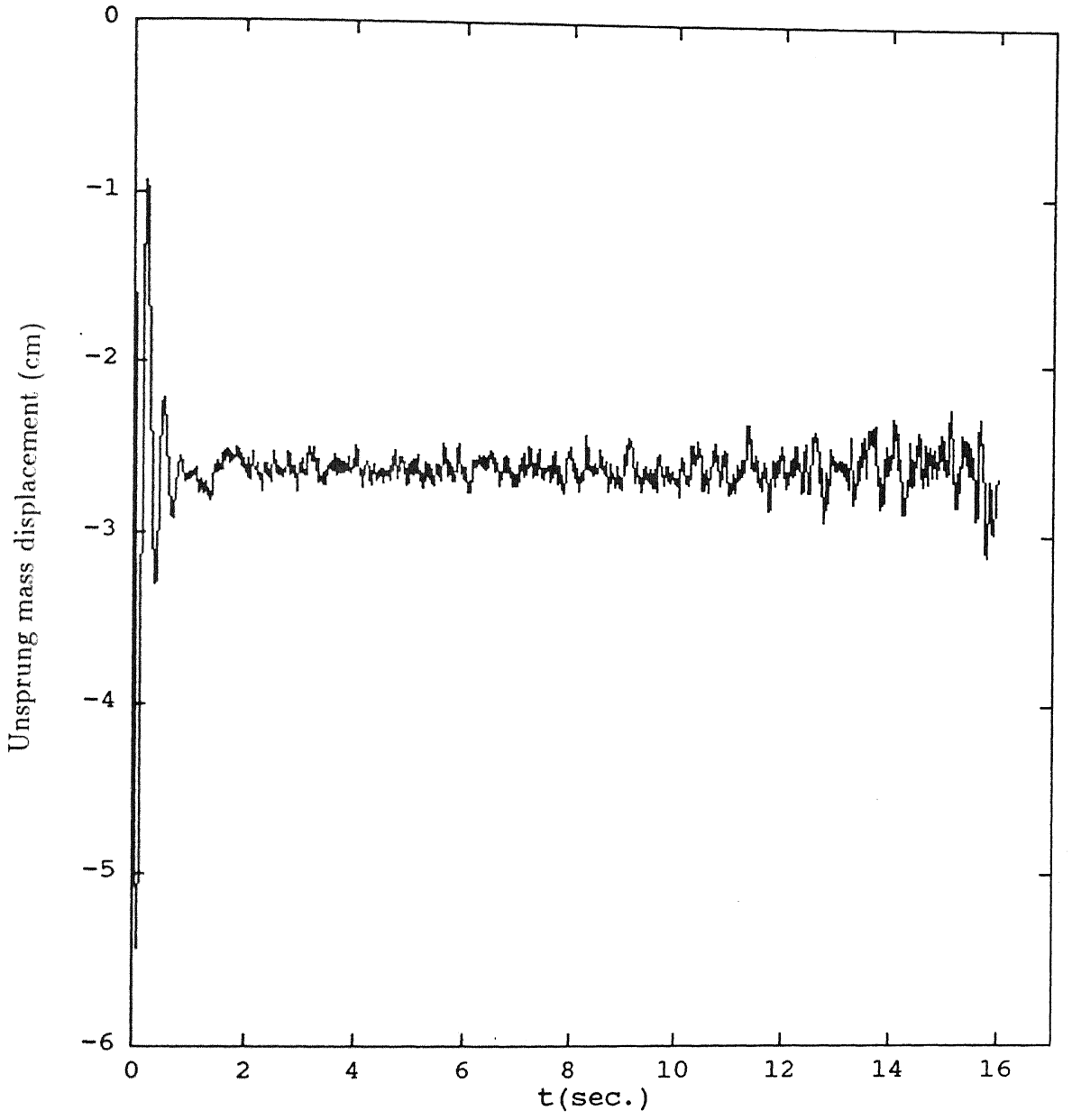

Figure 5.29: Unsprung mass displacement for zero mean runway, Glide velocity=90.67 m/s, Sink velocity=1.0 m/s

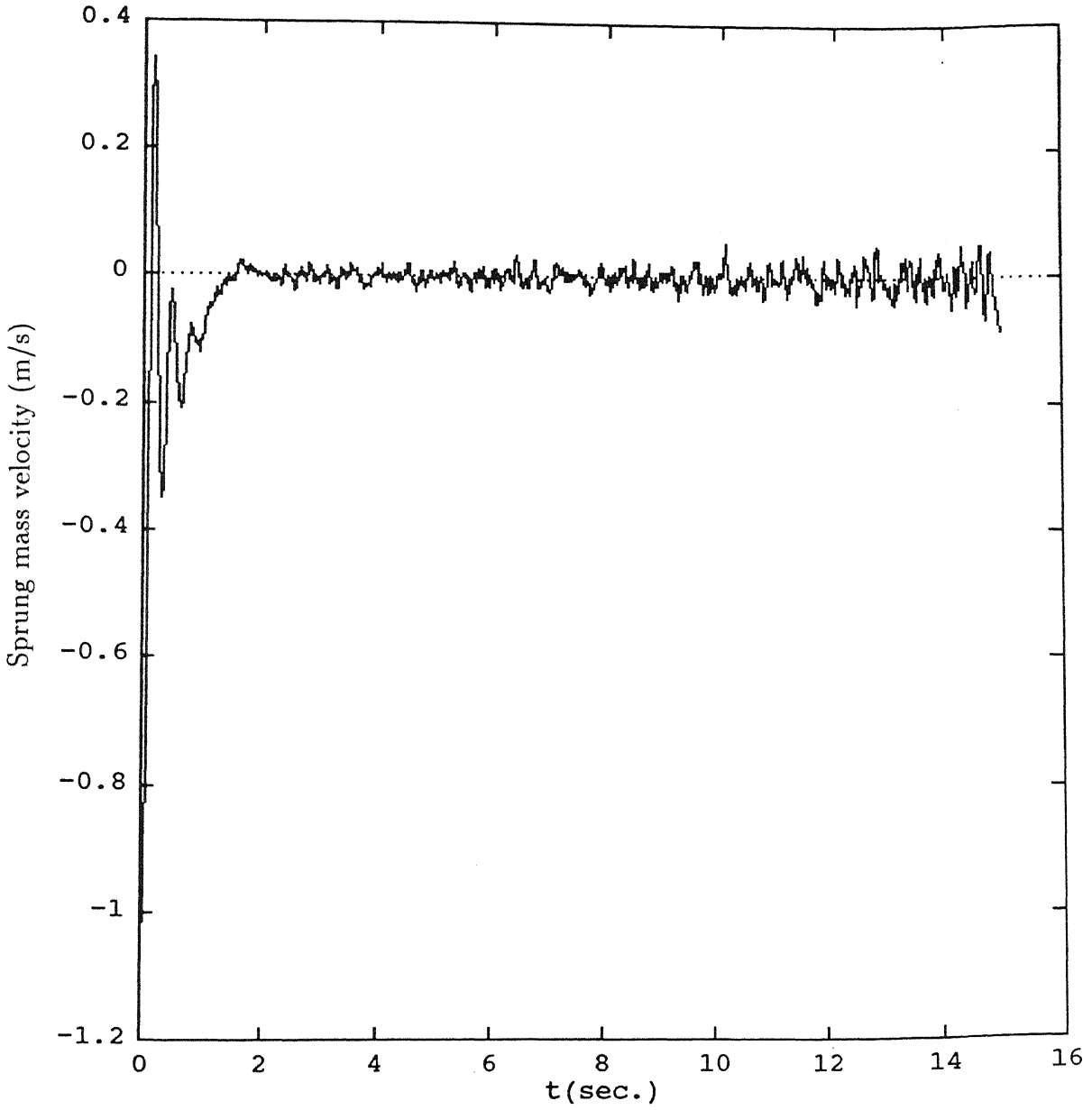

Figure 5.30: Sprung mass velocity for zero mean runway, Glide velocity=83.12 m/s, Sink velocity=1.0 m/s

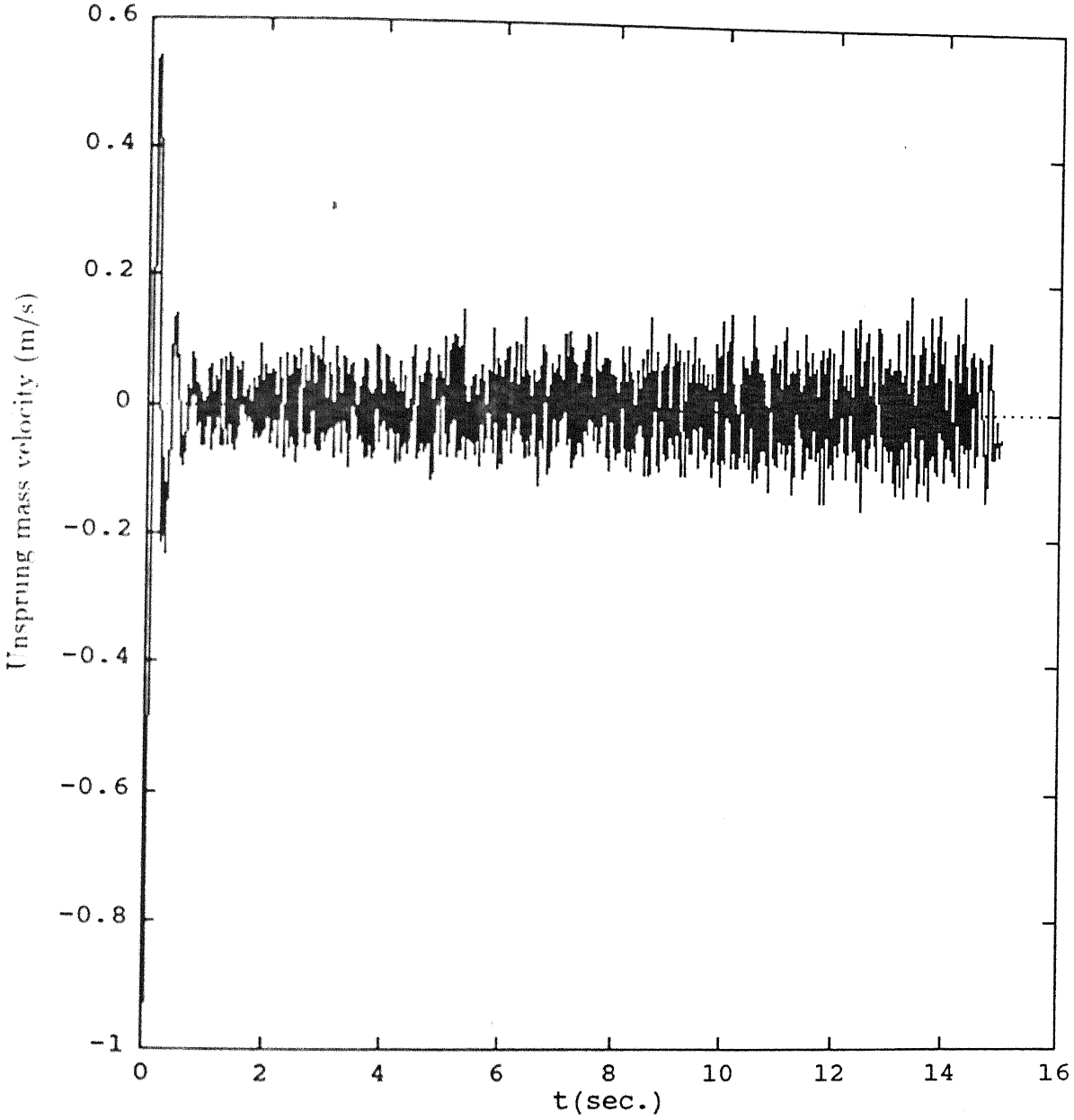

Figure 5.31: Unsprung mass velocity for zero mean runway, Glide velocity=83.12 m/s, Sink velocity=1.0 m/s

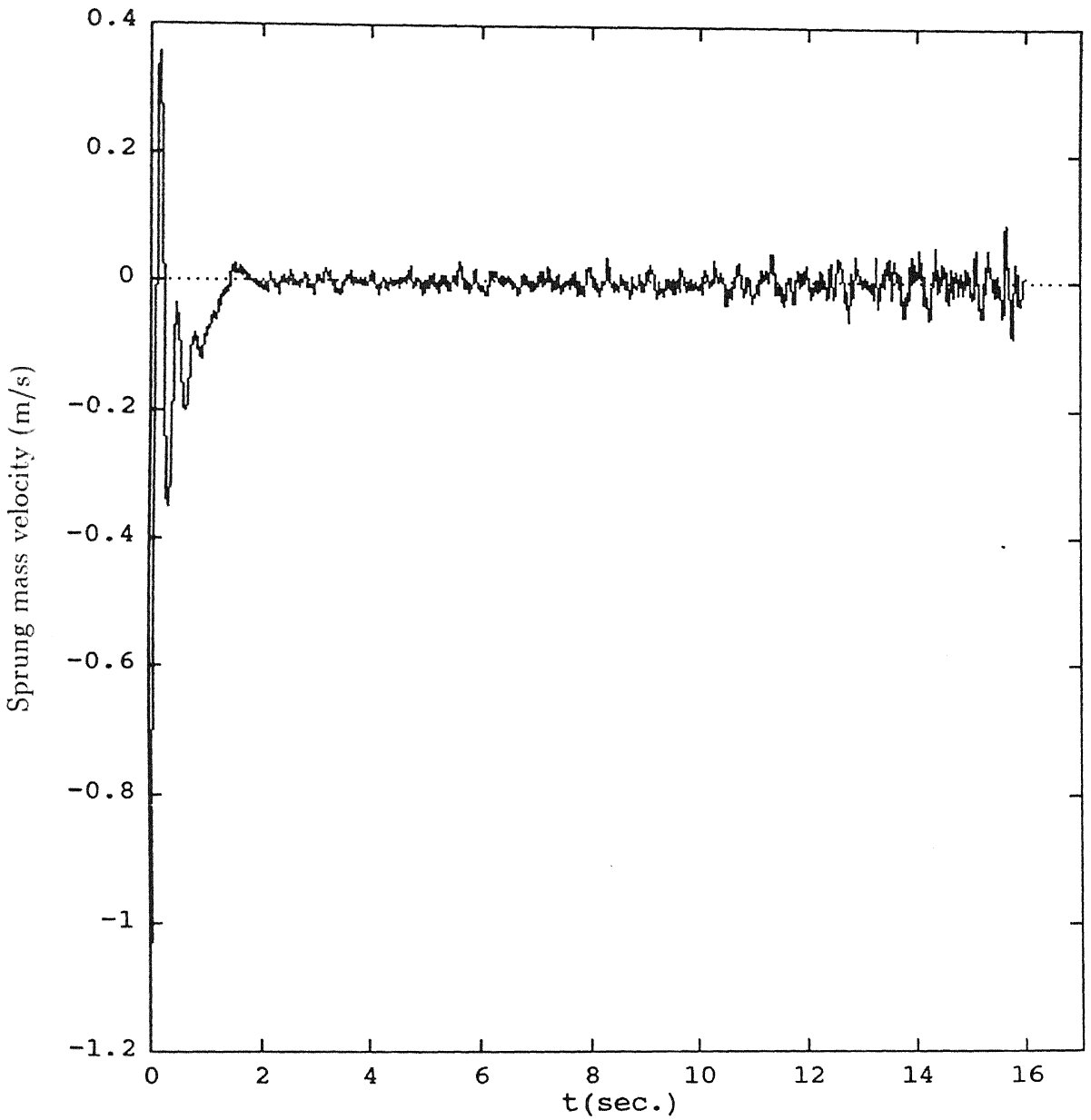

Figure 5.32: Sprung mass velocity for zero mean runway, Glide velocity=90.67 m/s, Sink velocity=1.0 m/s

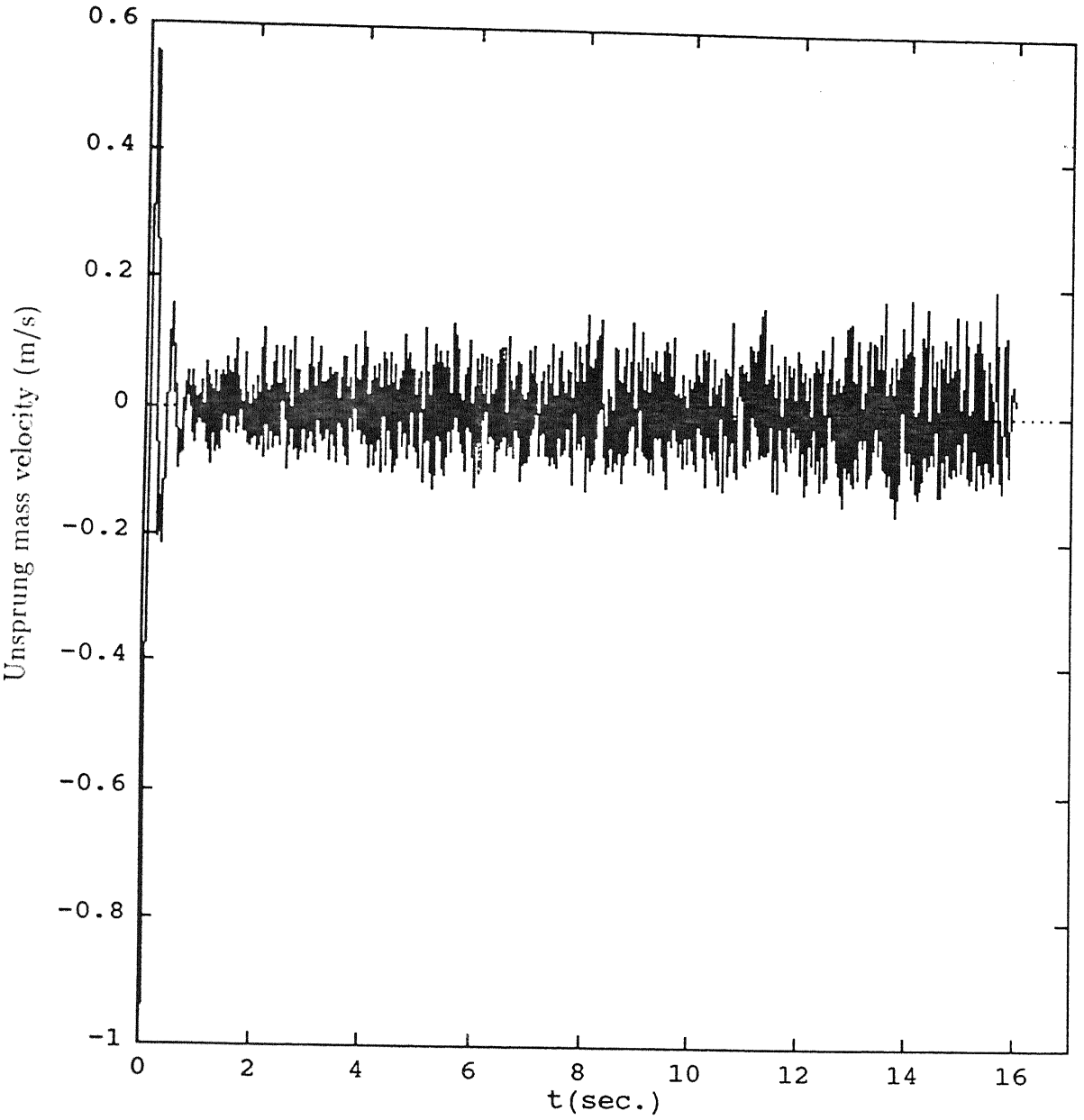

Figure 5.33: Unsprung mass velocity for zero mean runway, Glide velocity=90.67 m/s, Sink velocity=1.0 m/s

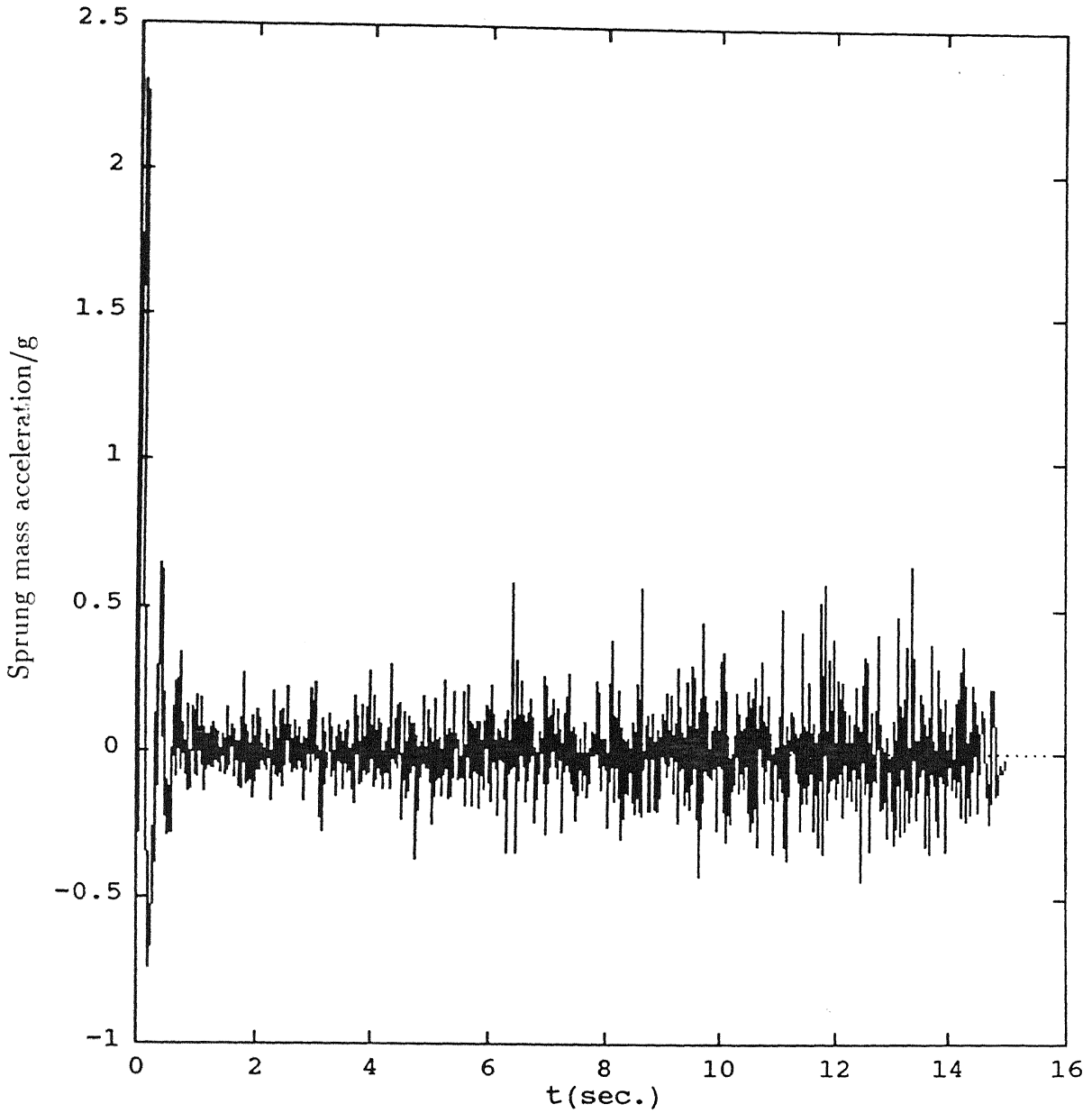

Figure 5.34: Sprung mass acceleration for zero mean runway, Glide velocity=83.12 m/s, Sink velocity=1.0 m/s

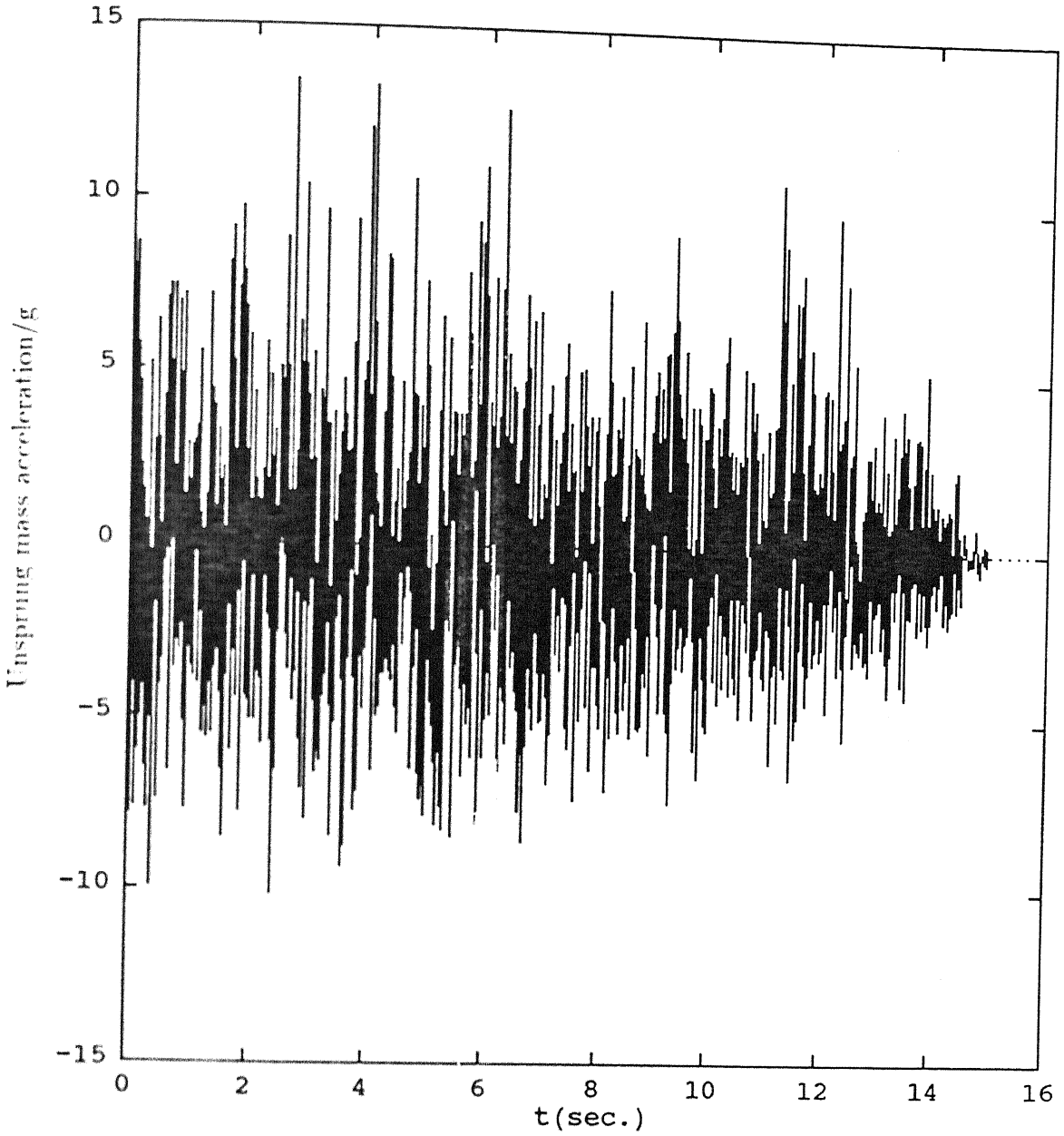

Figure 5.35: Unsprung mass acceleration for zero mean runway, Glide velocity=83.12 m/s, Sink velocity=1.0 m/s

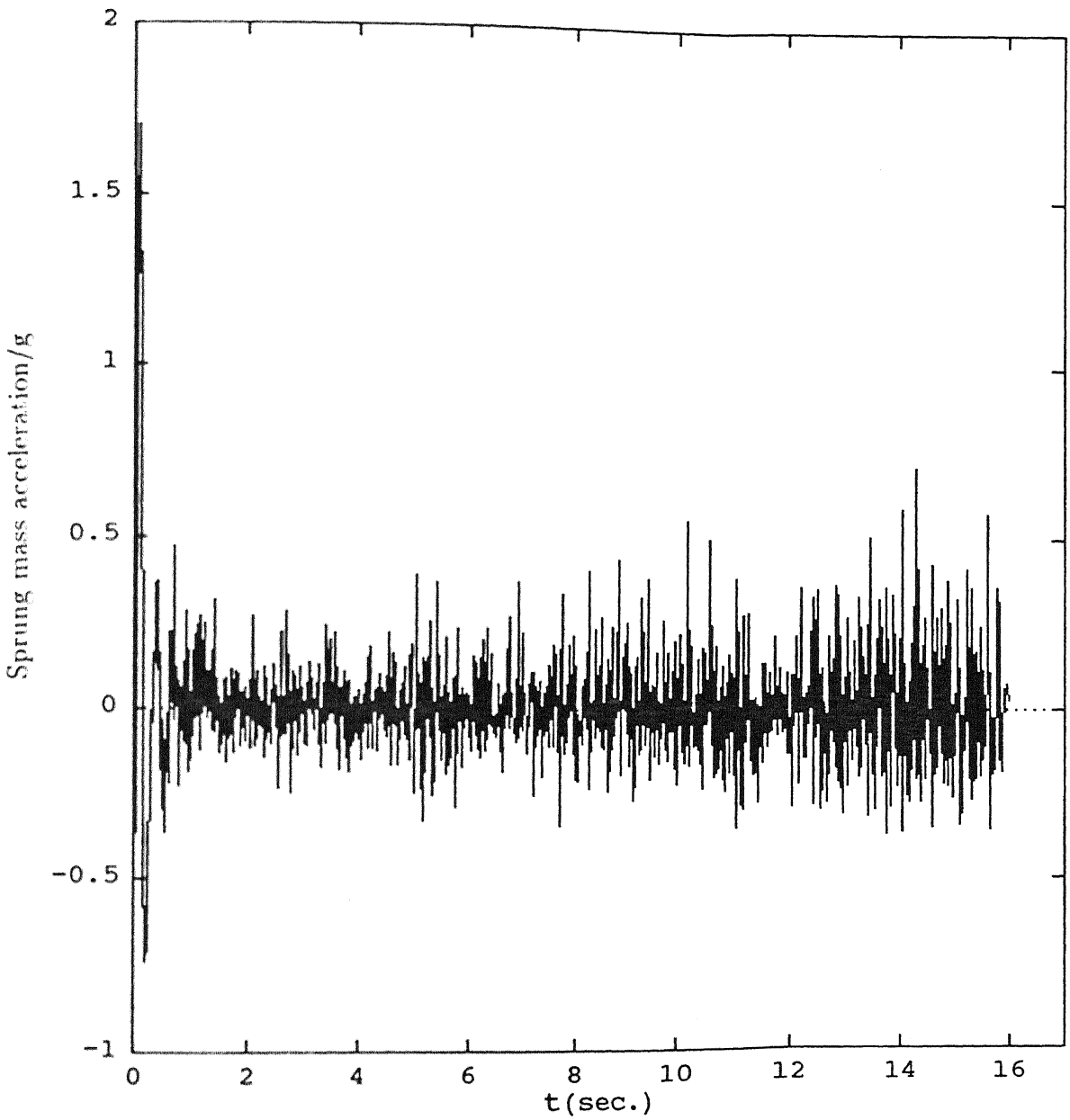

Figure 5.36: Sprung mass acceleration for zero mean runway, Glide velocity=90.67 m/s, Sink velocity=1.0 m/s

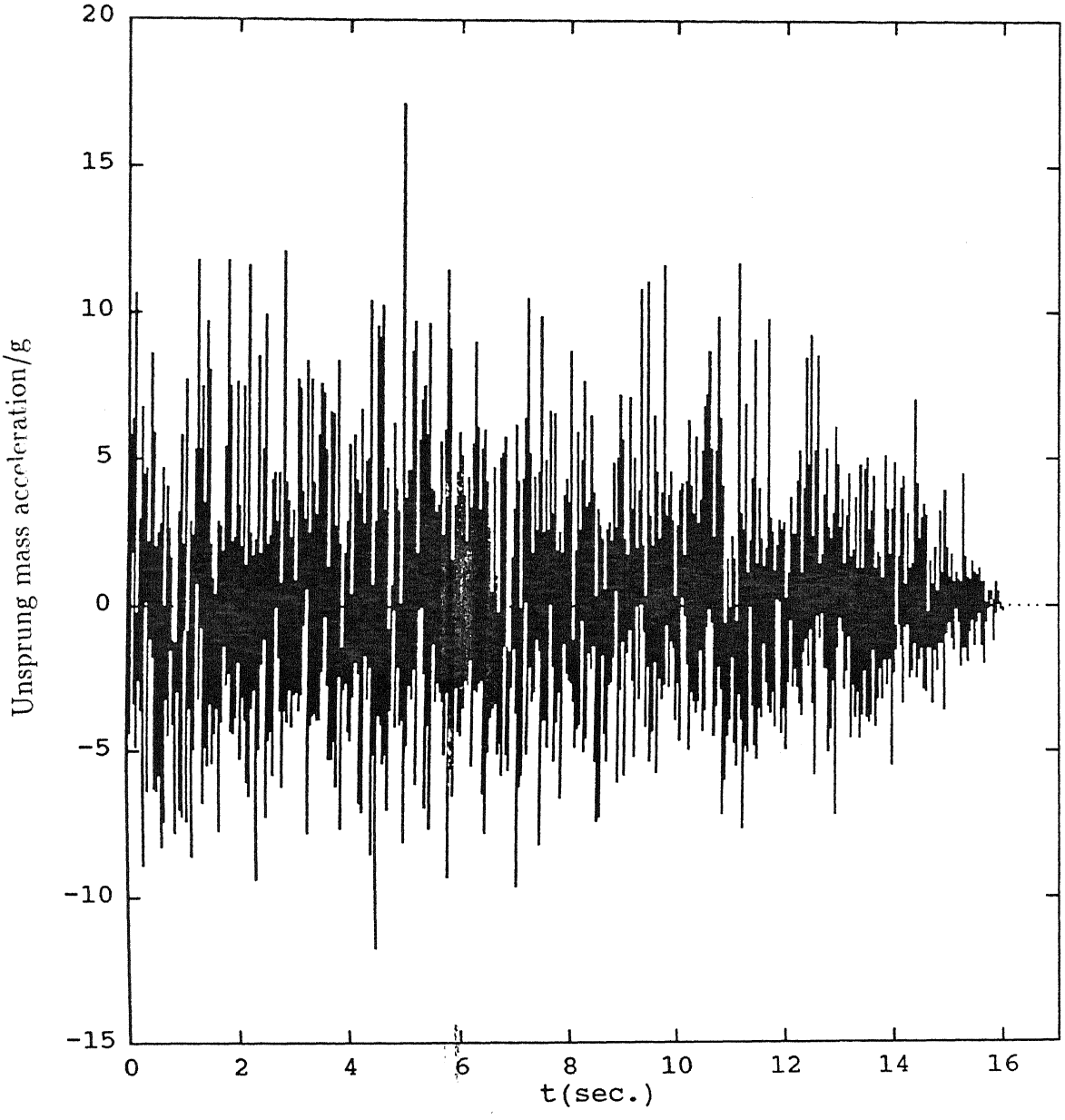

Figure 5.37: Unsprung mass acceleration for zero mean runway, Glide velocity=90.67 m/s, Sink velocity=1.0 m/s

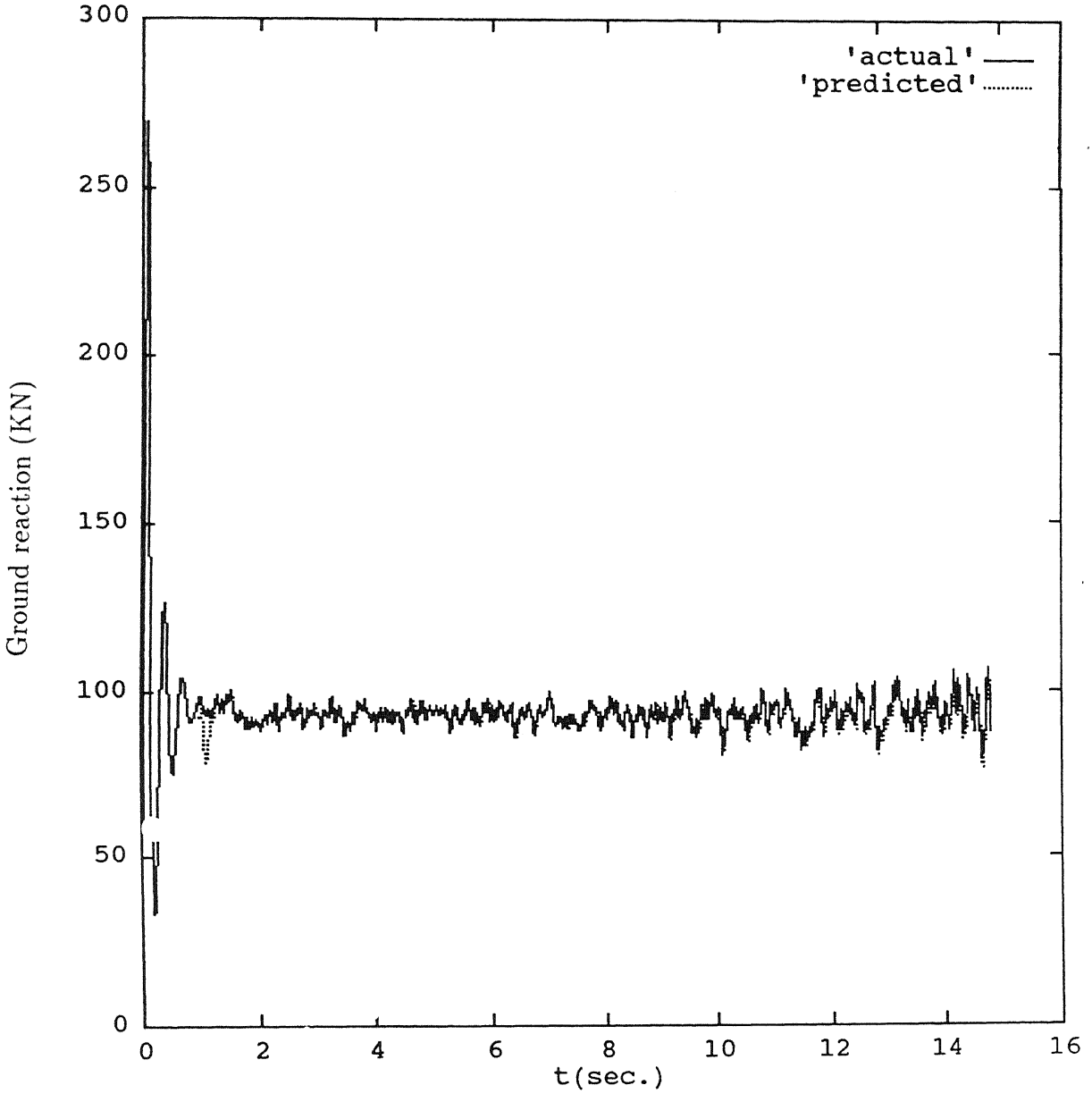

Figure 5.38: Ground Reaction for zero mean runway, Glide velocity=83.12 m/s, Sink velocity=1.0 m/s

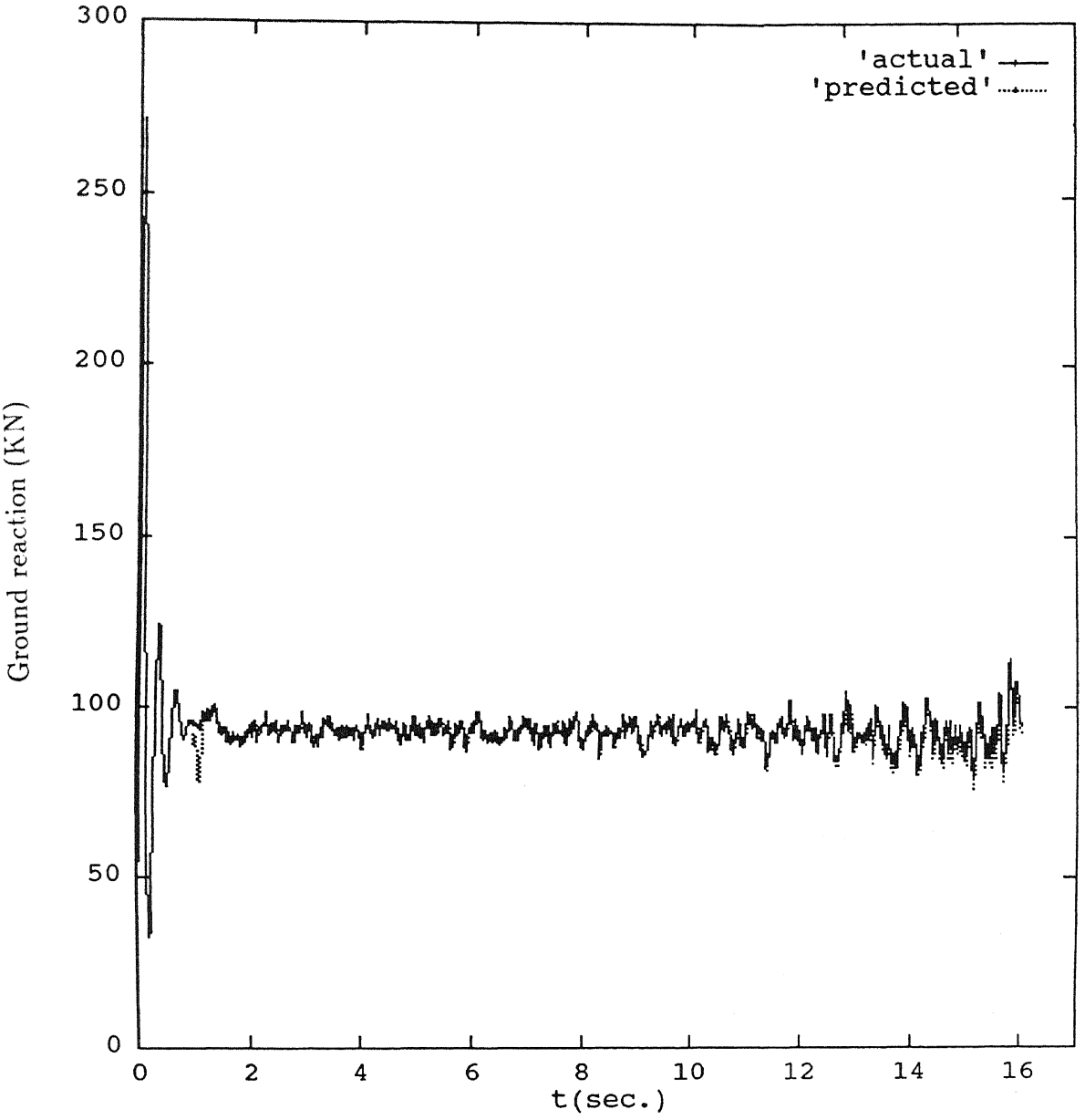

Figure 5.39: Ground Reaction for zero mean runway, Glide velocity=90.67 m/s, Sink velocity=1.0 m/s

There is almost no change in the pattern of aircraft forward velocity as compared to the first case (Fig. 5.40 and 5.41). One variation seen is that with increase in glide velocity stopping time also increases.

5.3.3 Variation in Mean Profile

The track mean profile is varied with the glide and the sink velocities same as in the first case.

The displacement response and velocity response pattern of both the masses do not change in case of inclined and stepped mean profile compared to the flat mean profile (Fig. 5.42 to 5.49).

In case of sinusoidal mean track profile, the peak values are less compared to other mean profiles (Fig. 5.50 to 5.53). Moreover, the frequencies of oscillation of displacement and velocity responses of both the masses have increased in this case. There is a sudden increase in amplitude of the responses towards the end of the curve. This may be due to the resonance occurring as a result of matching the frequency of sinusoidal track with the frequency of oscillation at that instant of time.

No change in the sprung mass acceleration pattern is observed in the inclined and the stepped mean profile compared to the flat mean profile (Fig. 5.54 and 5.55). However, the amplitude of vibration is increased in case of sinusoidal mean track profile (Fig. 5.56).

The amplitude of vibration of unsprung mass acceleration is decreased in inclined mean profile (Fig. 5.57), but is increased in stepped and sinusoidal mean profile (Fig. 5.58 and 5.59).

Due to lower peak values of unsprung mass displacement response over sinusoidal mean profile, the ground reaction also has lower peak values compared to other mean profiles (Fig. 5.60 to 5.62). The prediction is also poorer in sinusoidal mean profile compared to inclined, stepped and flat mean profile.

The stopping time of the aircraft is almost the same in all the track profiles (Fig. 5.63 to 5.65), resulting in almost equal ground distances.

The variation of stopping time and ground distance as a function of different system parameters is shown in table 5.3. The expected landing ground roll for the aircraft used in this study is 740 m. In the present work, it is found to vary from 480.4 m for glide velocity 75.56 m/s and sink velocity 3.0 m/s to 664.1 m for glide velocity 90.67 m/s and sink velocity 1.0 m/s.

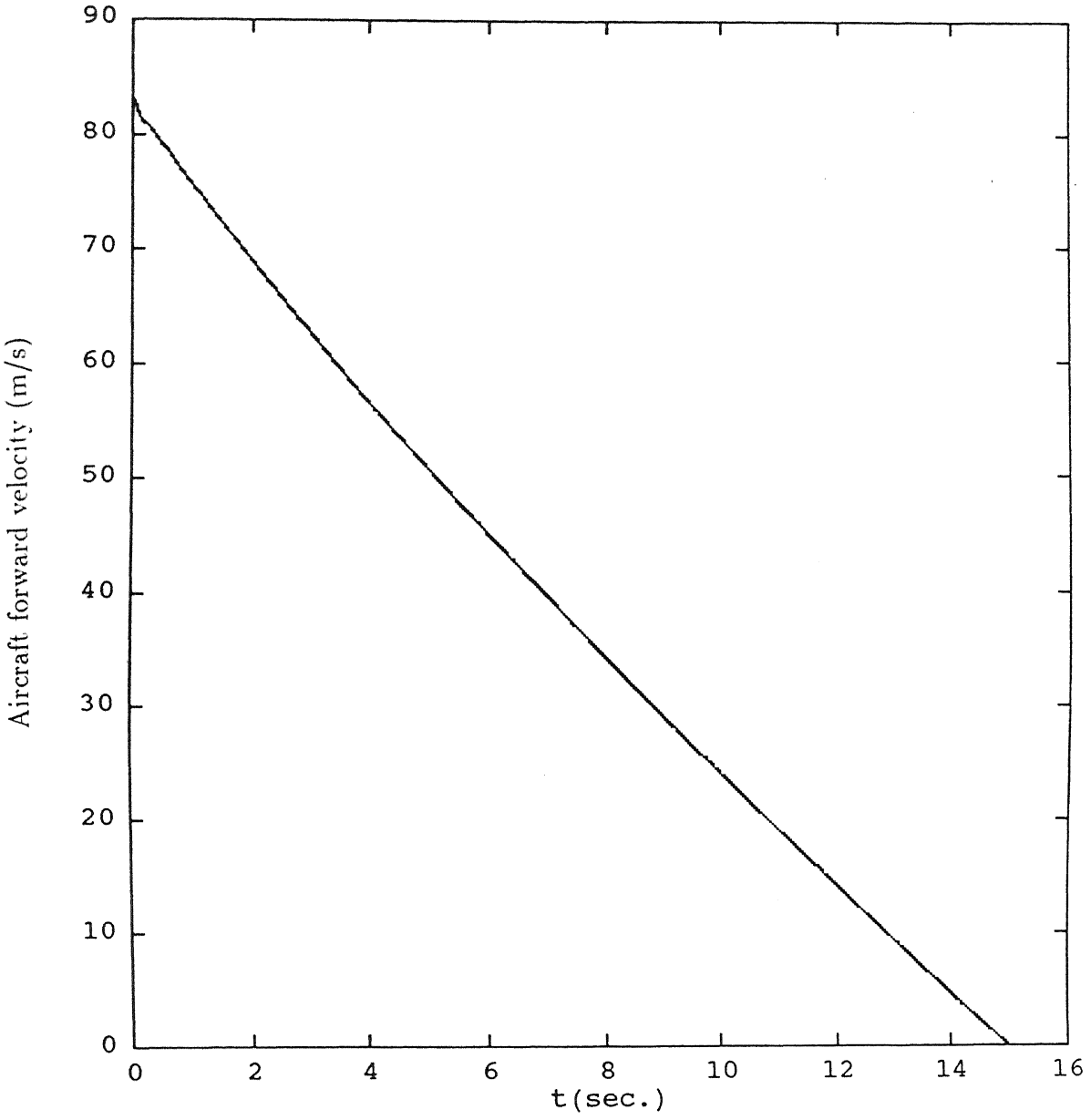

Figure 5.40: Aircraft forward velocity for zero mean runway, Glide velocity=83.12 m/s, Sink velocity=1.0 m/s

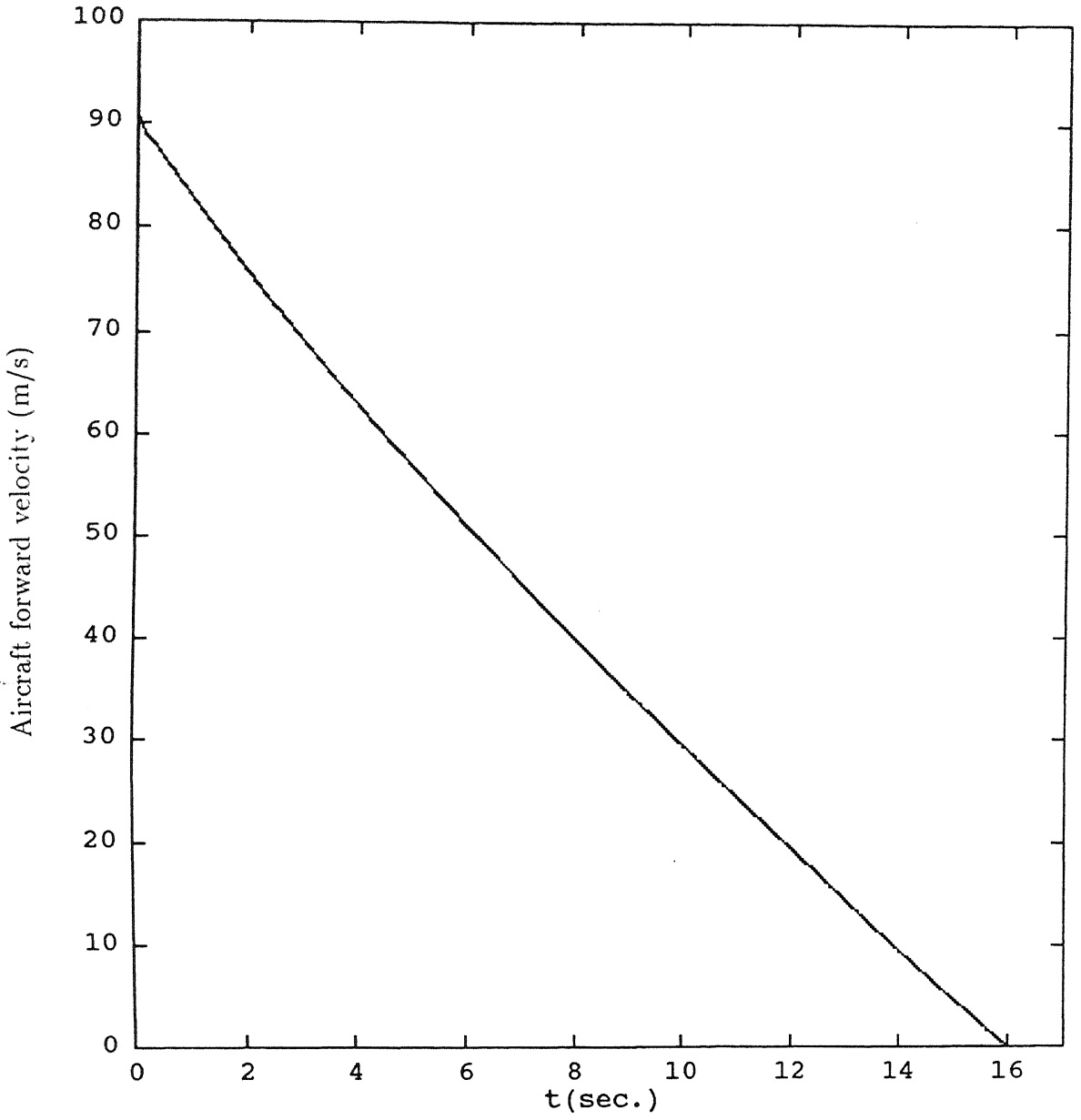

Figure 5.41: Aircraft forward velocity for zero mean runway, Glide velocity=90.67 m/s, Sink velocity=1.0 m/s

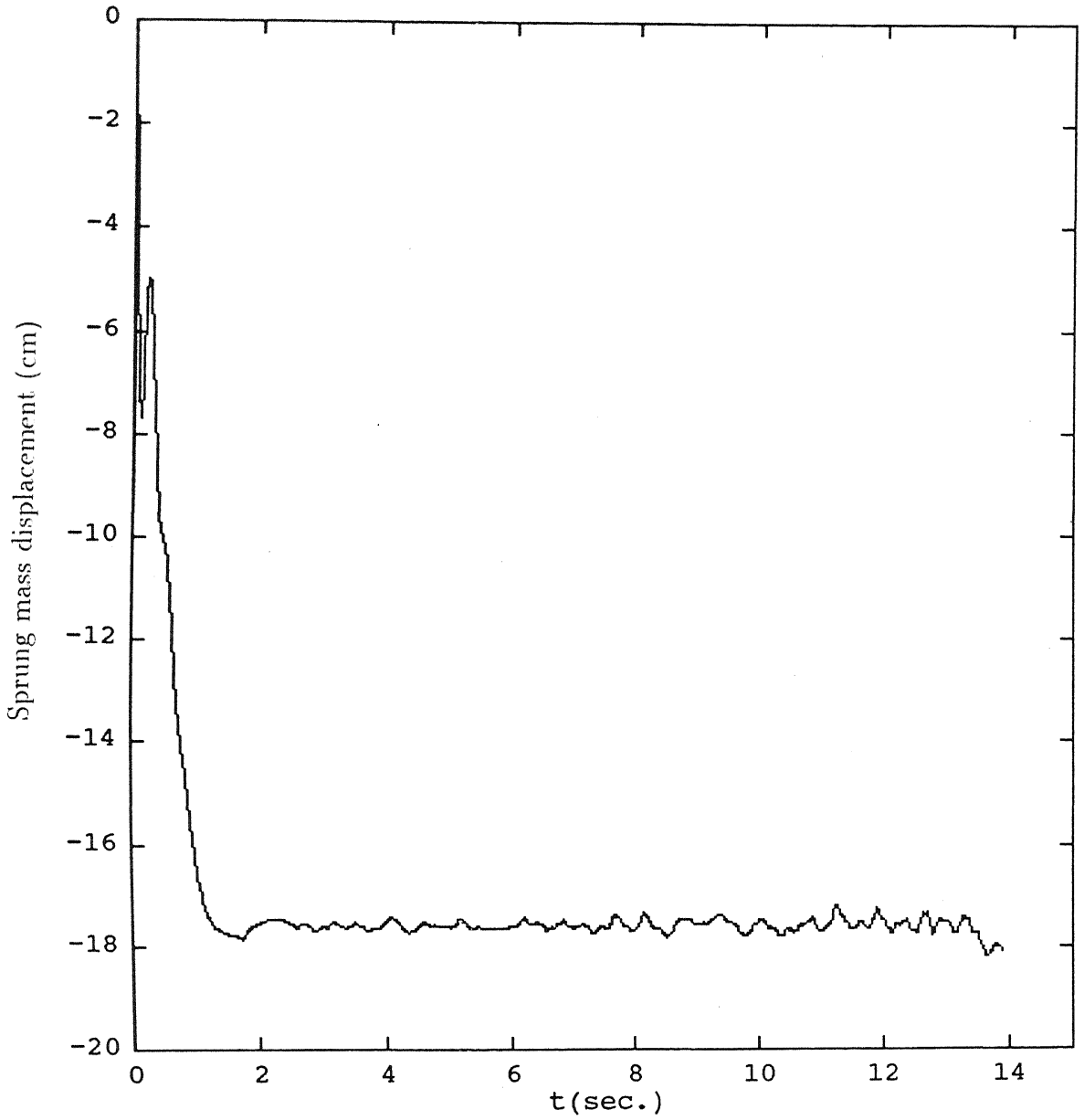

Figure 5.42: Sprung mass displacement for inclined runway, Glide velocity=75.56 m/s, Sink velocity=1.0 m/s

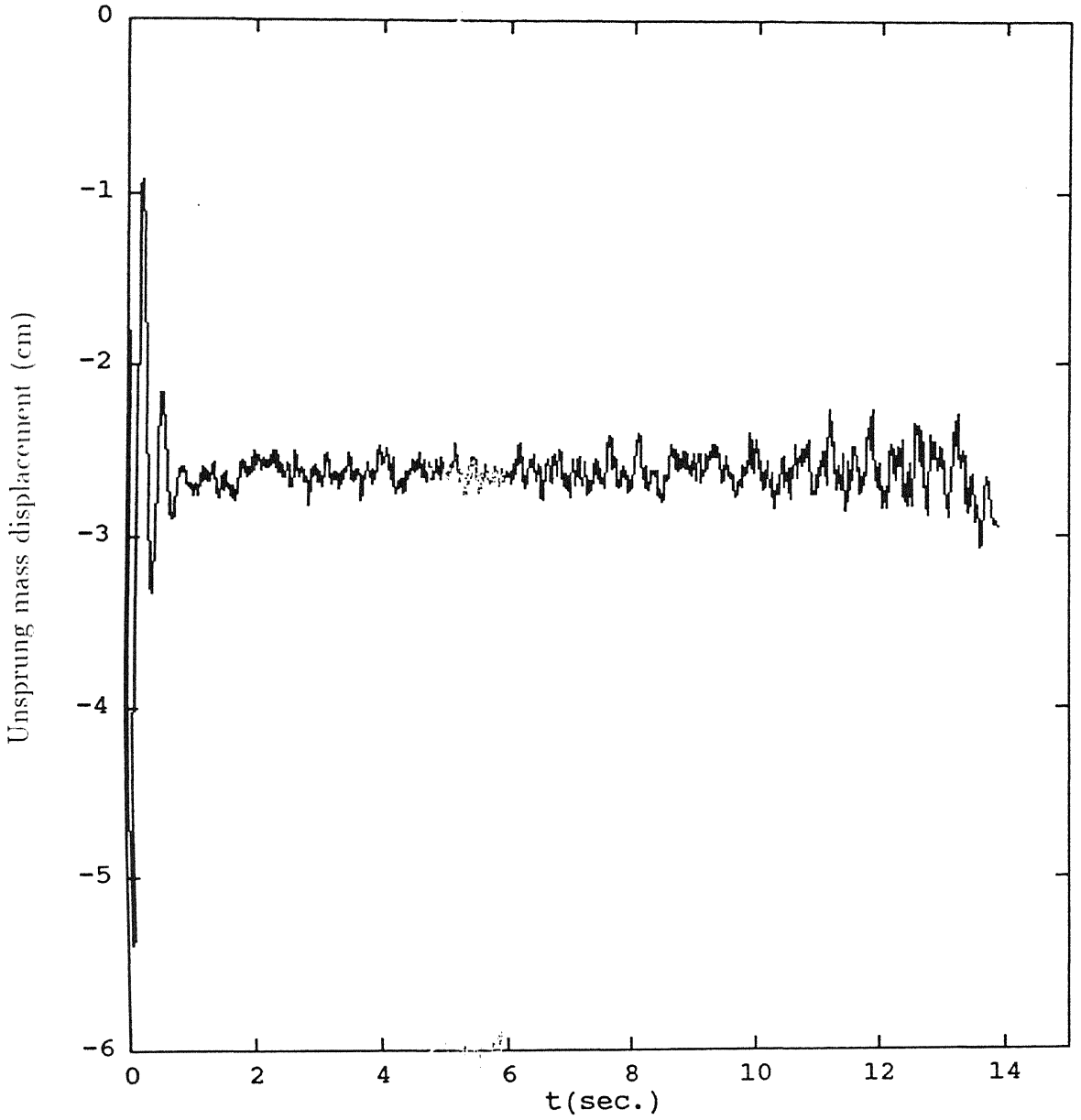

Figure 5.43: Unsprung mass displacement for inclined runway, Glide velocity=75.56 m/s, Sink velocity=1.0 m/s

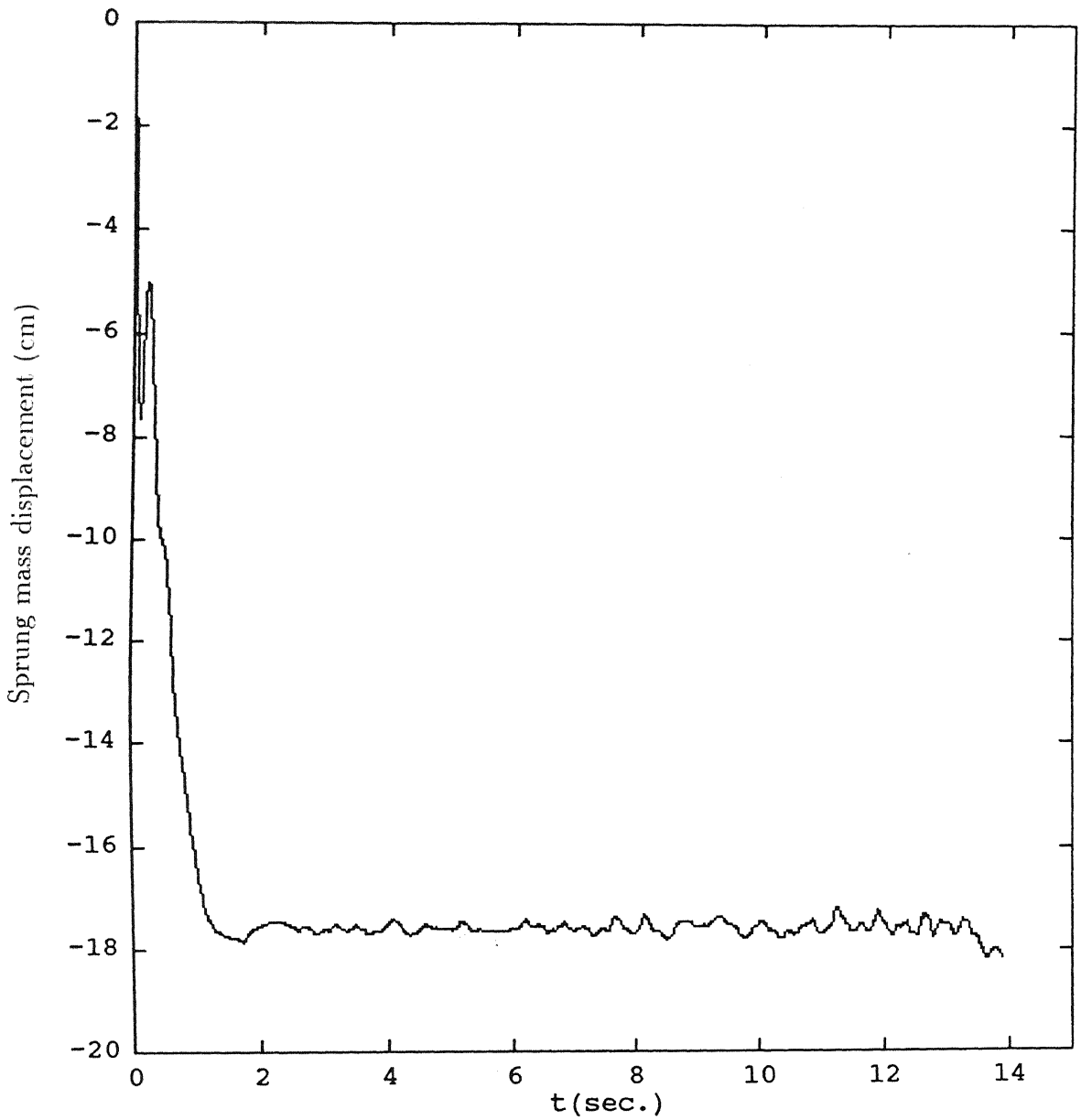

Figure 5.44: Sprung mass displacement for stepped runway, Glide velocity=75.56 m/s, Sink velocity=1.0 m/s

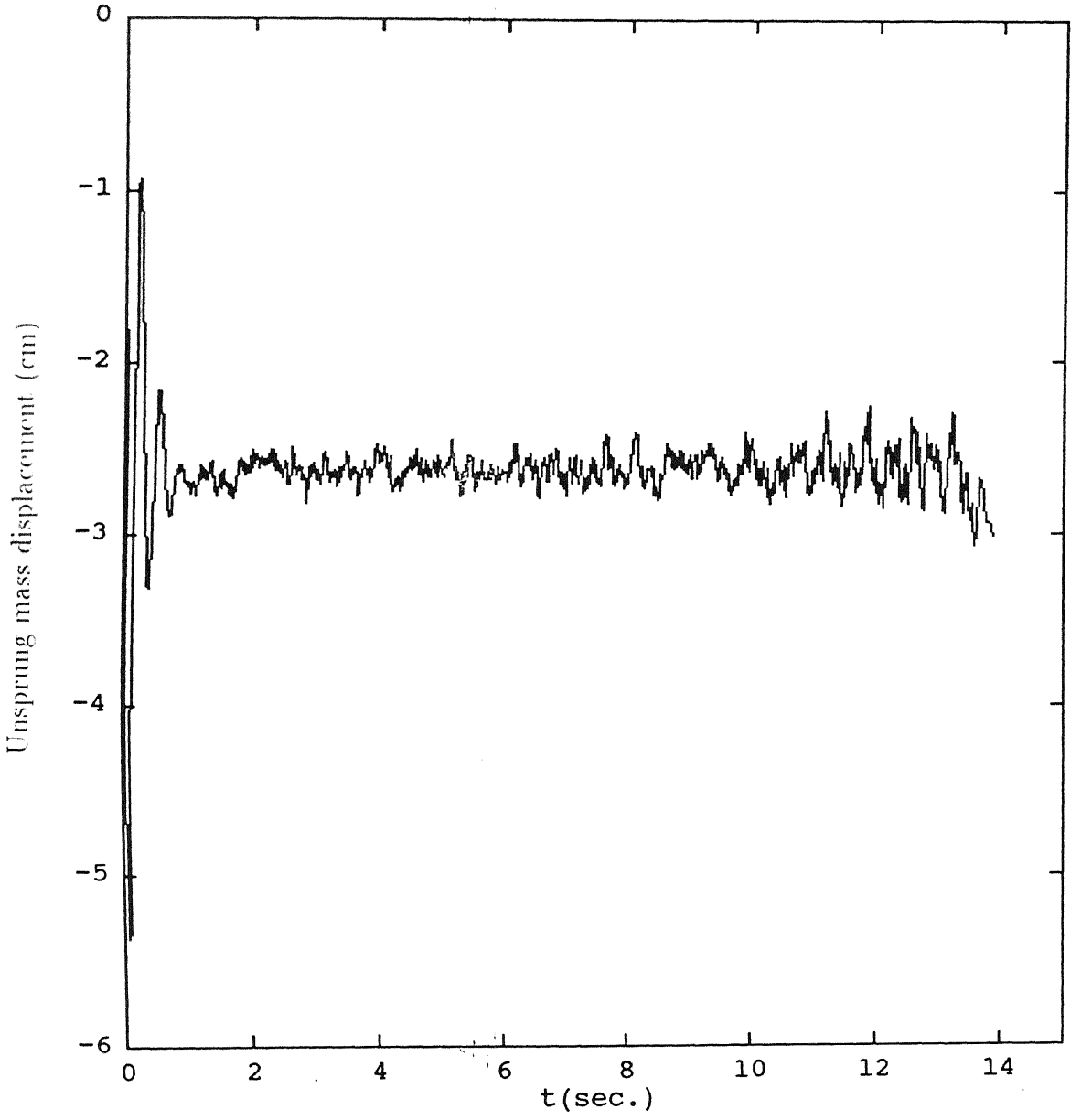

Figure 5.45: Unsprung mass displacement for stepped runway, Glide velocity=75.56 m/s, Sink velocity=1.0 m/s

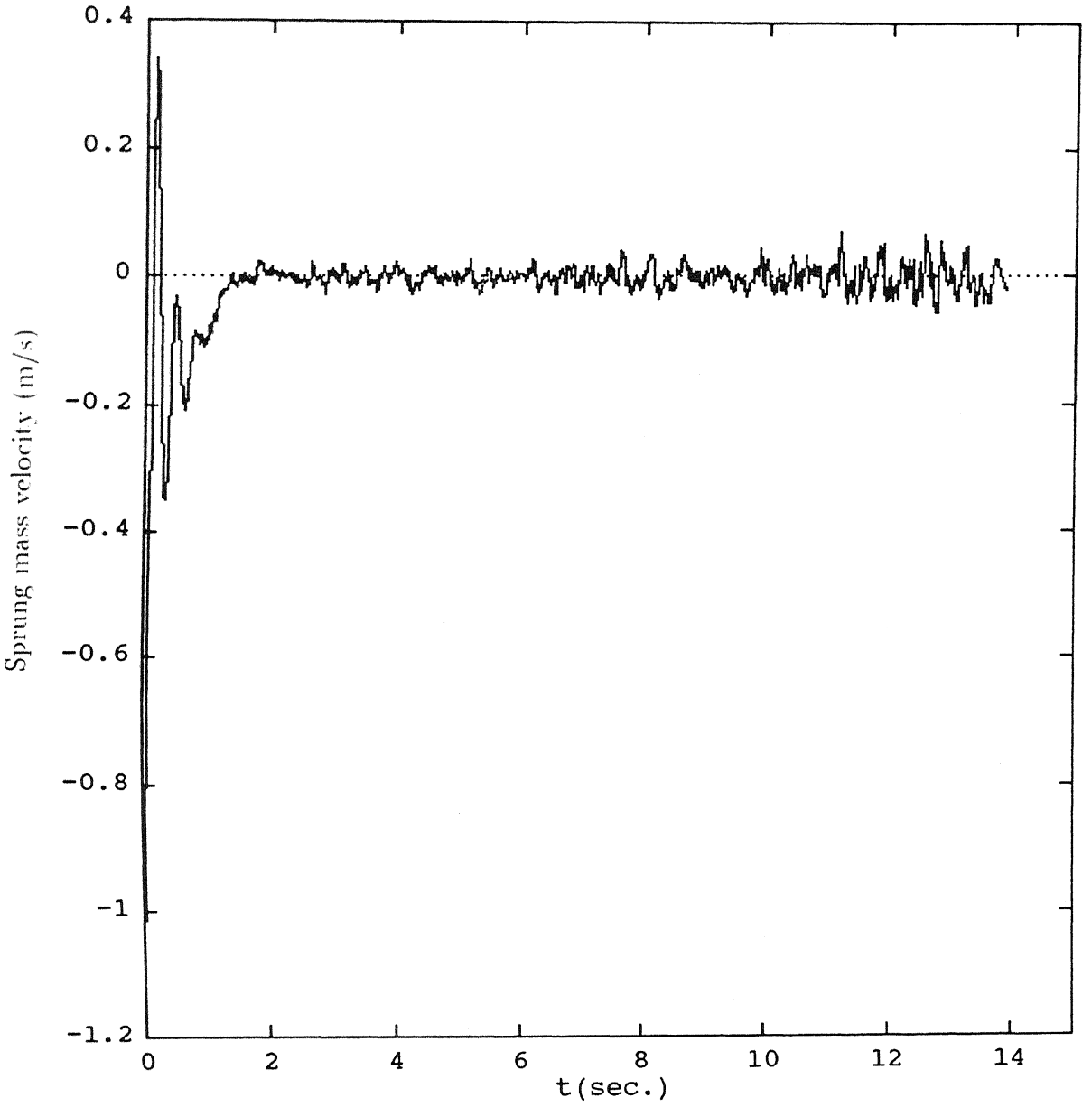

Figure 5.46: Sprung mass velocity for inclined runway, Glide velocity=75.56 m/s, Sink velocity=1.0 m/s

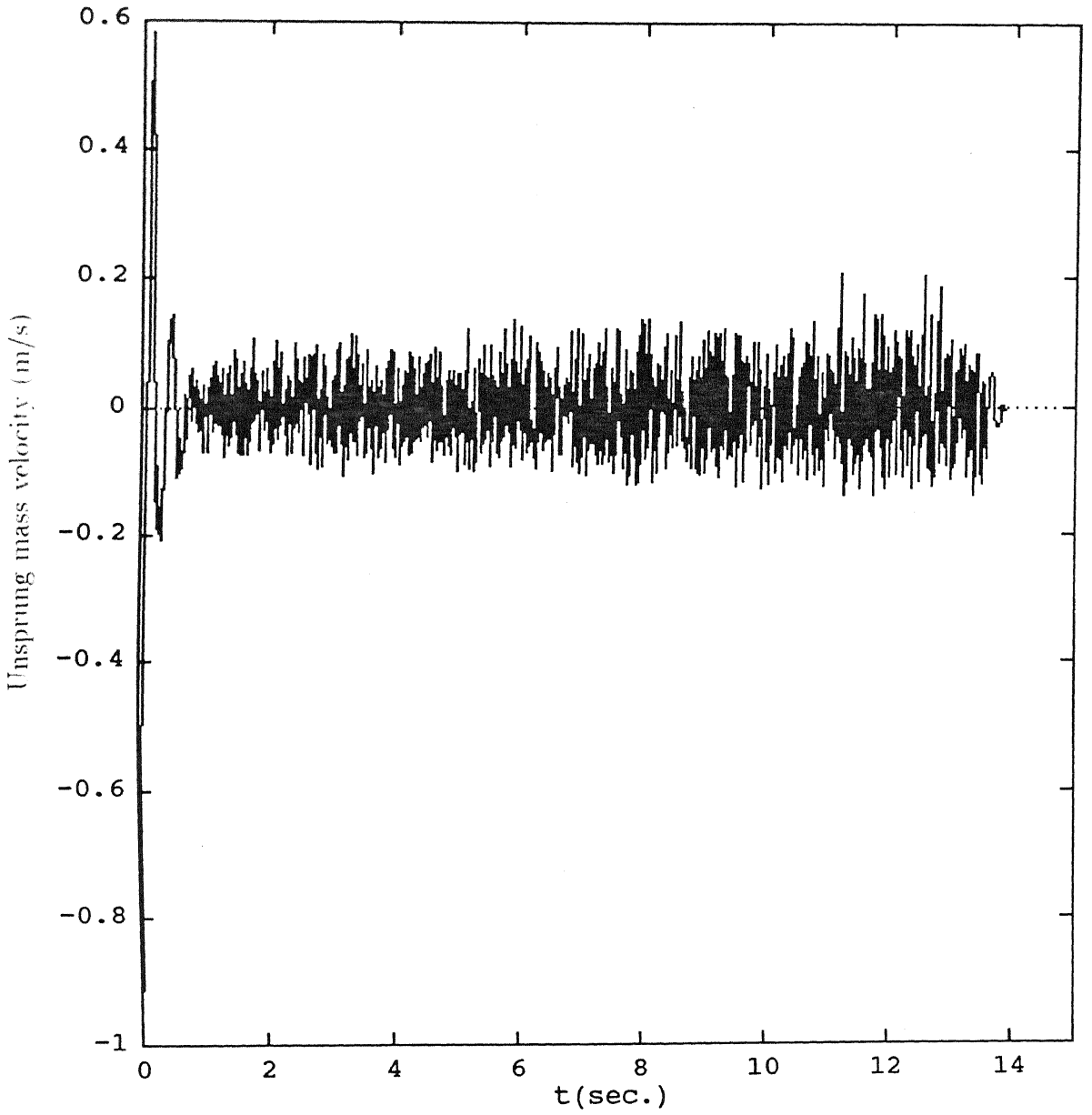

Figure 5.47: Unsprung mass velocity for inclined runway, Glide velocity=75.56 m/s, Sink velocity=1.0 m/s

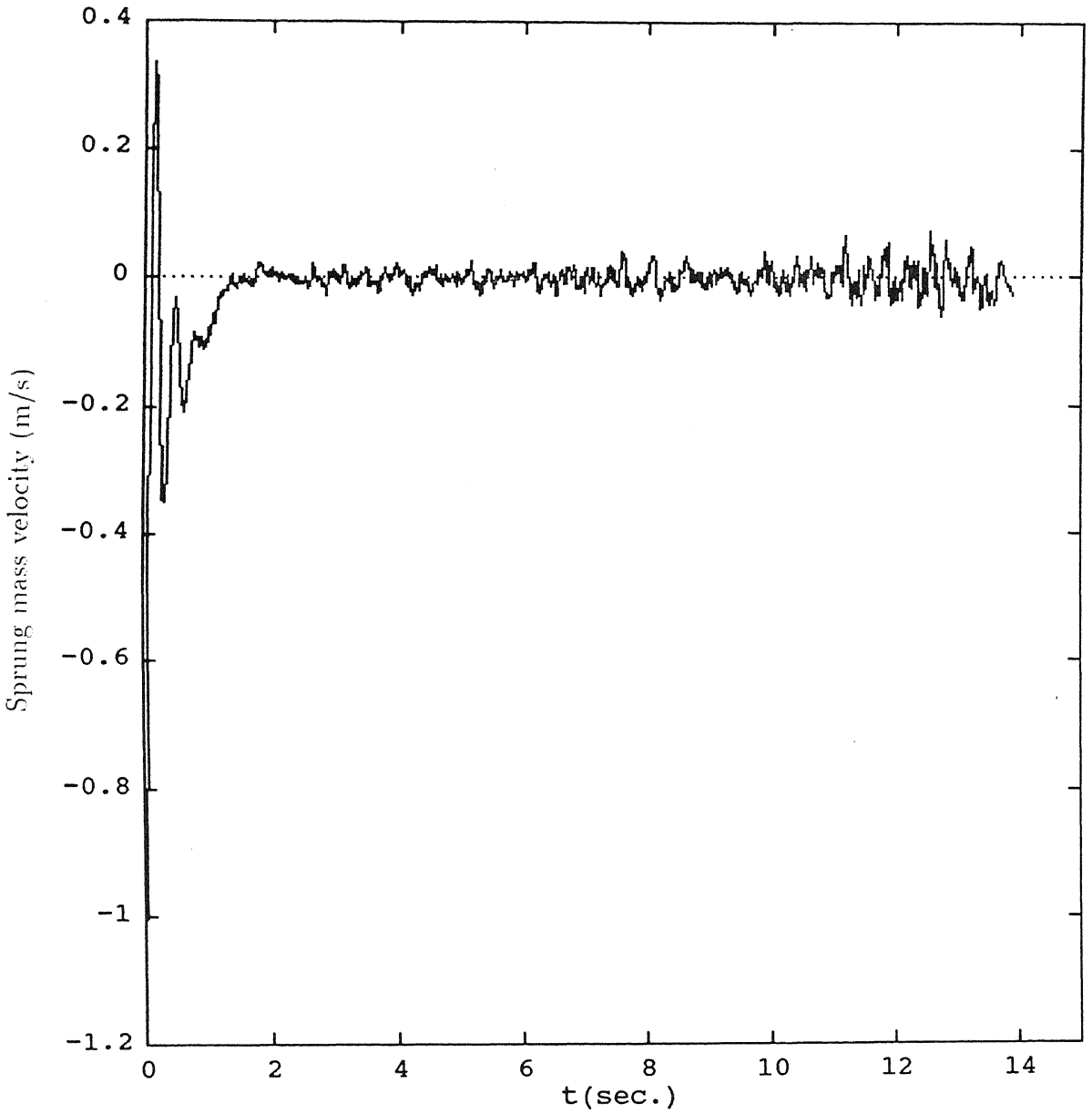

Figure 5.48: Sprung mass velocity for stepped runway, Glide velocity=75.56 m/s, Sink velocity=1.0 m/s

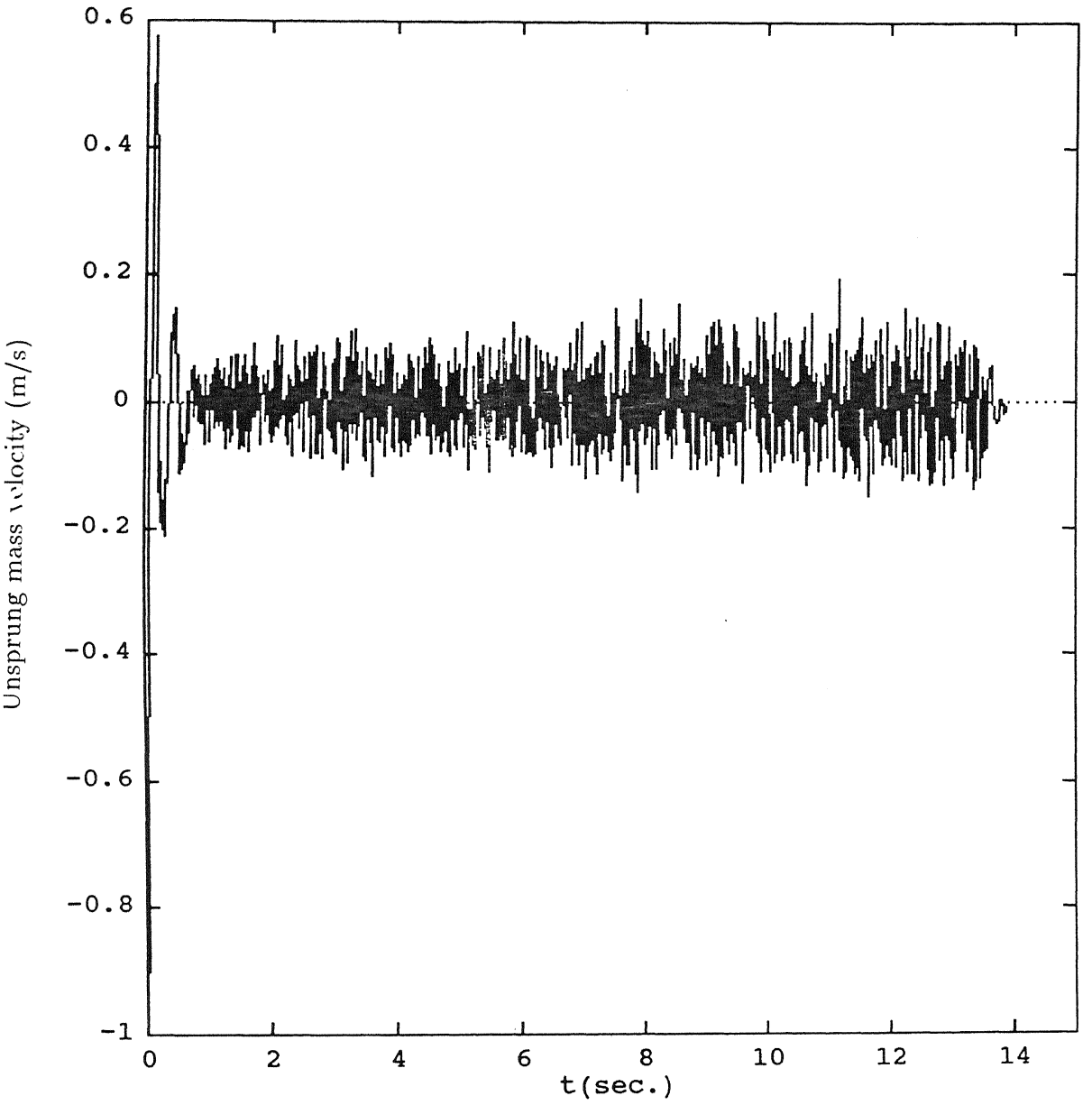

Figure 5.49: Unsprung mass velocity for stepped runway, Glide velocity=75.56 m/s, Sink velocity=1.0 m/s

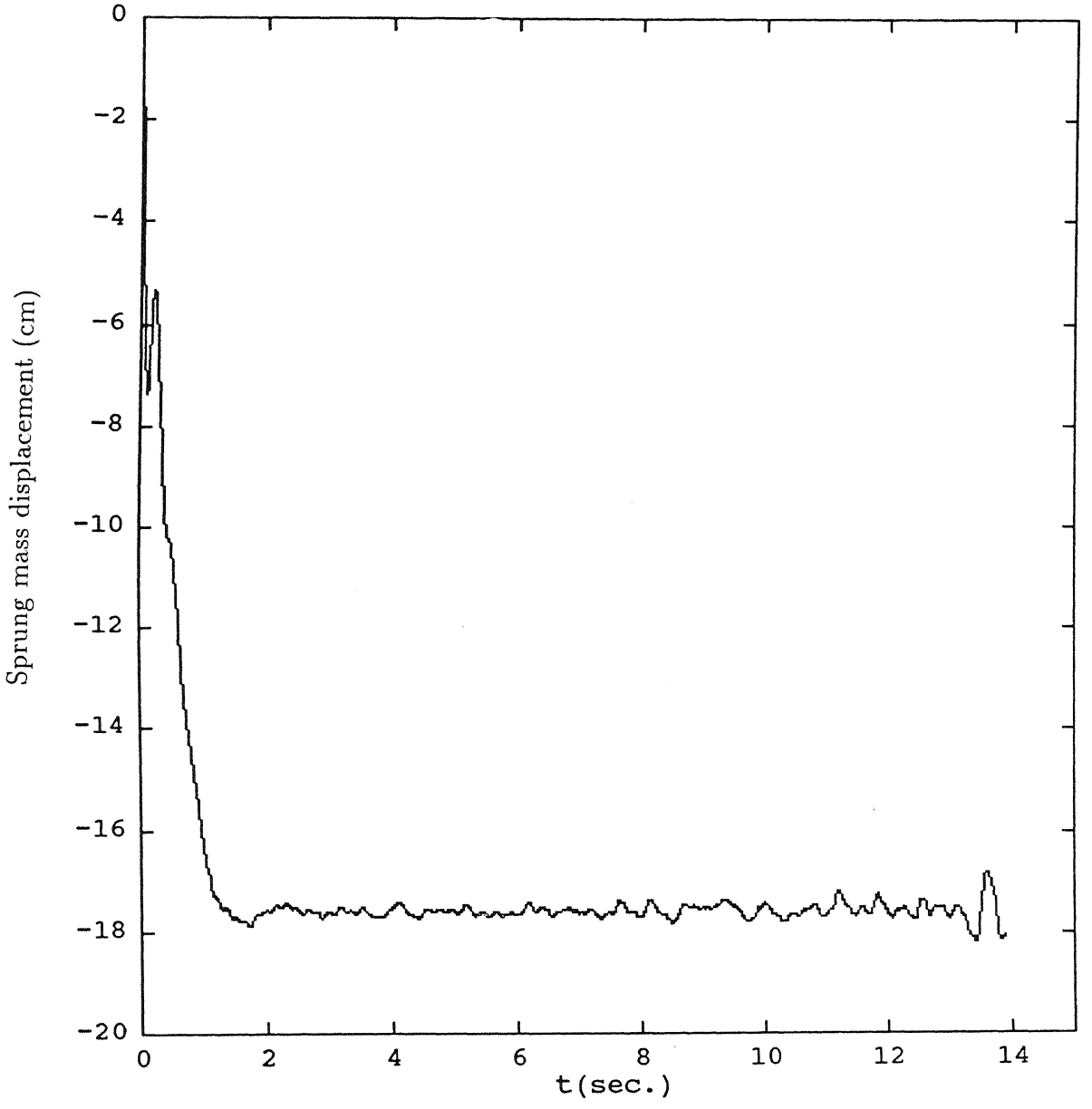

Figure 5.50: Sprung mass displacement for sinusoidal runway, Glide velocity=75.56 m/s, Sink velocity=1.0 m/s

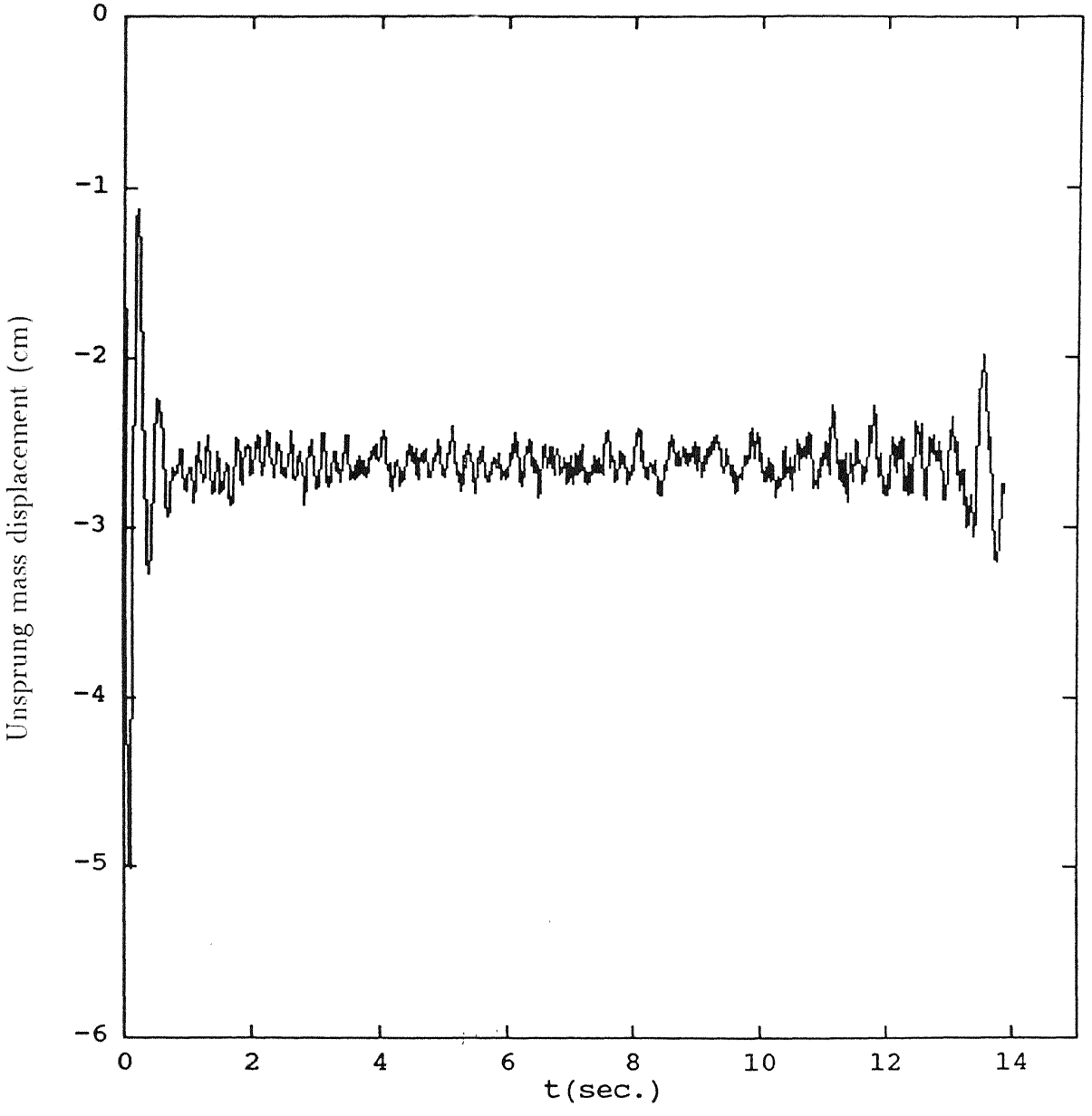

Figure 5.51: Unsprung mass displacement for sinusoidal runway, Glide velocity=75.56 m/s, Sink velocity=1.0 m/s

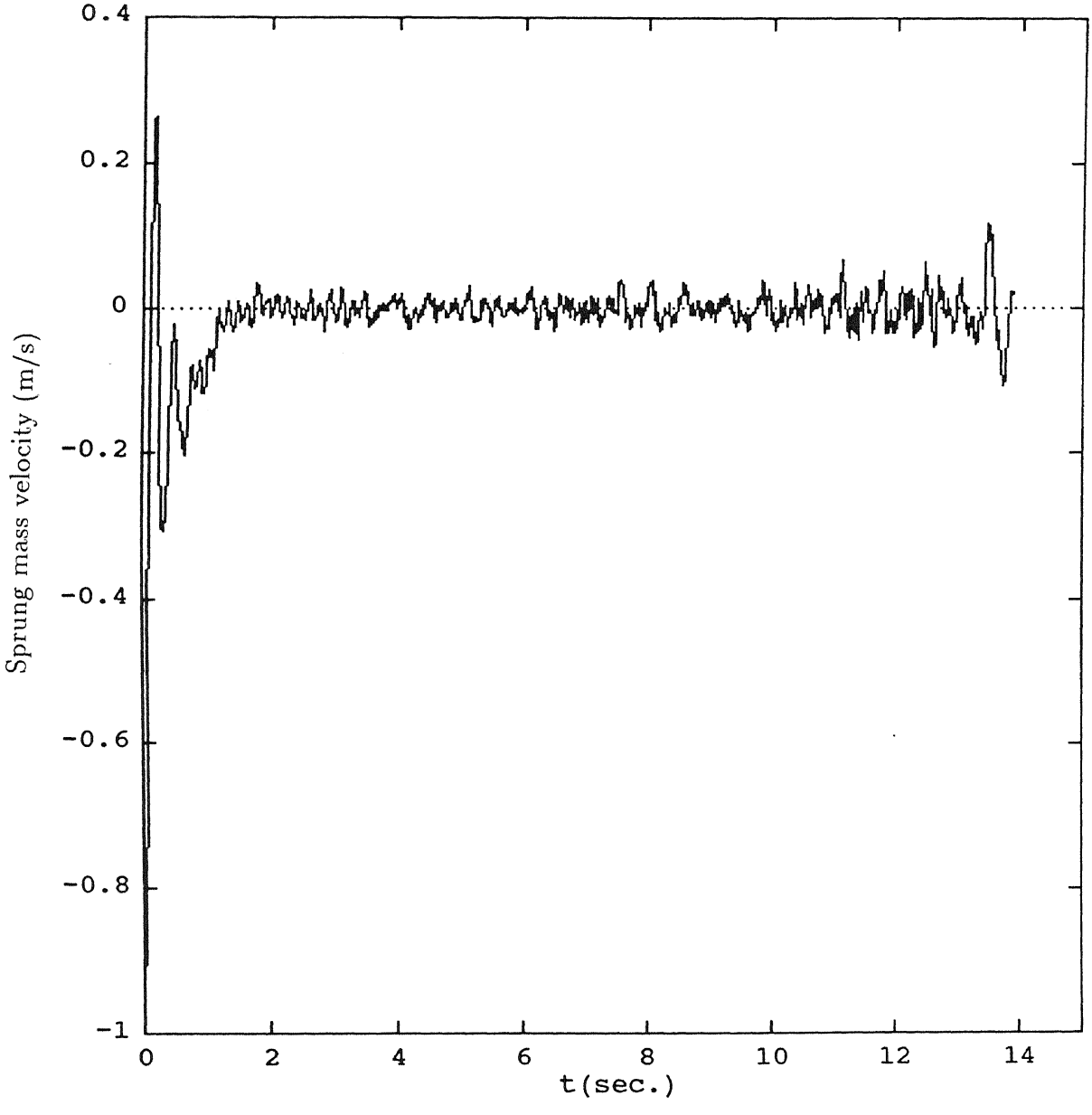

Figure 5.52: Sprung mass velocity for sinusoidal runway, Glide velocity=75.56 m/s, Sink velocity=1.0 m/s

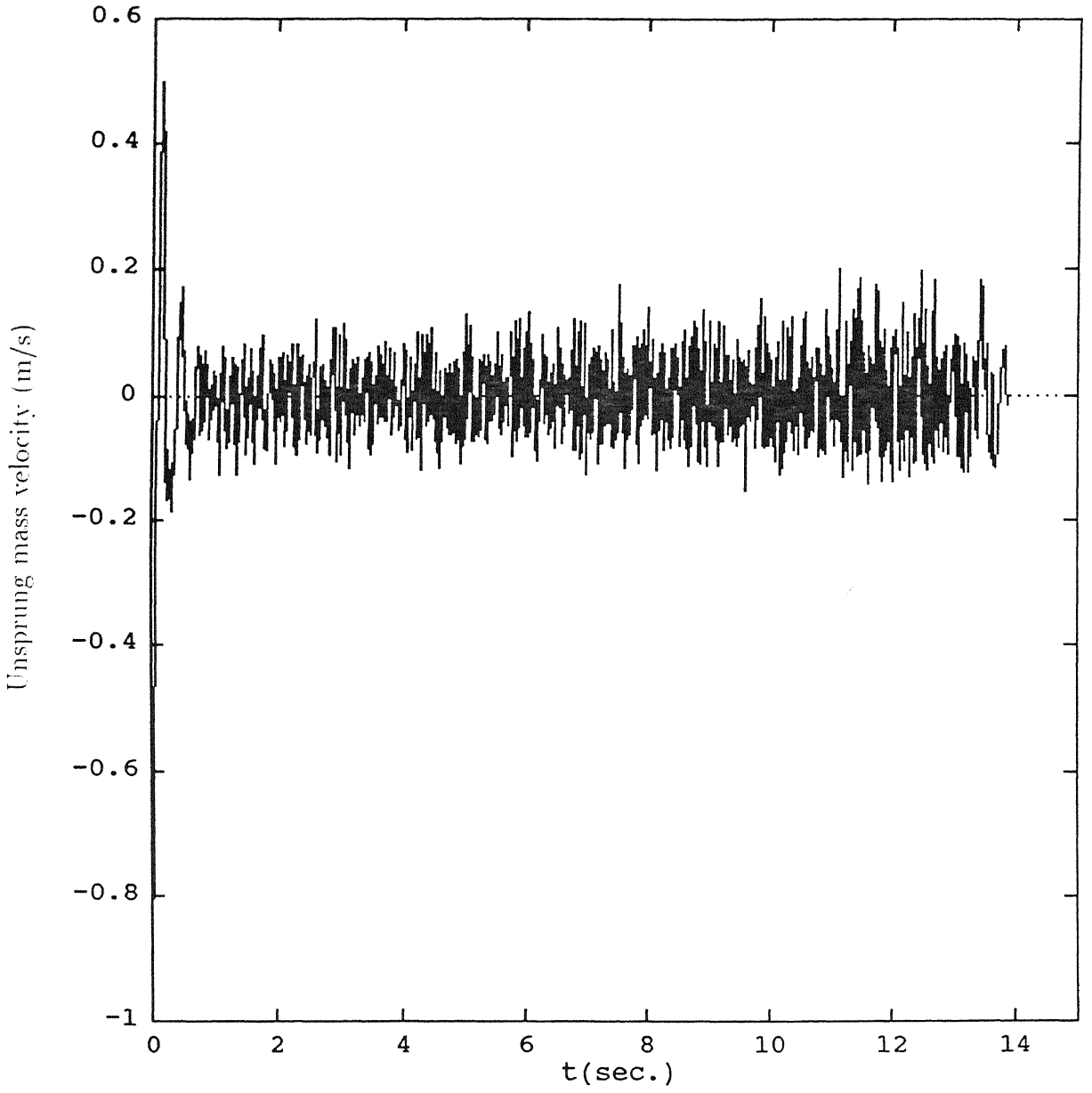

Figure 5.53: Unsprung mass velocity for sinusoidal runway, Glide velocity=75.56 m/s, Sink velocity=1.0 m/s

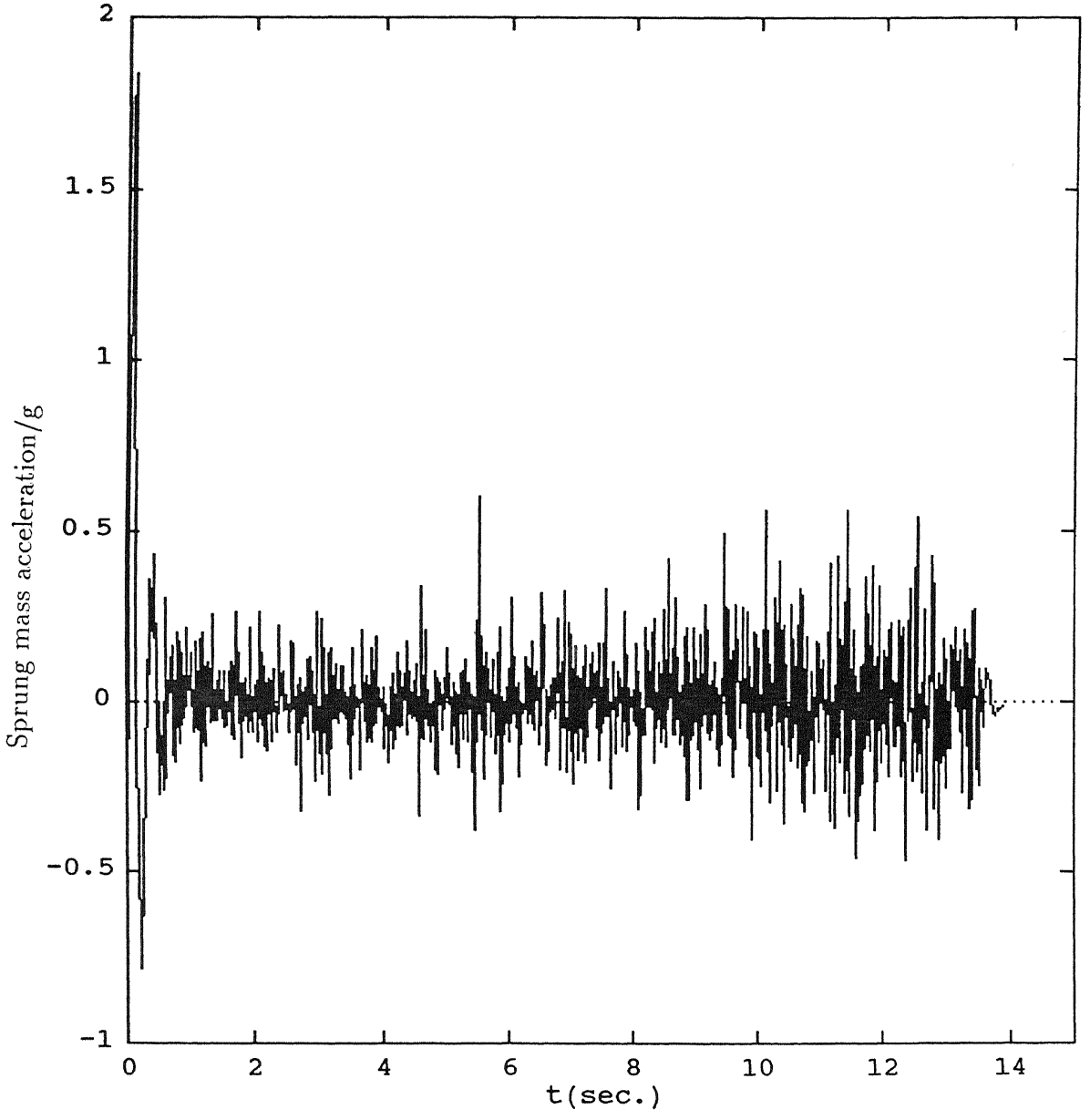

Figure 5.54: Sprung mass acceleration for inclined runway, Glide velocity=75.56 m/s, Sink velocity=1.0 m/s

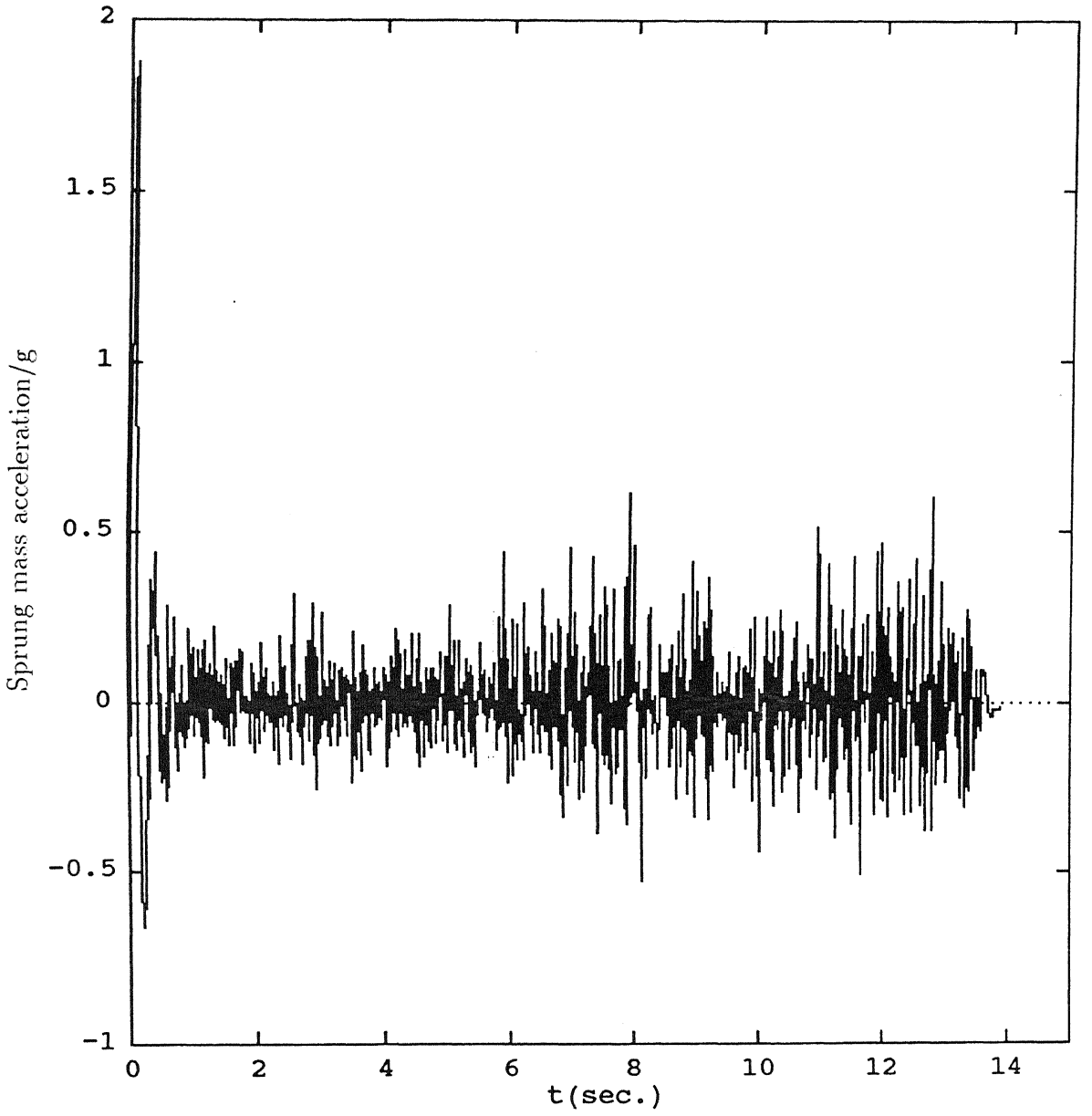

Figure 5.55: Sprung mass acceleration for stepped runway, Glide velocity=75.56 m/s, Sink velocity=1.0 m/s

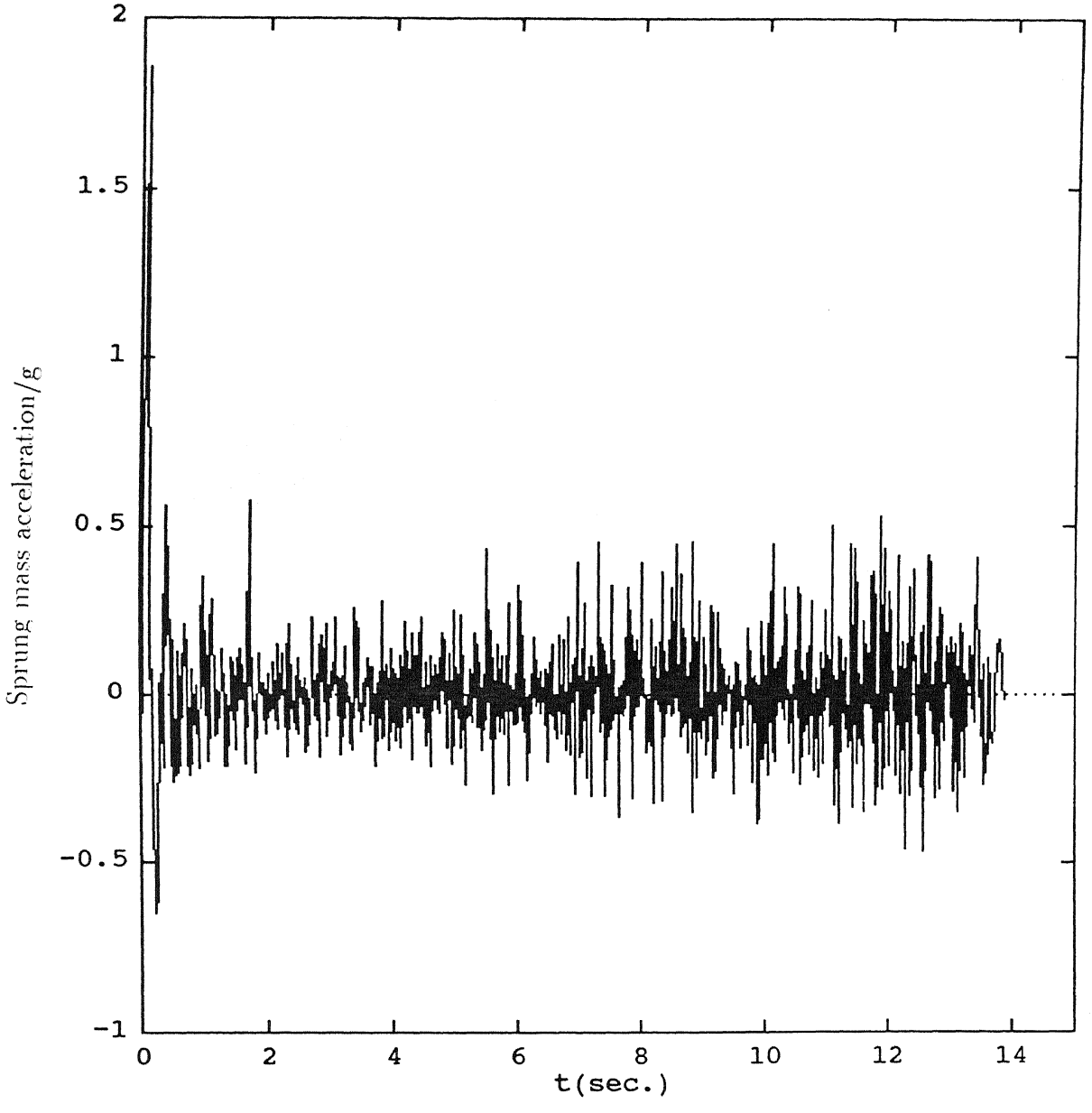

Figure 5.56: Sprung mass acceleration for sinusoidal runway, Glide velocity=75.56 m/s, Sink velocity=1.0 m/s

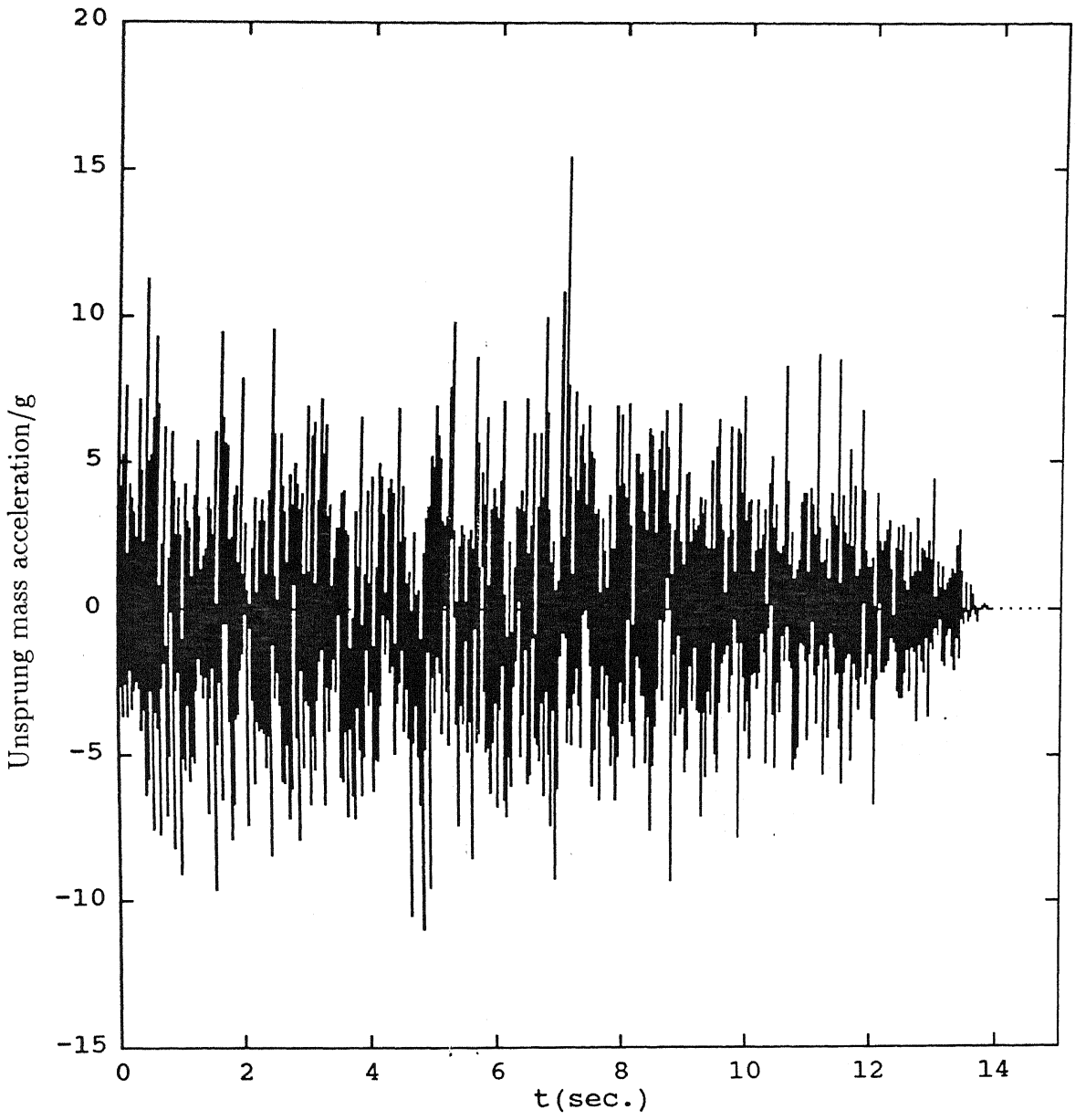

Figure 5.57: Unsprung mass acceleration for inclined runway, Glide velocity=75.56 m/s, Sink velocity=1.0 m/s

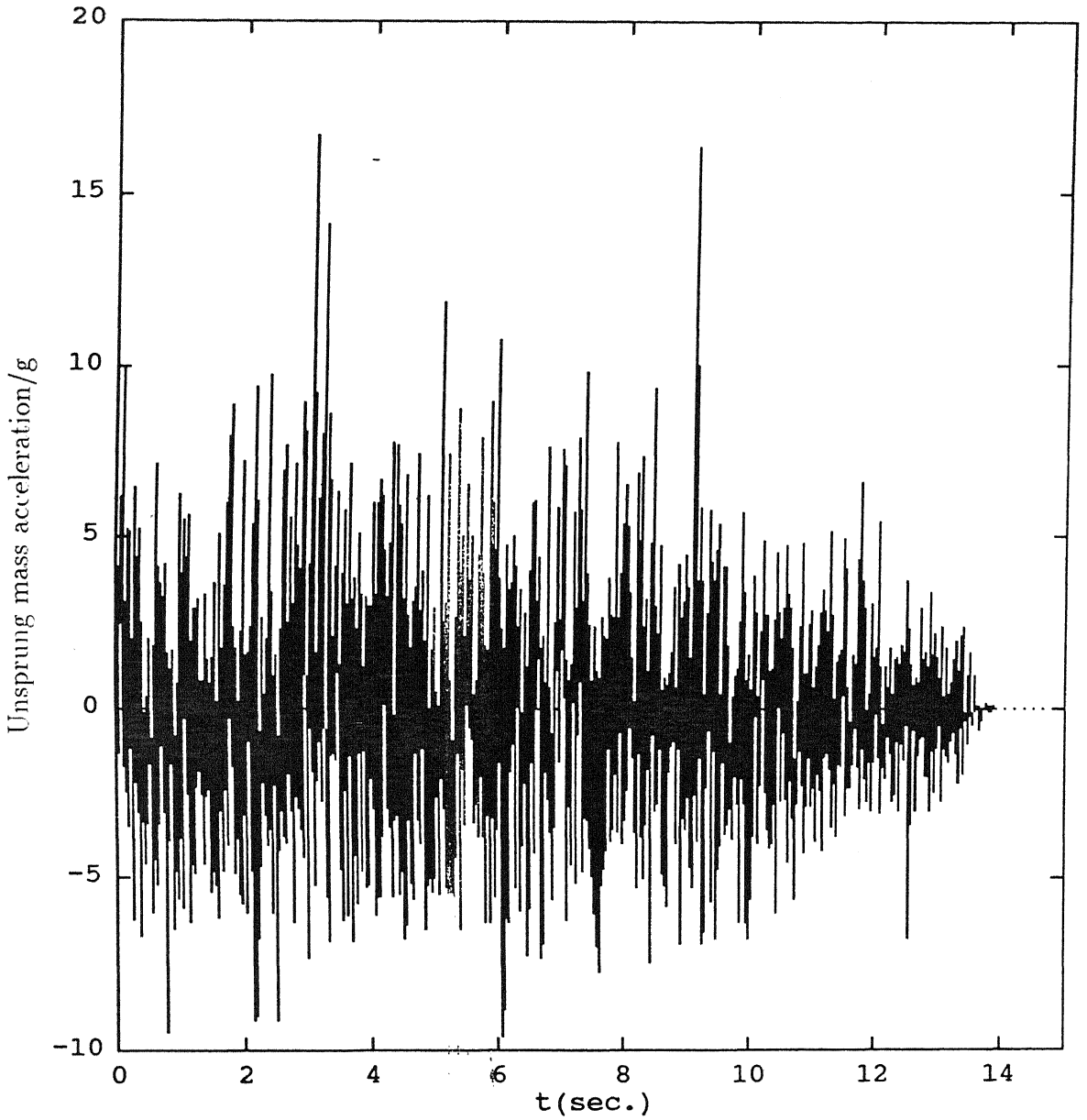

Figure 5.58: Unsprung mass acceleration for stepped runway, Glide velocity=75.56 m/s, Sink velocity=1.0 m/s

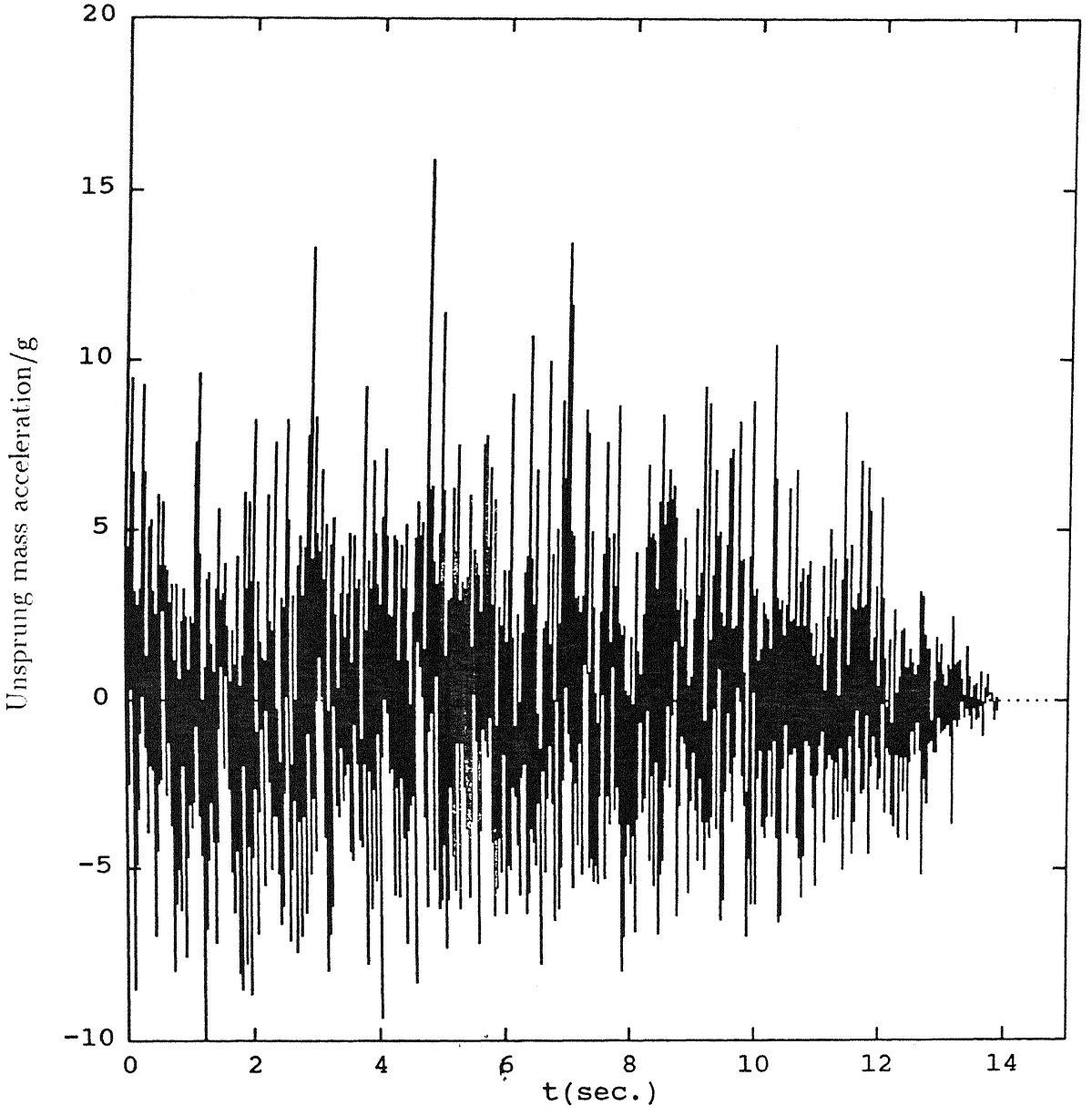

Figure 5.59: Unsprung mass acceleration for sinusoidal runway, Glide velocity=75.56 m/s, Sink velocity=1.0 m/s

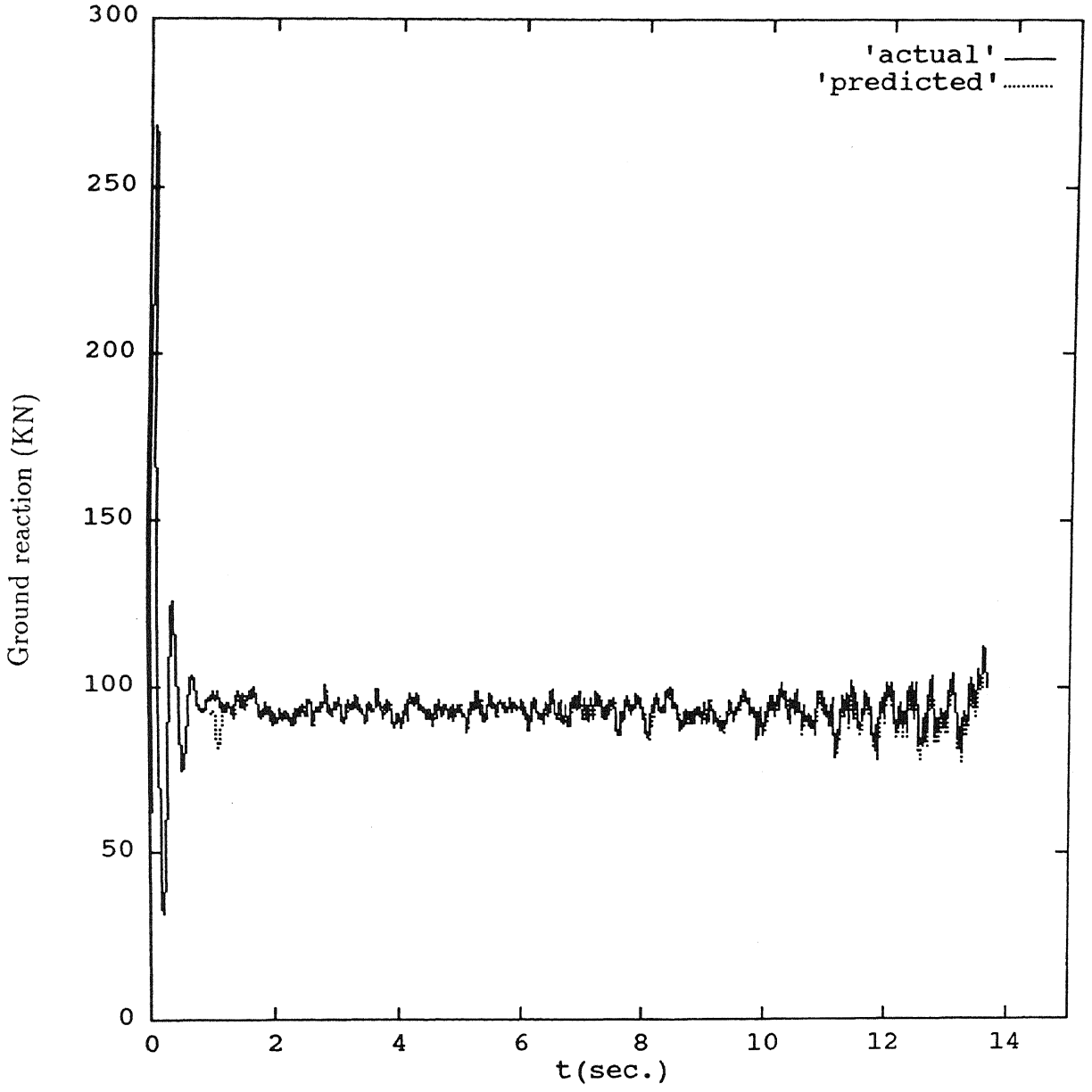

Figure 5.60: Ground Reaction for inclined runway, Glide velocity=75.56 m/s, Sink velocity=1.0 m/s

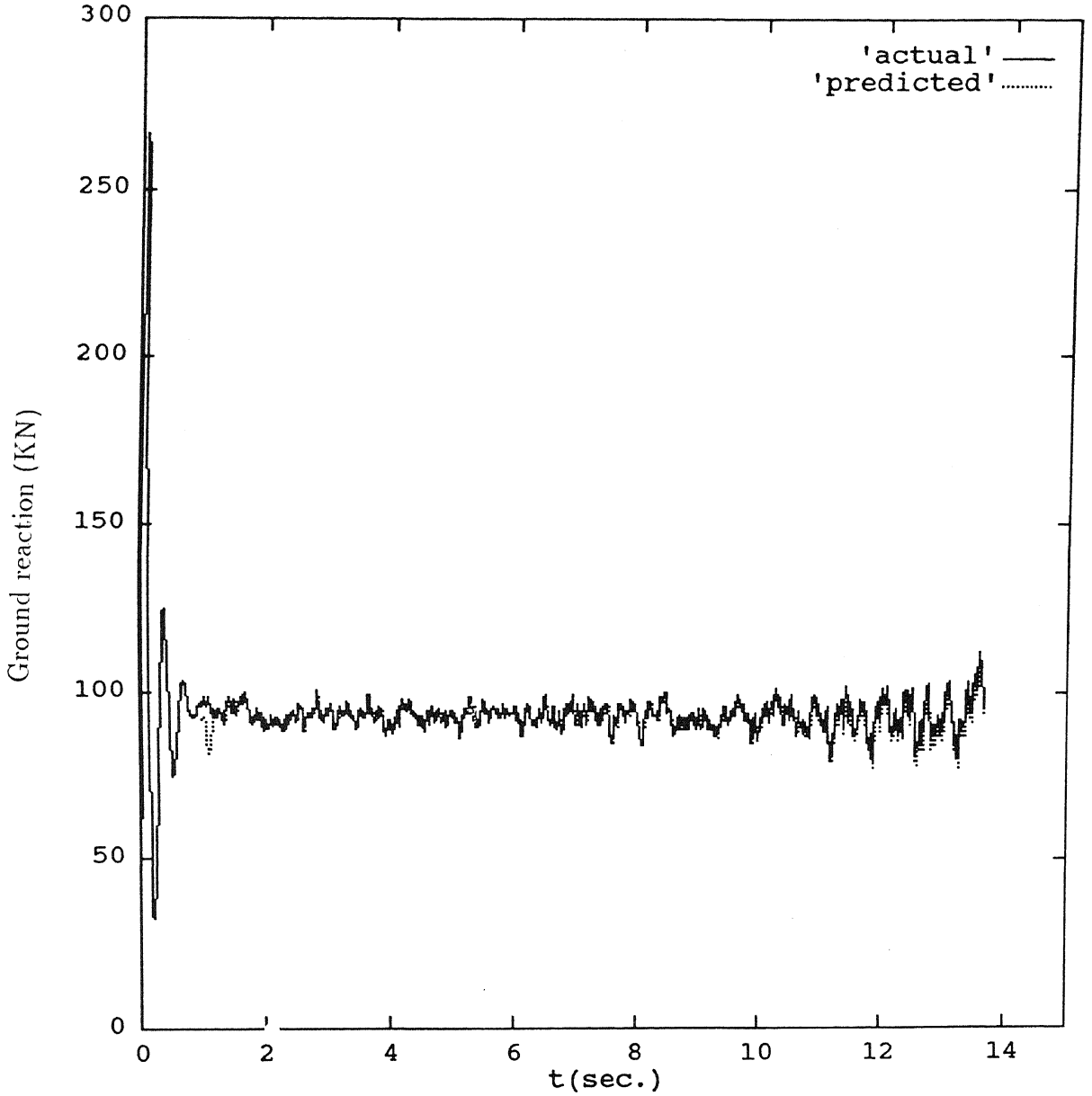

Figure 5.61: Ground Reaction for stepped runway, Glide velocity=75.56 m/s, Sink velocity=1.0 m/s

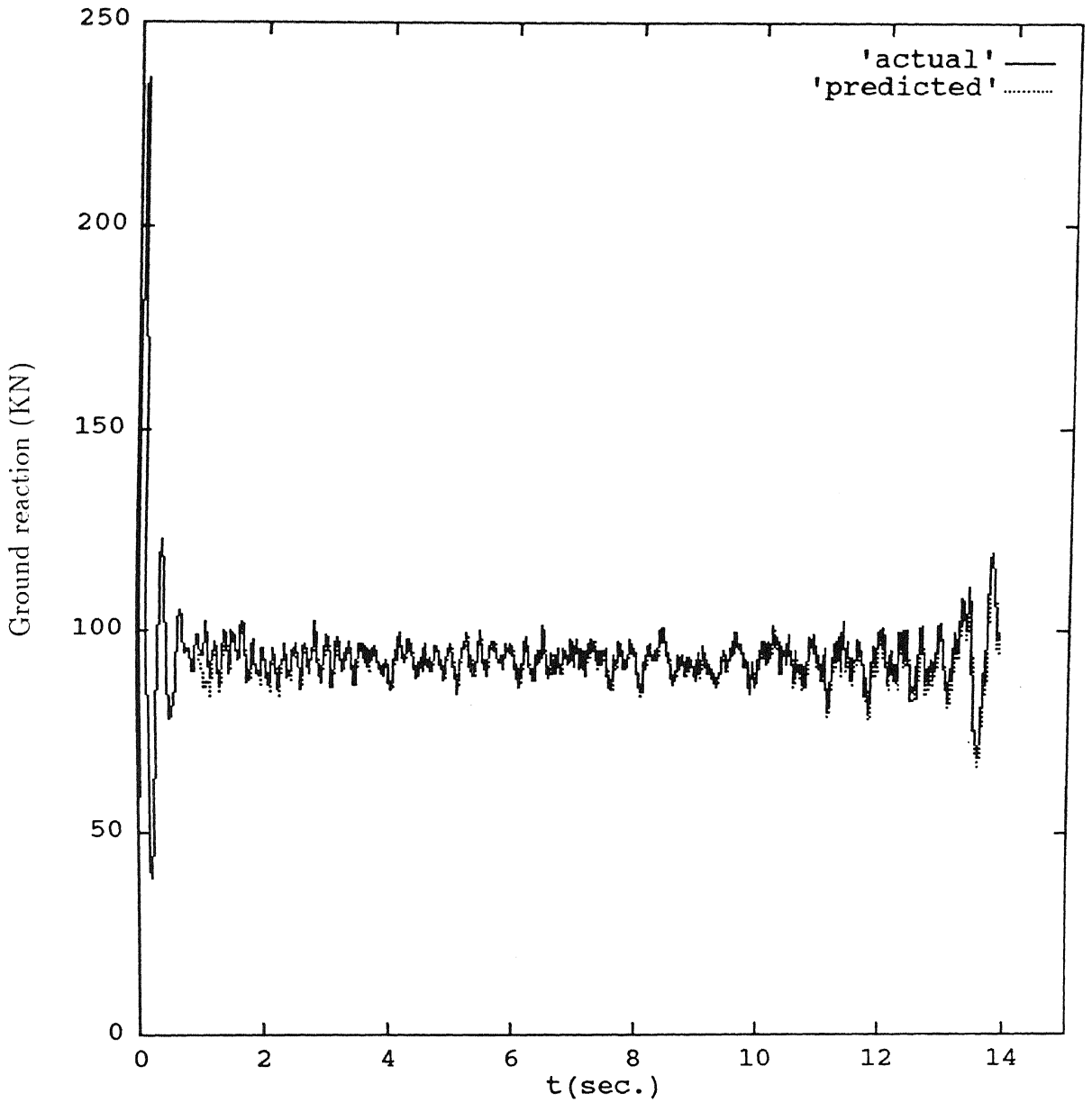

Figure 5.62: Ground Reaction for sinusoidal runway, Glide velocity=75.56 m/s, Sink velocity=1.0 m/s

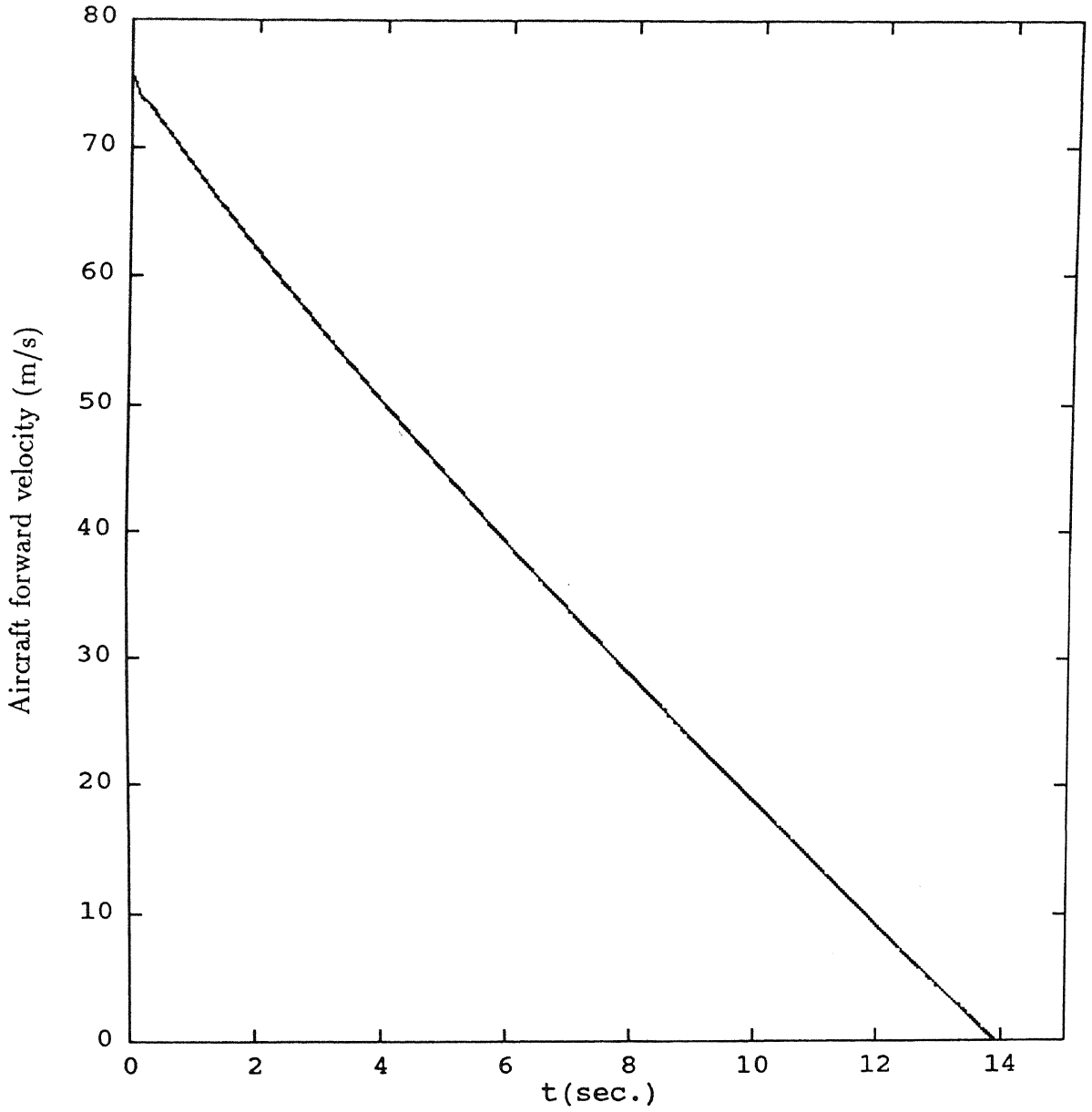

Figure 5.63: Aircraft forward velocity for inclined runway, Glide velocity=75.56 m/s, Sink velocity=1.0 m/s

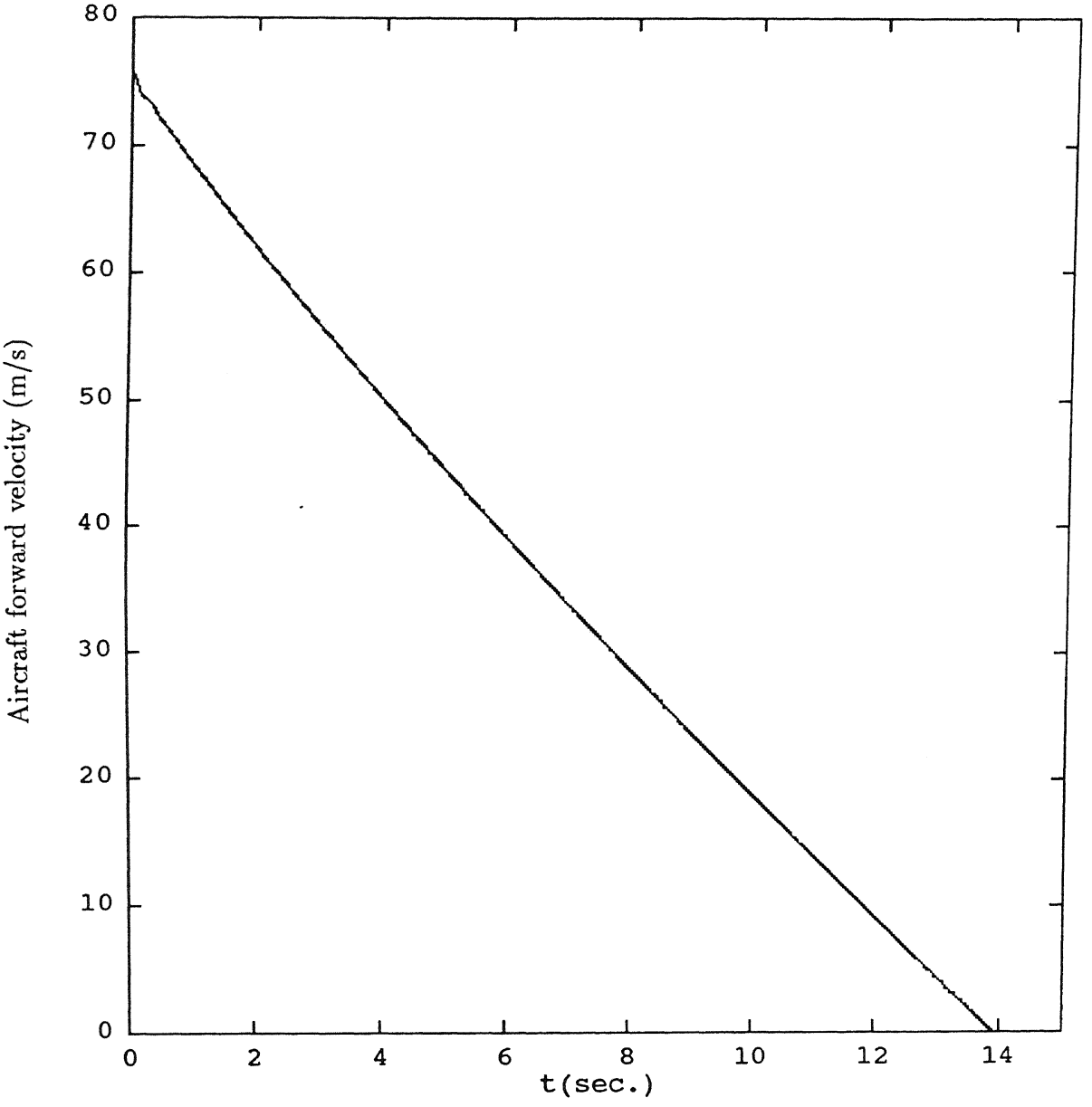

Figure 5.64: Aircraft forward velocity for stepped runway, Glide velocity=75.56 m/s, Sink velocity=1.0 m/s

Table 5.3: Landing distance variation with different parameters

Glide velocity (m/s)	Sink velocity (m/s)	Mean profile	Stopping time (sec.)	Ground distance travelled (m)
75.56	1.0	Flat	13.9	491.7
75.56	2.0	Flat	13.8	485.9
75.56	3.0	Flat	13.7	480.3
83.12	1.0	Flat	15.0	576.7
90.67	1.0	Flat	16.0	664.1
75.56	1.0	Inclined	13.9	491.7
75.56	1.0	Stepped	13.9	491.7
75.56	1.0	Sinusoidal	13.9	492.3

Chapter 6

Conclusions

Following conclusions are drawn from the work done in the present study :

- Considerable reduction in the ground distance travelled is obtained showing the efficacy of the anti-skid optimal braking scheme.
- The landing run decreases with increase in sink velocity.
- The landing run increases with increase in glide velocity.
- Change in the mean profile has no significant effect on the landing run length.
- With increase in glide velocity, the increase in stopping time is much less compared to the increase in landing run length. This shows the optimality of the present scheme towards the change in the landing glide velocity of the aircraft.
- The predicted ground reaction is in close agreement with the actual value, except sometimes at the peaks.
- The prediction is improved with increase in sink velocity.
- The change in glide velocity has no significant effect on the accuracy of the predictor.
- The prediction is poorer for sinusoidal mean profile.
- It is observed that system response is not much effected with change in the mean profile. But, in case of sinusoidal mean, the amplitude of the response

is increased for lower forward velocity of the aircraft. This indicates that any dominant frequency content in the track profile should be avoided.

- The ballooning of the aircraft increase with increase in sink velocity. It can be suppressed by appropriately controlling the shock struts parameters.

Following suggestions are made for further research in this area :

The heave model of the aircraft is used in the present study. The work can be extended by taking heave-pitch and heave-pitch-roll models. This would enable the case of one point and two point landings to be investigated. The shock strut can be articulated as well as telescopic in nature.

Only one sample of ground variation is taken in the present work. The true nature of the system response can be predicted only by taking large number of samples and studying the statistical characteristics of the responses.

The system response is studied only for three different sink velocities. But, in general, the sink velocity of an aircraft is never fixed. The work can be extended by assuming the sink velocity to be random in nature having a particular mean and standard deviation. The same is valid for the glide velocity as well.

The slip in the present study is assumed to be always in the optimal range, which may not be true. A feed back control mechanism could be used to keep the slip in the desirable range.

The coefficient of friction μ, between the tyre and the ground, varies with ground surface conditions. The present study has been conducted only for one value of μ. The coefficient of friction can also be taken as random.

References

[1] "Data on Various Aircrafts and Landing Gears", *Private Communications with Research Labs.*

[2] John. C. Houbolt, (1961), "Runway roughness studies in the aeronautical field", *Proceedings of the American Society of Civil Engineers, Journal of the Air Transport Division*, Vol. 87, pp 11-31.

[3] Norman. S. Silsby, (1962), "An analytical study of effects of some airplane and landing gear factors on the response to runway roughness with application to supersonic transports", *NASA TN D-1492.*

[4] C. C. Tung, J. Penzien and R. Horonjeff, (1964), "The effect of runway unevenness on the dynamic response of supersonic transports", *NASA CR-119.*

[5] C. L. Kirk and P. J. Perry, (1971), "Analysis of taxing induced vibrations in aircraft by the power spectral density method", *The Aeronautical Journal of the Royal Aeronautical Society*, Vol. 75, pp 182-194.

[6] C. L. Kirk, (1971), "The random heave-pitch response of aircraft to runway roughness", *The Aeronautical Journal of the Royal Aeronautical Society*, Vol. 75, pp 476-483.

[7] V. J. Virchis and J. D. Robson, (1971), "Response of an accelerating vehicle to random road undulation", *Journal of Sound and Vibration*, Vol. 18, No. 1, pp 423-427.

[8] K. Sobczyk and D. B. Macvean, (1976), "Nonstationary random vibration of systems travelling with variable velocity", *Symposium on Stochastic*

Problems in Dynamics, University of Southhamton (editor B. L. Clarkson), pp 412-434.

[9] D. Yadav and N. C. Nigam, (1978), "Ground induced nonstationary response of vehicles", *Journal of Sound and Vibration*, Vol. 61, No. 1, pp 117-126.

[10] J. K. Hammond and R. F. Harrison, (1981), "Nonstationary response of vehicles on rough ground-a state space approach", *Journal of Dynamic Systems, Measurement and Control, Transactions of the American Society of Mechanical Engineers*, Vol. 103, pp 245-250.

[11] R. F. Harrison and J. K. Hammond, (1986), "Evolutionary (frequency/time) spectra analysis of vehicles moving on rough ground by using "covariance equivalent" modelling", *Journal of Sound and Vibration*, Vol. 107, No. 1, pp 29-38.

[12] R. F. Harrison and J. K. Hammond, (1986), "Approximate, time domain, nonstationary analysis of stochastically excited, nonlinear systems with particular reference to the motion of vehicles on rough ground", *Journal of Sound and Vibration*, Vol. 105, No. 3, pp 361-371.

[13] D. Yadav and K. E. Kapadia, (1990), "Non-homogeneous track induced response of vehicles with non-linear suspension during variable velocity runs", *Journal of Sound and Vibration*, Vol. 143, No. 1, pp 51-64.

[14] S. Narayanan and G. V. Raju, (1990), "Stochastic optimal control of nonstationary response of a single degree of freedom vehicle model", *Journal of Sound and Vibration*, Vol. 141, No. 3, pp 449-463.

[15] D. Yadav and R. P. Ramamoorthy, (1991), "Aircraft heave-pitch dynamics to track induced excitation", *Journal of Aero. Soc. of India*, Vol. 43, No. 1, pp 19-28.

[16] D. Yadav and H. C. Upadhyay, (1991), "Nonstationary dynamics of train and flexible track over inertial foundation during variable velocity runs", *Journal of Sound and Vibration*, Vol. 147, No. 1, pp 57-71.

[17] D. Yadav and H. C. Upadhyay, (1992), "Dynamics of vehicles in variable velocity runs over non-homogeneous flexible track and foundation with two

point input models", *Journal of Sound and Vibration*, Vol. 156, No. 2, pp 247-268.

[18] D. Yadav and C. V. K. Singh, (1995), "Landing response of aircraft with optimal anti-skid braking", *Journal of Sound and Vibration*, Vol. 181, No. 3, pp 401-416.

[19] M. Shinozuka, (1971), "Simulation of multivariate and multidimensional random processes", *The Journal of the Acoustical Society of America*, Vol. 49, No. 1, pp 357-368.

[20] I. H. Witten, (1980), "Algorithms for adaptive linear prediction", *The Computer Journal*, Vol. 23, No. 1, pp 78-84.

[21] P. Jayarami Reddy, V. T. Nagaraj and V. Ramamurti, (1984), "Analysis of semi-levered suspension landing gear with some parametric study", *Journal of Dynamic Systems, Measurement and Control*, Vol. 106, No. 3,pp 218-224.

[22] B. Milwitzky and F. E. Cook, (1963), "Analysis of landing gear behaviour", *NACA*, TR 1154.

[23] Mahinder. K. Wahi, (1976), "Oil compressibility and polytropic air compression analysis of oleo-pneumatic shock strut", *Journal of Aircraft*, Vol. 13, No. 7, pp 527-530.

[24] N. C. Nigam, (1983), *Introduction to Random Vibrations*, MIT Press, Cambridge, Massachussetes.

[25] S. H. Crandall and W. D. Mark., (1963), *Random Vibrations in Mechanical Systems*, Academic, New York

[26] Y. K. Lin, (1967), *Probabilistic Theory of Structural Dynamics*, McGraw Hill Book Company

[27] H. G. Conway, (1958), *Landing Gear Design*, Chapman and Hall, London.

[28] C. V. K. Singh, (1991), "Induced response of vehicles during anti-skid braking", *M. Tech. Thesis, Deptt. of Aerospace Engg., I.I.T.Kanpur.*